FE-2229-12
Distribution Category UC-90c

# SURFACE STRUCTURE AND MECHANISMS OF GASIFICATION CATALYST DEACTIVATION

**Final Report**

**P. J. Reucroft**
**E. B. Bradley**
**R. J. De Angelis**
**G. A. Sargent**

UNIVERSITY OF KENTUCKY
Lexington, Kentucky 40506

March 1980

PREPARED FOR THE UNITED STATES
DEPARTMENT OF ENERGY

Under Contract No. EX-76-C-01-2229
(formerly E(49-18)-2229)

---

# Table of Contents

# Introduction

Since June 1974, methanation catalyst characterization studies have been in progress at the University of Kentucky. The initial project was supported by the Institute for Mining and Minerals Research (IMMR) and Catalysts and Chemicals, Inc. (now United Catalysts, Inc.), headquartered in Louisville, Kentucky. The project was aimed at obtaining information on the average catalyst particle size and the particle size distribution in typical supported nickel methanation catalysts by x-ray diffraction, hydrogen chemisorption and electron microscopy techniques. In the initial phase of the project, x-ray profile analysis techniques were developed that allowed determination of the particle size distribution in both unreduced and reduced nickel catalysts. The catalysts that were investigated were supplied by United Catalysts, Inc.

In February 1976, the research project was expanded considerably to include catalyst characterization and surface studies by ESCA (x-ray photoelectron spectroscopy), auger spectroscopy, infrared spectroscopy and Raman spectroscopic techniques, in addition to the initial methods. Studies on gas/solid interactions at nickel single-crystal surfaces were also initiated. In these latter studies, the techniques primarily employed included LEED (low-energy electron diffraction), auger spectroscopy and laser Raman spectroscopy.

The broad objectives of the expanded program have been to:

(1) Obtain insight into the mechanism of the methanation reaction at metal surfaces;

(2) Obtain a better understanding of chemical poisoning mechanisms; and,

(3) Determine thermal deactivation (sintering) mechanisms.

The ultimate objective is to design catalysts that are more selective and have increased thermal stability and poison resistance.

The program since February 1976 (supported by the U.S. Department of Energy (DOE), Contract No. EX-76-C-01-2229, IMMR and United Catalysts, Inc., who have also supplied fresh catalysts), used activity-tested catalysts and sulfur-poisoned catalysts for the characterization studies. A program to develop a sulfur-resistant catalyst by measuring the methanation activity of various catalyst formulations in the presence of sulfur has been carried out concurrently at United Catalysts, Inc. (ERDA Contract No. EX-76-C-01-2032). This final report to the Department of Energy includes studies on the characterization of both fresh and activity-tested catalysts and covers all work done on the project since its inception.

# Brief Summary of Progress to Date

Considerable information has been obtained on the chemical state of nickel in typical coprecipitated alumina and silica supported nickel catalysts. In these catalysts it appears that a significant fraction of the metal is chemically complexed with the support material forming aluminate and silicate, respectively, in alumina and silica supported catalysts. This leads to incomplete reduction of nickel at low temperatures, resulting in less metal being available in a catalytically active form. Recent studies indicate that less metal-support interaction takes place in magnesium silicate-supported nickel catalysts.

Studies on the effect of time and temperature on the nickel particle size distribution in unreduced (nickel oxide) and reduced (nickel metal) catalysts indicate that the sintering mechanism, which leads to a larger average particle size, appears to be different in the two forms of the catalyst. In the unreduced catalyst, the number of nickel oxide particles increases at both the low and the high ends of the distribution in the sintered catalyst relative to the fresh catalyst. In the reduced catalyst, on the other hand, the number of nickel metal particles increases at the high end of the distribution in the sintered reduced catalyst relative to the fresh reduced catalyst. These results indicate that a particle transport and particle-particle coalescence mechanism may be dominant in the reduced catalysts. In the unreduced catalyst, on the other hand, a sintering mechanism by which atoms escape from the catalyst particles, diffuse through the matrix and are acquired by other catalyst particles, may be operative in addition to a particle-particle coalescence mechanism.

ESCA studies on sulfided alumina and magnesium-silicate supported nickel catalysts and sulfided magnesium-silicate supported nickel-chromium catalysts indicate that a significant fraction of the sulfur acquired by the catalysts appears to be in the sulfate form in the nickel-chromium catalyst. The sulfur is primarily in the sulfide form in both the alumina and magnesium-silicate supported nickel catalysts. These results suggest that the presence of chromium in a magnesium-silicate supported matrix favors the formation of sulfate rather than sulfide. This may be one reason for the higher methanation activity observed by United Catalysts, Inc., in their activity studies on sulfided magnesium-silicate supported nickel-chromium catalysts compared to many other catalysts that were evaluated in the program. Similar results were found for magnesium-aluminate supported nickel-chromium catalysts. Studies on the chemical form of sulfur in these catalysts are now underway.

The interaction of carbon monoxide at the nickel (111) surface has been investigated by LEED, auger spectroscopy and laser Raman spectroscopy. The results indicate that carbon monoxide dissociates into a complex form of carbon at temperatures higher than 100°C. These results support methanation mechanisms (and Fischer-Tropsch mechanisms) in which surface carbon formation has been proposed as the first step in the synthesis process. Raman lines have been obtained from the Ni(111) surface that are thought to be associated with the carbon complex. Studies are continuing to clarify the nature of the carbon species and to obtain information on the chemical bonding situation.

A number of scientific papers have been published as these studies have progressed. Reprints and preprints of the publications listed below, as well as thesis abstracts, are included in Appendix I; Appendix II includes abstracts of presentations made at various technical meetings; and, Appendix III contains concise statements of research accomplishments on the project. These were prepared for the U.S. Department of Energy Conference on University Coal Research which was held in Lexington, Kentucky on August 23-24, 1978.

# Publications


1. P. J. Reucroft, E. B. Bradley, R. J. DeAngelis and G. A. Sargent, *"Surface Structure and Mechanisms of Gasification Catalyst Deactivation,"* Quarterly Reports Nos. 1-11, Contract No. EX-76-C-01-2229 (Reports FE-2229, Nos. 1-11) covering the period February 1, 1976 to October 31, 1978.

2. R. B. Shalvoy and P. J. Reucroft, *"Quantitative Analysis of ESCA Signal Intensities from Coprecipitated Nickel on Alumina Catalysts,"* **Journal of Electron Spectroscopy and Related Phenomena,** Vol. 12, p. 351 (1977).

3. A. Kidron, R. J. DeAngelis and P. J. Reucroft, *"Particle Size Distribution of NiO in Coprecipitated $NiO$-$Al_2O_3$ Powders,"* **Journal of Applied Physics,** Vol. 48, p. 5296 (1977).

4. P. Ganesan, H. K. Kuo, A. Saavedra and R. J. DeAngelis, *"Particle Size Distribution Function of Supported Metal Catalyst by X-Ray Diffraction,"* **Journal of Catalysis,** Vol. 52, p. 310 (1978).

5. C. H. Lin, *"A Study of Metal Surface Area in Supported Nickel Catalysts by Hydrogen Chemisorption,"* M.S. Thesis, University of Kentucky (1977).

6. K. H. Ho, *"Surface Area Studies on Variable Composition Nickel-Alumina Methanation Catalysts,"* M.S. Thesis, University of Kentucky (1977).

7. H. K. Kuo, *"Structural Characteristics of Catalytic Materials Containing Nickel Supported on Alumina or Silica,"* M.S. Thesis, University of Kentucky (1977).

8. E. B. Bradley and J. M. Stencel, *"Infrared Spectra of Some Nonreduced Methanation Catalysts,"* **Applied Spectroscopy,** Vol. 32, p. 496 (1978).

9. J. M. Stencel and E. B. Bradley, *"Raman Spectra of CO, $H_2$ and $O_2$ Adsorbed on Ni(111),"* **Spectroscopy Letters,** Vol. 11, p. 563 (1978).

10. J. M. Stencel, D. M. Noland, E. B. Bradley and C. A. Frenzel, *"An Ultrahigh-Vacuum Chamber for Raman Studies on Gases Adsorbed on Metals,"* **Review of Scientific Instruments,** Vol. 49, p. 1163 (1978).

11. R. B. Shalvoy, P. J. Reucroft and B. H. Davis, *"Characterization of Coprecipitated Nickel on Silica Methanation Catalysts by X-Ray Photoelectron Spectroscopy,"* **Journal of Catalysis,** Vol. 56, p. 336 (1979).

12. J. W. Park, *"The Effect of Reduction Time and Temperature on the Surface Area of Nickel Methanation Catalysts,"* M.S. Thesis, University of Kentucky (1979).

13. R. B. Shalvoy and P. J. Reucroft, *"Characterization of a Sulfur Resistant Methanation Catalyst by X-Ray Photoelectron Spectroscopy,"* **Journal of Vacuum Science Technology,** Vol. 16, p. 567 (1979).

14. J. M. Stencel, E. Heinz and E. B. Bradley, *"Structural Changes in a Sulfur-Resistant Methanation Catalyst as Determined from Infrared Spectroscopy,"* **Applied Spectroscopy,** Vol. 33, p. 118 (1979).

15. J. M. Stencel and E. B. Bradley, *"Raman Spectra of Carbon Monoxide Adsorbed on Oriented Crystalline Nickel Surfaces,"* **Journal of Raman Spectroscopy**, Vol. 8, p. 203 (1979).

16. D. M. Noland, *"Far Infrared Investigation of Aluminate and Silicate Support Nickel Methanation Catalysts,"* M.S. Thesis, University of Kentucky (1979).

17. H. K. Kuo, P. Ganesan and R. J. De Angelis, *"A Method to Study Sintering of a Supported Metal Catalyst,"* **Proceedings of the Twelth Annual Conference of the International Metallographic Society**, Tamiment, Pennsylvania, July 8-10, 1979, in press.

18. R. B. Shalvoy, P. J. Reucroft and B. H. Davis, *"Studies of the Metal-Support Interaction in Coprecipitated Nickel on Alumina Methanation Catalysts using X-Ray Photoelectron Spectroscopy (XPS),"* **Surface and Interface Analysis**, in press.

19. J. M. Stencel, E. B. Bradley and F. R. Brown, *"Infrared and Raman Spectra of a Surface-Resistant Methanation Catalyst,"* **Applied Spectroscopy**, in press.

20. J. L. R. Chao, *"A Surface Analysis Study of Carbon Monoxide and Hydrogen Adsorption and Desorption on Ni(111) Crystals,"* Ph.D. Dissertation, University of Kentucky (1979).

The following papers have been presented by faculty, postdoctoral research associates and graduate students associated with the project:

1. *"Surface Structure and Mechanisms of Gasification Catalyst Deactivation,"* presented by P. J. Reucroft at the ERDA/EPRI/NSF University Principal Investigators Conference – Coal Research, Golden, Colorado, September 3-4, 1976.

2. *"Characterization of Heterogeneous Catalysts,"* presented by R. B. Shalvoy at the Northeast Users Group Meeting, Wilmington, Delaware, May 20, 1977.

3. *"ESCA Characterization of Methanation Catalysts,"* by P. J. Reucroft, B. H. Davis and R. B. Shalvoy; presented by P. J. Reucroft at the Symposium on Catalysis of Coal Conversion Processes, Second Joint CIC/ACS Conference, Montreal, May 29 - June 2, 1977.

4. *"Particle Size Distribution Functions of Supported Metal Catalysts by X-Ray Diffraction,"* by R. J. DeAngelis, P. Ganesan and A. Saavedra; presented by R. J. DeAngelis at the Symposium on Catalysis of Coal Conversion Processes, Second Joint CIC/ACS Conference, Montreal, May 29 - June 2, 1977.

5. *"Infrared and Raman Spectra of a Heterogeneous Nickel-Alumina Catalyst,"* by J. M. Stencel and E. B. Bradley; presented by J. M. Stencel at the 32nd Symposium on Molecular Spectroscopy, Ohio State University, Columbus, Ohio, June 13-17, 1977.

6. *"Surface Analysis of Nickel Methanation Catalysts by ESCA,"* by P. J. Reucroft and R. B. Shalvoy; presented by P. J. Reucroft at the 9th ACS Central Regional Meeting, Charleston, West Virginia, October 12-14, 1977.

7. *"Surface Structure and Mechanisms of Gasification Catalyst Deactivation,"* presented by P. J. Reucroft at the ERDA/EPRI/NSF University – Principal Investigators Conference – Coal Research, Carnegie-Mellon Institute of Research, Pittsburgh, Pennsylvania, August 25-26, 1977.

8. *"Correlation of ESCA Signal Intensities and Average Particle Size in Methanation Catalysts,"* presented by R. B. Shalvoy at the Northeast ESCA Users Group Meeting, Picatinny Arsenal, Dover, New Jersey, December 2, 1977.

9. *"A Cell for* In Situ *Infrared and Raman Studies,"* by J. M. Stencel and E. B. Bradley; presented by J. M. Stencel at the 1977 Fall Meeting of the American Physical Society, Miami, Florida, November 21-24, 1977.

10. *"Comparison of the Infrared Spectra of Coal Methanation Catalysts,"* by J. M. Stencel and E. B. Bradley; presented by J. M. Stencel at the 1977 Fall Meeting of the American Physical Society, Miami, Florida, November 21-24, 1977.

11. *"ESCA Characterization of Nickel Methanation Catalysts,"* by R. B. Shalvoy and P. J. Reucroft; presented by R. B. Shalvoy at the 175th ACS National Meeting, Anaheim, California, March 13-17, 1978.

12. *"On Measuring the Average Particle Size of Nickel in Coprecipitated NiO-$Al_2O_3$ and NiO-$SiO_2$ Catalytic Materials,"* by K. B. Patel, C. H. Lin, P. Ganesan, R. J. Reucroft and R. J. DeAngelis; presented by P. Ganesan at the Conference on Catalysts Deactivation and Poisoning, University of California, Berkeley, California, May 24-26, 1978.

13. *"Raman Spectra Associated with Gas Adsorption on Nickel (111),"* by J. M. Stencel and E. B. Bradley; presented by J. M. Stencel at the Molecular Spectroscopy Symposium, Ohio State University, June 12-16, 1978.

14. *"Surface Characterization of Methanation Catalysts,"* presented by P. J. Reucroft at the Fifth Annual DOE/Fossil Energy Conference on University Coal Research, Lexington, Kentucky, August 23-24, 1978.

15. *"Auger Electron Spectroscopy and Desorption Studies of CO on Sulfur Poisoned Nickel (111) Single-Crystal Surfaces,"* by G. A. Sargent, G. B. Freeman and J. L. Chao; presented by G. B. Freeman at the 176th National SCS Meeting, Miami Beach, Florida, September 10-15, 1978.

16. *"Characterization of a Sulfur Resistant Methanation Catalyst by XPS,"* by R. B. Shalvoy and P. J. Reucroft; presented by R. B. Shalvoy at the 25th National Vacuum Symposium, American Vacuum Society, San Francisco, November 27 - December 1, 1978.

17. *"An Ultrahigh Vacuum Cell for Infrared Reflection Studies of Gases Adsorbed on Metals,"* by J. M. Stencel, E. B. Bradley and E. Heinz; presented by E. Heinz at the APS Southeastern Section Meeting, Blacksburg, Virginia, October 26, 1978.

18. *"Raman Spectra Associated with Gas Adsorption on Nickel (110),"* by J. M. Stencel and E. B. Bradley; presented by E. B. Bradley at the Annual Meeting of the Optical Society of America, San Francisco, California, October 21 - November 4, 1978.

19. *"Investigation of the Metal Support Interaction in Coprecipitated Nickel on Alumina Methanation Catalysts Using X-Ray Photoelectron Spectroscopy,"* by R. B. Shalvoy, P. J. Reucroft and B. H. Davis; presented by R. B. Shalvoy at the 26th National Meeting of the American Vacuum Society, New York, New York, October 1-5, 1979.

20. *"Raman Spectra of CO Adsorbed on Oriented Nickel Surfaces,"* by E. B. Bradley and J. M. Stencel; presented by E. B. Bradley at the Annual Meeting, Optical Society of America, Rochester, New York, October 8-12, 1979.

21. *"Apparatus for the Measurement of the Infrared and Raman Spectra of Gases Adsorbed on Clean Metal Surfaces,"* by R. E. Heinz, J. M. Stencel and E. B. Bradley; presented by E. Heinz at the Molecular Spectroscopy Symposium, Columbus, Ohio, June 11-15, 1979.

22. *"Auger Electron Spectroscopy (AES), Low-Energy Electron Diffraction (LEED) and Thermal Desorption Studies of CO on Clean and Sulfur Poisoned Ni(111) Single Crystals,"* by G. A. Sargent, J. Chao and G. Freeman; presented by G. A. Sargent at the 1979 International Metallographic Society Meeting, Tamiment, Pennsylvania, July 8-11, 1979.

23. *"The Sintering Behavior of a Silica-Supported Nickel Catalyst,"* by H. K. Kuo, P. Ganesan and R. J. De Angelis, presented by R. J. De Angelis at the 12th Annual International Metallographic Convention, Tamiment, Pennsylvania, July 8-11, 1979.

# Acknowledgements

Research personnel who have participated in the project, in addition to the co-principal investigators, include Drs. P. Ganesan, J. M. Stencel, P. Zanzucchi and C. H. Huang (postdoctoral research associates), Drs. R. B. Shalvoy, G. B. Freeman and B. H. Davis (Institute for Mining and Minerals Research), and H. K. Kuo, J. Chao, D. M. Noland, E. Heinz, C. H. Lin, K. H. Ho, J. W. Park and S. N. Russell (graduate assistants).

# Appendix I.
# **Reprints and Preprints of Papers Resulting from this Research**

# Quantitative Analysis of ESCA Signal Intensities from Coprecipitated Nickel on Alumina Catalysts

**R. B. Shalvoy and P. J. Reucroft**
Department of Metallurgical Engineering and
Materials Science
University of Kentucky
Lexington, Kentucky 40506

## Introduction

Heterogeneous catalysts are complex, non-uniform, systems. ESCA has been applied to a variety of simple and complex systems, often providing valuable information on the surface electronic structure. Increasingly, ESCA has been used to characterize heterogeneous catalyst systems[1]. Positive correlations between ESCA peak intensities and catalyst properties, such as dispersion and particle size have been obtained from a quantitative analysis of the ESCA spectra[2-4]. These results indicate that ESCA data, properly interpreted, can provide much basic information on catalysts in addition to characterizing the charge state of the dispersed metal.

We have been investigating a series of coprecipitated nickel oxide/alumina methanation catalysts. Catalysts prepared by this technique have not been extensively studied using ESCA. In addition, these samples have a higher metal content (10–47% nickel, by weight) than previously studied catalysts*. As the method of preparation appears to have an influence on the properties of the catalyst[4], it is of interest to learn how the coprecipitation method affects the ESCA spectra, and hence the properties of the catalyst itself.

The catalyst samples were prepared by coprecipitation of a nickel salt with an aluminum salt to obtain carbonates of nickel and aluminum. The samples were then calcined to their oxide states. This method of preparation has yielded very active catalysts following reduction of the nickel oxide to nickel metal[5, 6]. Particle sizes in the unreduced form, determined by X-ray diffraction, range from 15–30 Å[7], although particle sizes for the 10–30% nickel samples have not been determined to date.

The intensity of a photoelectron peak for a sample of uniform composition may be described in terms of the following[8]

$$I = I_0 n \sigma \lambda(\varepsilon)\, D(\varepsilon) \qquad (1)$$

Where $I_0$ is the X-ray flux, $n$ the density of atoms, $\sigma$ the photoexcitation cross section, $\lambda(\varepsilon)$ the mean free path of the electron of energy $\varepsilon$ in the sample material, and $D(\varepsilon)$ is the detector efficiency. We assume $I_0$ to be constant and the variations of the mean free path between different catalyst samples to be small. The ratio of intensities of the Ni $2p_{3/2}$ and Al $2s_{1/2}$ core levels, abbreviated to Ni and Al, may be expressed as

$$R\left(\frac{Ni}{Al}\right) = \frac{I_{Ni}}{I_{Al}} = \frac{n_{Ni}}{n_{Al}}\left(\frac{\sigma_{Ni}\lambda(\varepsilon_{Ni})D(\varepsilon_{Ni})}{\sigma_{Al}\lambda(\varepsilon_{Al})D(\varepsilon_{Al})}\right) = \left(\frac{n_{Ni}}{n_{Al}}\right) Y \qquad (2)$$

The term relating the relative atomic density to the ratio of ESCA signal intensities (Y) may be determined from standard samples of known composition. Thus by measuring the relative ESCA signal intensities for the Ni $2p_{3/2}$ and Al $2s_{1/2}$ core levels, the relative atomic abundances of nickel and aluminum in the surface region of the catalyst may be estimated.

* Catalyst samples were supplied by Catalyst and Chemicals Inc., Louisville, KY, who also supplied information on chemical composition and physical properties.

## Results and Discussion

The samples were examined as pellets, the form in which the catalyst is utilized and as supplied by the manufacturer. The flat end of the pellet was mounted in a copper block holder, dusted clean and then inserted into the spectrometer analysis chamber (AEI ES200B, vacuum: $5 \times 10^{-9}$ torr, Mg X-rays). Brief argon ion etching (less than 1 minute, 1KV beam voltage) was performed. Etching up to 30 minutes beyond this did not cause any further changes in signal intensity ratios.

The Ni $2p_{3/2}$, O 1*s*, and Al 2*s* peak regions were scanned in repetitive sequence using the AEI-supplied DS100 computer based data acquisition system. When a good signal to noise ratio was obtained, typically with 20,000 net counts on the Ni peak, the data were plotted and the peak areas determined. It was observed that the peak binding energies, relative to the Au $4F_{7/2}$ peak binding energy of 84.0 eV[9], remained unchanged for the various samples showing that the chemical form of the nickel did not change with the metal loading. The ESCA spectra shown in Fig. 1 (binding energies are not corrected for the sample charging of 4 eV) are typical of the results obtained on the catalysts investigated.

The peak areas were measured over the areas shown in Fig. 1. The area of the Al 2*s* peak was truncated on the low binding energy side as the Ni 3*s* peak occurs just

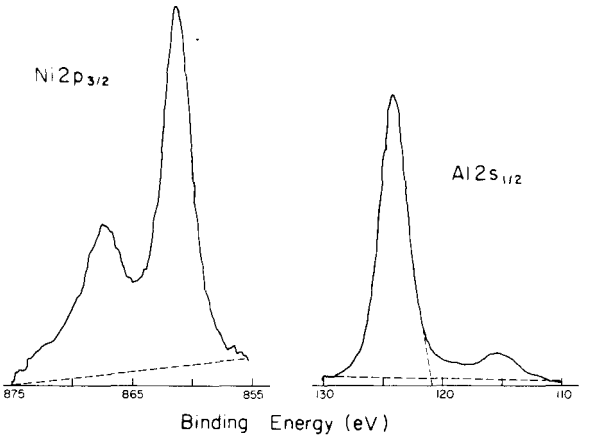


**Figure 1. Typical ESCA peak areas measured (10% nickel content sample).**

**Table 1. Experimental and Calculated R (Ni/Al) Intensity Ratios.**

| Sample | Nickel wt. percent | Atomic abundance Ni | Atomic abundance Al | R( Ni/Al) Exp. | R( Ni/Al) Calc. |
|---|---|---|---|---|---|
| 1 | 10 | 0.04 | 0.37 | 0.29 | 0.25 |
| 2 | 20 | 0.08 | 0.34 | 0.45 | 0.59 |
| 3 | 30 | 0.13 | 0.30 | 0.92 | 1.07 |
| 4 | 40 | 0.18 | 0.26 | 1.61 | 1.79 |
| 5 | 47.5 | 0.23 | 0.22 | 1.91 | 2.64 |

below the Al 2*s* peak. The Ni 3*s* peak is not distinctly visible in Fig. 1 because the nickel content is low. The peak was discernible, however, in the samples of greater nickel content.

The anticipated intensity ratio for these samples was calculated by assuming a sample composition of $(NiO)_x$ $(Al_2O_3)_{1-x}$ and determining the atomic abundances as a function of the specified nickel weight contents. The ESCA peak area ratios were then estimated using eqn. (2). The atomic abundances, calculated ESCA signal ratios and the experimentally determined peak area ratios are listed in Table 1. The experimentally determined peak area ratios and the calculated ratios are plotted in Fig. 2 as a function of increasing nickel content.

The agreement between the experimental data and the calculated curve is quite good except for the 47% nickel content sample. Within the experimental uncertainties there is no appreciable difference between theory and experiment in the case of the lower nickel content samples. This result supports the assumptions concerning the sample uniformity and variation of the mean free path between catalyst samples. The result also suggests that the particle size of the unreduced nickel oxide remains relatively constant over the range of nickel contents studied. Particle sizes observed independently by X-ray diffraction for these materials with metal loadings in the range 40–60% are all about equal to the mean free path for the photoelectrons (~ 15A)[7, 10]. We were not able to obtain particle size data for the lower metal loading samples due to experimental difficulties. It would be surprising, however, to find large particle sizes for these samples in view of the fact that the coprecipitation technique produces a small particle size in the case of the higher metal loading samples. We are attempting to verify this by the X-ray diffraction technique.

The deviation of the higher nickel content sample from the calculated curve may be due to this sample having been reduced prior to the study and thereby possessing a larger particle size. This effect has been noted for other lower metal content samples[4] and in work on these catalysts in this laboratory. This possibility will be tested by examining reduced and/or sintered forms of the lower nickel content samples and determining their particle sizes independently. It may be possible in this way to determine particle sizes of dispersed metals from ESCA signal intensities while the sample is maintained under vacuum, or for samples which are difficult to evaluate in conventional fashion.

In Fig. 2, the relationship between the signal intensity ratio and the nickel content corresponds more closely to that observed for low metal content catalysts prepared by a cation exchange method rather than the relationship observed for impregnated catalysts[4]. The catalysts prepared by the cation exchange method were considered to have smaller particle sizes for a given metal loading and this resulted in a curve similar to that observed for the coprecipitated catalysts. The high activity observed for catalysts prepared by the coprecipitation method may be thus related to the small particle size, evidenced even for the high nickel content samples by the shape of the observed curve as well as by the generally good agreement between the experimental and calculated signal intensity ratios.

A quantitative analysis of ESCA spectra of the dispersed catalyst metal and the support material suggests that the coprecipitation method of preparation provides a good dispersion of the metal even for high metal contents. The reduction process which causes a degree of sintering is reflected in a lower Ni/Al signal intensity ratio. Hence ESCA provides a convenient method of monitoring catalyst particle sizes, even under vacuum conditions. The analysis on which these conclusions are based is still quite approximate. The reasonable results obtained at this level of analysis is encouraging, however, and indicates that further refinement in the method will lead to the development of a useful catalyst characterization technique.

## Acknowledgements

Support for this project was provided by U.S. ERDA, through Contract No. E(49-18)2229, and the Institute for Mining and Minerals Research, University of Kentucky.

We would also like to thank A. L. Hausberger, W. A. Kustes and M. Miller (Catalysts and Chemicals, Inc., Louisville, KY) for the catalyst samples and useful technical information.

## References

1 W. N. Delgass, T. R. Hughes and C. S. Fadley, *Catal. Rev.*, 4 (1970) 179.
2 J. S. Brinen, T. L. Schmitt, W. R. Doughman, R. J. Achorn, L. A. Siegel and W. N. Delgass, *J. Catal.*, 40 (1975) 295.
3 L. H. Scharpen, *J. Electron Spectrosc. Relat. Phenom.*, 5 (1974) 369.
4 D. Briggs, *J. Electron Spectrosc. Relat. Phenom.*, 9 (1976) 487.
5 A. L. Hausberger, K. Atwood and C. B. Knight, *Development of Methanation Catalysts for Synthetic Natural Gas Processes*, presented at the Symposium on Methanation of Synthesis Gas, Division of Fuel Chemistry (ACS), Atlantic City, NJ, September 1974.
6 A. L. Hausberger and W. A. Kustes, *Sulfur Resistant Methanation Catalysts*, First Annual Report, U. S. ERDA Contract No. E(49-18)2032, July 1976 (FE-2032-4).
7 P. J. Reucroft, E. B. Bradley, R. J. De Angelis and G. A. Sargent, *Surface Structure and Mechanisms of Gasification Catalyst Deactivation*, First Annual Report, U. S. ERDA Contract No. E(49-18)2229, March 1977 (FE-2229-4).
8 D. R. Penn, *J. Electron Spectrosc. Relat. Phenom.*, 9 (1976) 29.
9 Further details on the binding energy calibration are given in: R. B. Shalvoy, G. B. Fisher and P. J. Stiles, *Phys. Rev. B*, 15 (1977) 1680.
10 C. J. Powell, *Surf. Sci.*, 44 (1974) 29.

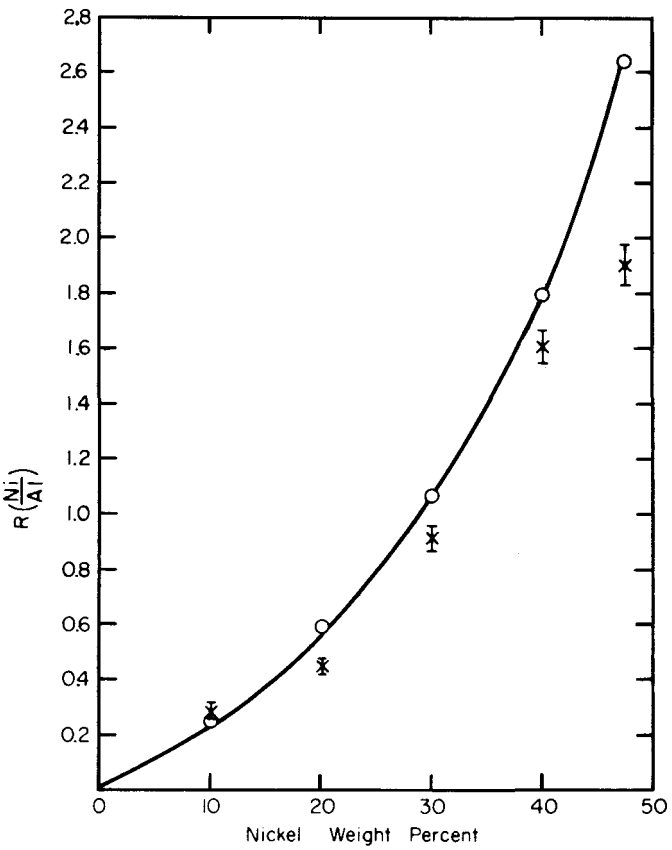


**Figure 2. Comparison of the experimental and calculated R (Ni/Al) intensity ratios for a range of alumina supported catalysts.**

# Characterization of Coprecipitated Nickel on Silica Methanation Catalysts by X-Ray Photoelectron Spectroscopy

R. B. Shalvoy and P. J. Reucroft
Department of Metallurgical Engineering and
Materials Science
University of Kentucky
Lexington, Kentucky 40506

and

B. H. Davis
Institute for Mining and Minerals Research
Kentucky Center for Energy Research Laboratory
P.O. Box 13015
Lexington, Kentucky 40583

## ABSTRACT

An X-ray photoemission spectroscopy study of a series of standard nickel compounds (Ni, NiO, $Ni(OH)_2$, and $NiSiO_3$) and silica-supported nickel methanation catalysts has been conducted. The binding energies and spectral shapes of the standard samples provide a data base which has been used to understand the catalyst spectra.

The activity and thermal stability of coprecipitated nickel catalysts has been attributed to the metal-support interaction. This interaction has been observed in two coprecipitated nickel-on-silica catalysts. The nickel spectra closely resemble those of amorphous $NiSiO_3$. The interaction varies somewhat between the two catalysts studied, as evidenced by the differences in their reducibility.

## INTRODUCTION

The production of pipeline quality substitute natural gas from coal requires the methanation of coal synthesis gas using metal catalysts such as nickel (*1*, *2*). These catalysts can be quickly deactivated by poisoning from sulfur in the gas stream and by sintering of the dispersed nickel particles (*1*). In general, catalysts that are more resistant to both chemical poisoning and thermal sintering while maintaining good activity are required if this process is to become economically viable in the future. In addition, a better understanding of the mechanism of methanation is highly desirable in order to develop catalysts with improved selectivity. A program has been initiated which has the broad objective of gaining a better understanding of the chemical and physical characteristics of typical methanation catalysts in order to provide a basis for designing improved catalysts. Some of the results obtained have been reported previously (*3–5*).

X-ray photoelectron spectroscopy (XPS) is a powerful tool for characterizing the chemical and physical state of surfaces (*6*). XPS has been found to be particularly useful in the study of catalyst poisoning (*7*, *8*) and changes in the chemical state occurring after reducing or oxidizing treat-

ments (*9*). The surface sensitivity of XPS (sampling depths are less than 18 Å (*10*)) makes the technique highly appropriate for the study of fresh and treated catalysts.

In the present work, the surfaces of silica-supported coprecipitated nickel methanation catalysts have been examined using XPS with the goal of characterizing the chemical state of the catalysts. Fresh (unreduced) samples have been evaluated.

These catalysts provide a good balance of methanation activity, selectivity, thermal stability, and reducibility (*11*). Interaction of the dispersed NiO particles and the silica support during catalyst preparation has been suggested as an important factor in providing this favorable set of properties (*11*).

The spectra of the dispersed nickel and the silica support show evidence of this interaction. How the interaction is affected by specific details of the coprecipitation technique used has also been investigated. From an understanding of how the method of preparation affects the chemical state of the dispersed nickel, improvements in catalyst performance may be obtained through refined preparational techniques.

## EXPERIMENTAL DETAILS

The data were acquired using a computer-controlled AEI ES200B electron spectrometer. This system used unmonochromatized Mg radiation and was operated in a variable analyzer transmission energy (of the electrons) mode giving good resolution (Au $4f_{7/2}$ full width at half maximum is 1.2 eV) and a linear (in electron kinetic energy) analyzer efficiency. Pressure in the analysis chamber was typically $5 \times 10^{-9}$ Torr. The spectrometer was calibrated in the present work by setting the kinetic energy difference between the Na 1*s* and 2*p* core levels (in $Na_2SO_3$) at 1041.1 eV or the Cu $2p_{\frac{3}{2}}$, $3p_{\frac{3}{2}}$ core level spacing (in copper) at 857.6 eV. The spectrometer work function was determined by using the Au $4f_{7/2}$ peak (binding energy = 84.0 eV (*12*) relative to spectrometer Fermi level). The calibration was checked at least weekly and adjusted as needed. Adjustments of more than 0.2 eV were seldom necessary.

Surface charging on an insulating sample introduces an additional complication in the determination of binding energies (*13*). Sample charging of 1 to 4 eV was observed for the standard samples and the catalysts. The best way of determining the charging shifts for powdered samples is still a matter of debate. In this work the shifting of the binding energy of the contaminant C 1*s* line from its neutral value of 285.0 eV was used as a measure of the surface charging. This method gives results which are of comparable reliability to those obtained using an electron flood gun to neutralize the surface charge (*13*). However, the binding energies obtained are still considered to contain uncertainties of ±0.3 eV.

The charging corrected binding energies determined using the C 1*s* line were found to be comparable with those obtained by a Ag spotting technique (*14*). The use of the C 1*s* line also gave consistent results for the variety of sample mounting techniques used (In foil, Cu-backed adhesive tape, or pressing the powder into a shallow cavity in a Cu block). Sample charging determined varied by over 1 eV as a function of the mounting technique used.

Recent studies have shown that core level binding energies determined in different laboratories for identical samples can differ by more than 1 eV for a specified strong peak, even in the case of conductive, clean metal foils (*13*, *15*). Consistency of data taken within a laboratory, however, was found to be quite good and reproducible. Variations in the techniques of spectrometer calibration appear to be primarily responsible for the systematic variation of data taken in different laboratories. Consequently, standard samples

of several forms of nickel likely to appear in the catalyst samples have been examined prior to studying the catalysts. This set of binding energies and peak shapes formed a data base for interpretation of the catalyst spectra.

The standard samples were obtained from commercial sources and were examined as powders mounted on copper backed adhesive tape or on In foil. The nickel silicate sample was prepared by precipitation from $Ni(NO_3)_2$ and $Na_2SiO_3$ solution followed by calcination in air at 400°C for 20 hr (*16*). The catalyst samples were furnished by United Catalysts, Inc. of Louisville, Kentucky. The C150-1-01 catalyst was obtained by precipitation a complex carbonate from a nickel nitrate solution which contained $SiO_2$ as a slurry. After aging for 1 hr at 82°C, the precipitate was filtered, washed, dried, and calcined for 8 to 16 hr at 371°C. The material was ground to a fine mesh, mixed with graphite (2–3%), and pressed into $\frac{1}{8}''$ or $\frac{3}{16}''$ tablets. The sample was then calcined further to remove any remaining water. The C150-1-02 catalyst was prepared in a similar manner except that in this case the complex carbonate precipitate was obtained from an aqueous solution which contained nickel nitrate and sodium silicate. These preparations gave catalysts of good activity and small catalyst particle size (*11*). Physical properties of these materials are summarized in Table 1. Methanation activity studies have been described previously (*11*).

**Table 1. Physical Properties of Catalysts.**

| | C150-1-01 | C150-1-02 |
|---|---|---|
| Percent Ni (by weight) | 51.7 | 46.6 |
| Percent C | 2.9 | 2.1 |
| Total surface area ($m^2g^{-1}$) | 183 | 235 |
| Metal surface area $(m^2g)^{-1}$ (reduced 450°C) | 76 | 59 |
| Pore volume ($cm^3g^{-1}$) | 0.34 | 0.58 |
| NiO crystallite size (Å) | 20.4 | 22 |
| Density (g $cm^{-3}$) | 1.05 | 0.88 |

**Table 2. Standard Sample Binding Energies.**[a]

| | Ni $2p_{3/2}$ | Ni satellite splitting | O $1s_{1/2}$ | Si 2p |
|---|---|---|---|---|
| Ni | 852.8 | | | |
| NiO | 856.0<br>854.6 | 7.0 | 529.6 | |
| $Ni_2O_3$[b] | 855.8 | 5.6 | 531.4 | |
| $Ni(OH)_2$ | 855.5 | 5.8 | 531.0 | |
| $NiSiO_3$ | 856.7 | 6.0 | 532.5 | 103.5 |
| $SiO_2$ | | | 532.6 | 103.4 |

[a] In electron volts.
[b] Ref. (19).

## RESULTS

The work was divided into two parts: measurements on the standard samples and studies on the catalysts. The experimental details were unchanged between the two runs.

### Standard Samples

Powdered samples of high purity Ni, NiO, $NiO–Ni_2O_3$, $Ni(OH)_2$, and $NiSiO_3$ were examined. The $2p_{\frac{3}{2}}$ peak in the nickel spectrum was used to characterize the chemical state of nickel. It has the largest cross section in nickel (*17*) and has been studied extensively in other laboratories (*18–29*). A summary of the binding energies of the core levels is given in Table 2. All energies are given in electron volts and have been corrected for sample charging.

It is observed that the binding energies of nickel $2p_{\frac{3}{2}}$ level in many of the different forms of nickel are similar if the uncertainty in the energies is recalled. To make an unambiguous identification of a particular compound, other core levels must

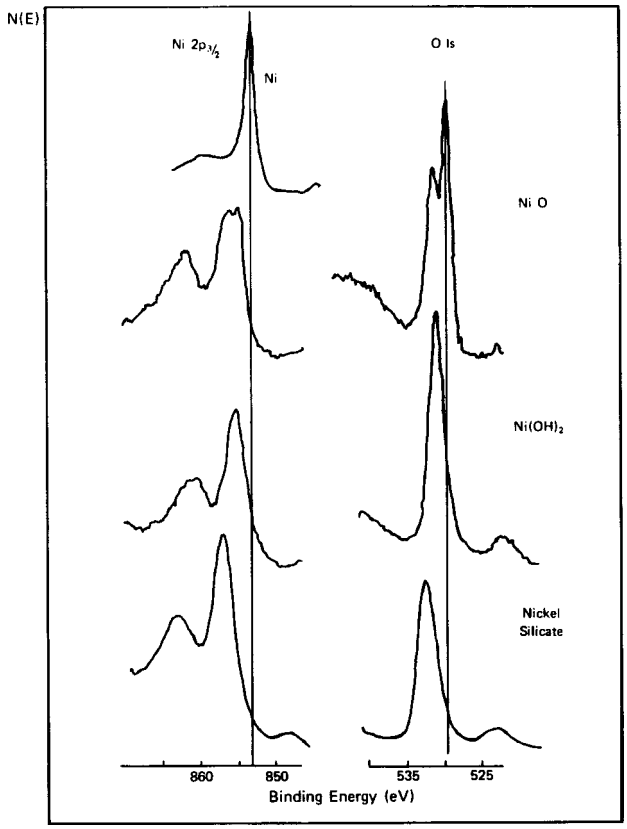


**Figure 1. Principal core level peaks (Ni $2p_{3/2}$, O 1s) for standard samples. All binding energies are corrected for charging (C 1s reference—285.0 eV).**

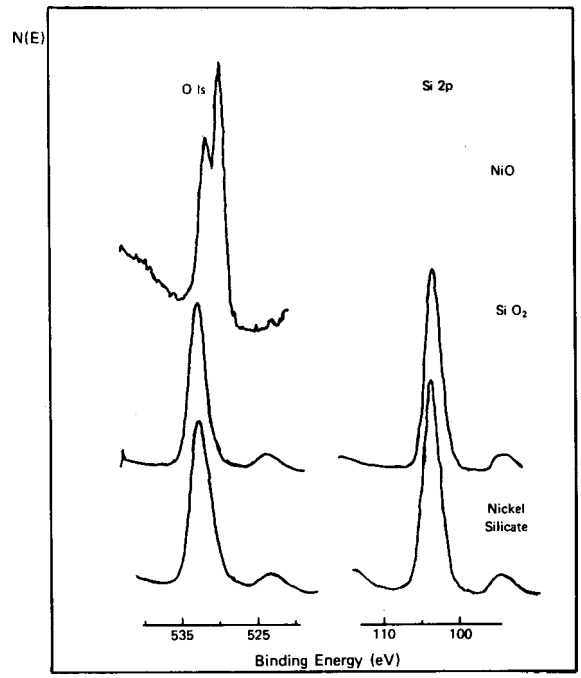


**Figure 2. O 1s and Si 2p core level peaks for NiO, $SiO_2$, and $NiSiO_3$.**

be examined, particularly the oxygen 1*s* level. The shape of the peaks also contains information. For example, the separation and intensity of the shakeup satellite of the Ni 2*p* level can be helpful in identifying a particular species. The spectra of the elements of interest are shown in Figs. 1 and 2 in the various standard compounds.

The chemical forms of nickel have certain characteristics which serve to identify their presence. These characteristics are summarized in Table 3. NiO has a unique doublet structure for the nickel $2p_{\frac{3}{2}}$ level as well as having the smallest binding energy for the oxygen 1*s* level. Conversely, the spacing of the Ni and O levels is larger than for the other standard compounds examined. $Ni_2O_3$ is similar spectrally to $Ni(OH)_2$. It appears to be present in the surface regions of most NiO samples, being evidenced by the higher binding energy oxygen peak typically observed in the spectrum of commercially obtained NiO samples and oxidized Ni foils (*18, 19, 21, 25–29*). It is not commonly found as a bulk material, however. This material has been described rather as a gross defect structure of NiO (*18, 19*). $Ni(OH)_2$ has binding energies which are relatively distinct from both NiO and $NiSiO_3$. It is also relatively dif-

**Table 3. Summary of Distinguishing NiX Characteristics.**

| Material | Characteristics |
|---|---|
| Ni metal | Ni 2p peak narrow, weak satellite structure. No charging, no chemical shift. |
| NiO | Ni 2p peak is doublet, large O 1s chemical shift. |
| $Ni_2O_3$ | Singlet Ni 2p peak of intermediate binding energy, reduced by $Ar^+$ etching. |
| $Ni(OH)_2$ | Intermediate Ni 2p binding energy, stable against $Ar^+$ ion induced reduction. |
| $NiSiO_3$ | High Ni 2p binding energy, High O 1s binding energy. |

ficult to reduce the $Ni^{+2}$ to $Ni^0$ by argon ion etching of this compound. Other compounds such as NiO and $NiSiO_3$ have been observed to be reduced by the argon ion etching process usually used to clean the sample surfaces *in situ*.

$NiSiO_3$ is observed to have high Ni and O binding energies. The nickel core level, as seen in Fig. 1, is distinct in shape from both Ni metal and NiO. The oxygen peak (Fig. 2) is similar to that observed in $SiO_2$ and again is quite distinct from that seen in NiO. The silicon 2*p* peak is similar to that for $SiO_2$, reflecting a similar chemical environment for silicon in these two materials.

The nickel in this sample can be reduced by argon ion etching although not as readily as the nickel in pure NiO. This material does not appear to be the $NiSiO_3$ spinel which is very difficult to reduce, however (*11*).

### Fresh (Unreduced) Catalysts

The fresh catalysts were examined as supplied (no pretreatment other than a light roughing up of the surface immediately prior to study). As coprecipitated catalysts display better performance than conventionally prepared catalysts (*11*) it was of interest to see how the two coprecipitation methods of preparation affect the chemical state, reducibility, and thermal stability of the nickel dispersion. The simplest spectrum would be a superposition of those of NiO and $SiO_2$. The relative signal intensities would be modulated by the NiO particle sizes (*3, 30*) and the physical character of the support itself, especially the pore size (*31*). The spectral characteristics of NiO as given in Table 3 would nonetheless be present. As nickel silicate has been observed to form under certain coprecipitation conditions (*11*), it would not be surprising to find some interaction between the NiO and $SiO_2$ which would affect the catalyst's properties.

The two catalyst samples (C150-1-01 and C150-1-02, referred to as 1-01 and 1-02 henceforth) have quite similar spectra (Figs. 3 and 4). These spectra are quite distinct in both peak binding energy and spectral shape from those of NiO. The spectra resemble (in shape and binding energy) those of the $NiSiO_3$ standard sample most closely although the matchup is not perfect. The variation in peak widths also suggests that the systems being examined are not necessarily simple compounds of one type, specifically that the catalysts are not solely composed of $NiSiO_3$. Nonetheless, the agreement between the catalyst's spectra and the spectra of the $NiSiO_3$ sample is quite good, particularly when the uncertainty in the binding energies is considered. It may be definitely said that NiO, as characterized by the Ni $2p_{\frac{1}{2}}$ doublet peak, is not present in the surface regions.

An argon ion etching study was performed additionally on each sample. According to previous reports (*18, 19*), some forms of nickel are reduced by the bombardment of the surface with charged

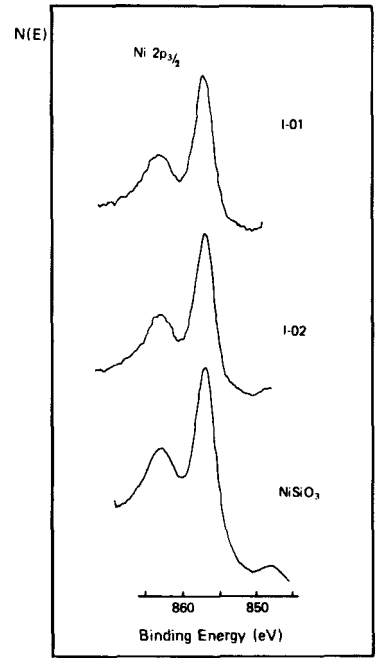


**Figure 3. The Ni $2p_{3/2}$ core level peak for the fresh (unreduced) catalysts and nickel silicate.**

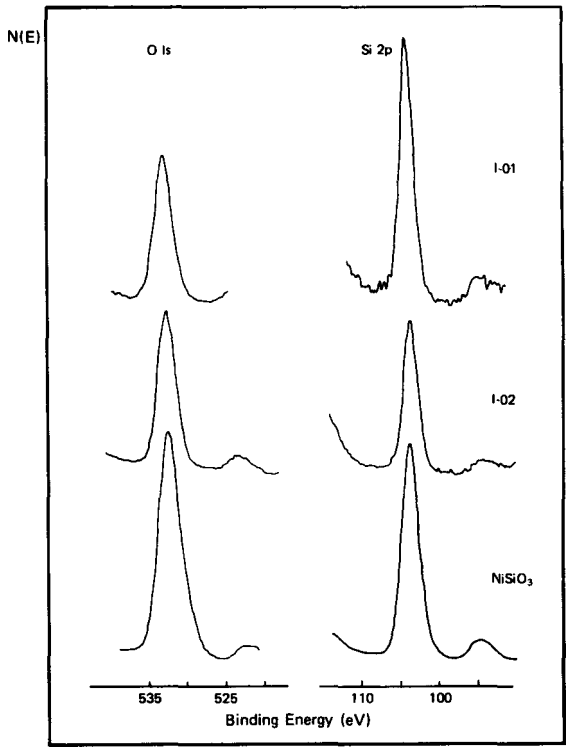


**Figure 4. The O 1s and Si 2p doublet core level peaks for the fresh catalysts and nickel silicate.**

energetic argon ions ($Ar^+$) as used in the etching process. The primary purpose of etching is to clean the surface by removing the exposed atoms on the surface thereby exposing the underlying material. However, nickel is reduced only for materials with a heat of formation of less than about 60 kcal/mole (*20*). This process may be used to further characterize the surface regions when the XPS spectra of two different chemical states of an atom are similar but where only one of the forms is reducible by argon ion etching.

The samples (in pellet form) were etched with a 2 kV Physical Electronics gun. The normal to the sample's surface was at a 30° angle to the axis of the incoming beam. A flow of research grade Ar giving a dynamic system pressure of $2 \times 10^{-5}$ Torr was established before etching was begun. An etching routine of 2 min (1 kV beam energy), 5 min (1 kV), and 28 min (1.5 kV) was performed sequentially on each sample with spectra recorded after each etch. The spectra recorded after the second and third etches are shown in Figs. 5 and 6. A repetition of the study at a later time gave similar results.

**Table 4. Catalyst Binding Energies and FWHM.***

| Sample | Ni $2p_{3/2}$ | Ni satellite splitting | O $1s_{1/2}$ | Si 2p |
|---|---|---|---|---|
| C150-1-01 | 857.0 (3.3) | 6.0 | 532.5 (2.8) | 103.5 (2.1) |
| C150-1-02 | 856.9 (3.1) | 5.9 | 532.5 (2.6) | 103.2 (2.1) |
| $NiSiO_3$ | 856.7 (3.8) | 6.0 | 532.5 (3.1) | 103.5 (2.4) |

*In electron volts.

The reduction of some nickel atoms to the metallic state is clearly seen for each sample. The amount of reduction, estimated from areas under the silicate and reduced nickel peaks measured with a planimeter using a linear baseline correction (*3*), is 45% for the 1-01 and 25% for the 1-02 catalyst. This difference in reduction is in agreement with that observed in Thermal Gravimetric Analysis

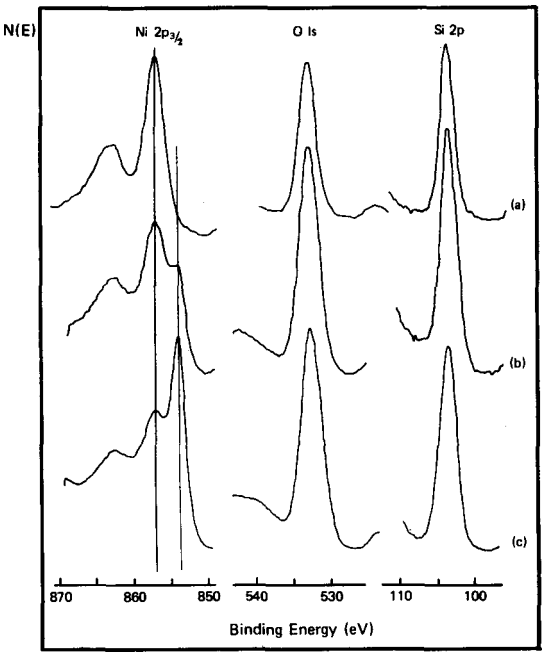


**Figure 5. Spectra for the C150-1-01 catalyst (unreduced): (a) unetched, (b) etched 7 minutes (total time) at 1-keV beam energy, (c) etched an additional 28 minutes at 1.5-keV beam energy.**

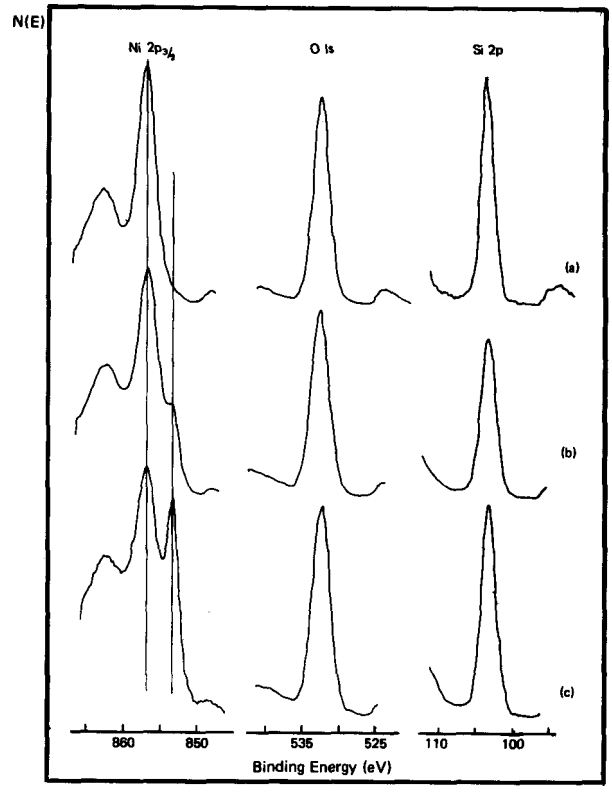


**Figure 6. Spectra for the C150-1-02 catalyst (unreduced): (a) unetched, (b) etched 7 minutes (total time) at 1-keV beam energy, (c) etched an additional 28 minutes at 1.5-keV beam energy.**

(TGA) studies of these samples (*32*). The reduction observed is less than that found for NiO when similarly treated. The occurrence of reduction for these samples is in agreement with the characterization of the surface by XPS as being primarily amorphous nickel silicate. An alternate form of nickel that could be indicated by XPS spectra, $Ni(OH)_2$, is not reduced by argon etching and hence is not the predominant form of nickel in the catalyst surfaces.

## DISCUSSION

The standard samples have sufficient characteristics (Table 3) to permit the different chemical forms of nickel to be distinguished. The fingerprint of NiO is of particular concern in this study. In other studies (*18–19*) of the nickel oxide system, two special features have been observed. The principal Ni $2p_{\frac{3}{2}}$ peak displays an unique doublet structure (splitting: 1.8 eV). No completely satisfactory explanation of this structure is known (*29*). This does not lessen its usefulness as an identifier of NiO. The O 1*s* spectrum is commonly found (*18, 19, 21, 23–28*) to consist of two peaks as shown in Figs. 1 and 2. Stoichiometric NiO has just the lower binding energy peak of the O 1*s* doublet (*18, 19*). The higher binding energy peak has been attributed to $Ni(OH)_2$ (*27*) and $Ni_2O_3$ (*18, 19, 26*). Both peaks of the doublet have similar depth profiles (*26*) indicating that the higher binding energy peak is not just a surface contaminant. This suggests that the higher binding energy peak is due to the presence of $Ni_2O_3$ at the surface of most commercially prepared samples in NiO. Care would need to be taken to eliminate the possible presence of $Ni(OH)_2$ when characterizing an unknown sample. This could be done using the Ni Auger spectrum (*18, 19*). Some of the ambiguity in characterization may be removed by the additional information obtained from argon ion etch-induced reduction of the samples. NiO and the $NiSiO_3$ sample are reduced by etching while $Ni(OH)_2$ is difficult to reduce. Hence, if a nickel compound (as in the catalysts) can be easily reduced by etching, it is unlikely that that compound is hydroxide. This capability has been used to clarify the characterization of the catalysts.

Some differences have been observed in the properties of the two catalysts that may be attributed to the different precipitation methods used to prepare them. The 1-02 catalyst is a "true" coprecipitated catalyst. The 1-01 catalyst, which was prepared with $SiO_2$ in a slurry with $Ni(NO_3)_2$, is not a coprecipitated catalyst in the same sense, but rather may be called a precipitated catalyst. The 1-01 catalyst preparation is thus an intermediate type between coprecipitation and

impregnation. Its properties (Table 1) and activity (*11*) are similar to those of the 1-02 catalyst, however.

The XPS spectra of the two catalysts indicate a similar chemical state (see below). The 1-01 sample charges up less than the 1-02 (2 vs 3.5 eV). The 1-01 sample is more readily reduced by argon etching than the 1-02. Bulk NiO reduces more readily than either, however. These reduction findings are paralleled in the TGA studies (*32*). It was also observed from analysis of the X-ray diffraction lines of NiO that the 1-01 catalyst sinters more rapidly than the 1-02 catalyst (*5, 32*). These results suggest that the nickel in the 1-01 catalyst is in a chemically more available form while the nickel in the 1-02 catalyst appears to be more stable regarding reduction and sintering. The coprecipitation method appears to lead to a catalyst in which more nickel has interacted with the support forming a more stable phase. The precipitation method used to prepare the 1-01 sample does, however, also lead to some nickel–silica interaction as indicated by the fraction of nickel not reduced at 400° (35% as compared with 60% for 1-02 and 0% for NiO). As it is possible to prepare an unreducible coprecipitated catalyst [due to the formation of the $NiSiO_3$ spinel (*11*)] it is reasonable to find a greater nickel–silica interaction in the 1-02 catalyst. That more than 80% of nickel in the catalysts could ultimately be reduced (at 500°C) shows that the interaction has not led to the formation of the $NiSiO_3$ spinel, however. This interaction, while hindering the reducibility of the nickel does give good stability and dispersion to the catalysts. The reducibility problem can be overcome by the higher metal content of the coprecipitated catalysts.

The reduction and sintering studies point toward a NiO–$SiO_2$ interaction of varying degrees of completeness in these two catalysts. The XPS spectra (Figs. 3 and 4) support this finding. The Ni $2p_{\frac{1}{2}}$ and O 1*s* spectra do not indicate NiO, but rather are similar to those for the $NiSiO_3$ sample both in binding energy and spectral shape. As the samples are pellets formed from the precipitate which is expected to be of reasonably homogeneous composition, we expected (and have found) that the spectra of the pellet surface also reflects the chemical composition of the interiors of the pellets.

This interpretation is in some conflict with the X-ray diffraction (XRD) spectra used to characterize the catalyst particle size (*5*). The diffraction spectra show lines due to NiO and none that are attributed to the $NiSiO_3$ spinel. A diffraction scan of the $NiSiO_3$ standard sample (calcined at 400°) did not show any lines at all. After being calcined at 1100°C for 20 hr lines due to NiO, $SiO_2$, and the $NiSiO_3$ spinel were observed. The XPS spectra of these samples before and after heating were essentially unchanged, however. This suggests that the $NiSiO_3$ present in the catalysts and the standard sample is basically amorphous in structure and that the core level XPS spectra of the $NiSiO_3$ spinel are similar to those of amorphous $NiSiO_3$, at least within the accuracy of the binding energy determinations for these samples.

However, a problem remains as to why NiO is not observed in the XPS spectra when it is readily visible in the XRD spectrum. In the reduction studies, it is found that some (30% for the 1-01 catalyst) of the nickel reduces almost immediately (at 400°C), while some (40%) of the nickel reduces more slowly, requiring 1 hr. The remainder of the nickel can only be fully reduced at 500°C. This behavior is attributed to, respectively, the presence of easily accessible NiO, less accessible NiO, and amorphous $NiSiO_3$. Any unreducible nickel would be due to the $NiSiO_3$ spinel. While the spinel was not

observed in these $Ni/SiO_2$ catalysts, it has been observed in another coprecipitated $Ni/SiO_2$ catalyst (*11*) and in coprecipitated $Ni/Al_2O_3$ catalysts (*33*). Hence, the NiO in the 1-01 and 1-02 catalysts is present either within pores in the $SiO_2$ support or is covered by an amorphous $NiSiO_3$ overlayer, as NiO in these locations would not be visible through XPS, but would be seen by XRD.

It is possible that small NiO particles dispersed on a silica support do not display the characteristic Ni $2p_{\frac{1}{2}}$ doublet structure if the doublet's origin requires a large-scale order that is not present in a small (20 Å) particle. However, we note that the spectra of a NiO on $MgSiO_3$ catalyst which was prepared similarly to the 1-01 catalyst do display the characteristic NiO spectra (*33*). As the porosity of the $MgSiO_3$ support is similar to that of the $SiO_2$ in the 1-01 catalysts, the appearance of the singlet Ni $2p_{\frac{1}{2}}$ peak in the one case and not the other is due to changes in the chemical form of the nickel and not to the small particle size.

## CONCLUSIONS

A study of the spectral shapes and binding energies of a series of nickel compounds and commercial coprecipitated nickel on silica catalysts has shown that the surface regions of the fresh (unreduced) catalysts are composed primarily, but not solely of amorphous $NiSiO_3$ with some NiO particles present either within the pores of the support or covered by a $NiSiO_3$ layer. A large fraction of the nickel present has interacted with the silica support which gives the catalysts good thermal stability and activity. The interaction is more complete in the coprecipitated 1-02 catalyst than the precipitated 1-01 catalyst, which affects the stability and reducibility of these materials accordingly.

## ACKNOWLEDGEMENTS

Support of this project was provided by the U.S. Department of Energy through Contract No. Ex-76C-01-2229, and the Institute for Mining and Minerals Research, University of Kentucky.

Catalyst samples and useful technical information were provided by A. L. Hausberger, W. A. Kustes, and M. Miller, United Catalysts, Inc., Louisville, Kentucky.

The assistance and helpful advice of R. J. DeAngelis, W. G. Lloyd, and T. Rebagay are also acknowledged.

## REFERENCES

1. Mills, G. A., and Steffgen, F. W., *Catal Rev.* **8**, 159 (1973).
2. Lom, W. L., and Williams, A. F., "Substitute Natural Gas." Wiley, New York, 1976.
3. Shalvoy, R. B., and Reucroft, P. J., *J. Electron Spectrosc.* **12**, 351 (1977).
4. Kidron, A., DeAngelis, R. J., and Reucroft, P. J., *J. Appl. Phys.* **48**, 5296 (1977).
5. Ganesan, P., Kuo, H. K., Saavedra, A., and DeAngelis, R. J., *J. Catal.* **52**, 310 (1978).
6. Siegbahn, K., Nordling, C., Fahlman, A., Nordbert, R., Hamrin, K., Hedman, J., Johansson, G., Bergmark, T., Karlsson, S. E., Lingren, I., and Lindberg, B., ESCA: Atomic, Molecular and Solid State Structure Studied by Means of Electron Spectroscopy, *Nova Acta Regiae Soc. Sci. Upsal. (IV)* **20**, Almquist and Wiksells, Uppsala (1967).
7. Delgass, W. N., Hughes, T. R., and Fadley, C. S., *Catal. Rev.* **4**, 179 (1970).
8. Brinen, J. S., *J. Electron. Spectrosc.* **5**, 377 (1974).
9. Ng, K. T., and Hercules, D. M., *J. Phys. Chem.* **80**, 2094 (1976).
10. Penn, D. R., *J. Electron Spectrosc.* **9**, 29 (1976).
11. Hausberger, A. L., Atwood, K., and Knight, C. B., *Adv. Chem. Ser.* **146**, 47 (1975).
12. Dianis, W. P., and Lester, J. E., *Anal. Chem.* **45**, 1416 (1973).
13. Madey, T. E., Wagner, C. D., and Joshi, A., *J. Electron Spectrosc.* **10**, 359 (1977).
14. Shalvoy, R. B., Fisher, G. B., and Stiles, P. J., *Phys. Rev. B* **15**, 1680 (1977).

*15.* Powell, C. J., personal communication.
*16.* Bailar, J. C., Emeleus, H. J., Nyholm, R., and Trotman-Dickinson, A. F., "Comprehensive Inorganic Chemistry." Pergamon, Oxford, 1973.
*17.* Scofield, J. H., *J. Electron Spectrosc.* **8**, 129 (1976).
*18.* Kim, K. S., and Davis, R. E., *J. Electron Spectrosc.* **1**, 251 (1972/73).
*19.* Kim, K. S., and Winograd, N., *Surface Sci.* **43**, 625 (1974).
*20.* Kim, K. S., Battinger, W. E., Amy, J. W., and Winograd, N., *J. Electron. Spectrosc.* **5**, 351 (1974).
*21.* Hirokawa, K., Honda, F., and Oku, J., *J. Electron Spectrosc.* **6**, 333 (1975).
*22.* Holm, R., *Appl. Phys.* **9**, 217 (1976).
*23.* Holm, R., and Storp, S., *J. Electron Spectrosc.* **8**, 139 (1976).
*24.* Matienzo, L. J., Yin, L. I., Grim, S. O., and Swartz, W. E., *Inorg. Chem.* **12**, 2762 (1973).
*25.* McIntyre, N. S., and Cook, M. G., *Anal Chem.* **47**, 2208 (1973).
*26.* Evans, S., Pielaszek, J., and Thomas, J. M., *Surface Sci.* **56**, 644 (1976).
*27.* Haber, J., Stoch, J., and Ungier, L., *J. Electron Spectrosc.* **9**, 459 (1976).
*28.* Wertheim, G. K., and Hufner, S., *Phys. Rev. Lett.* **28**, 1028 (1972).
*29.* Oku, M., and Hirokawa, K., *J. Electron Spectrosc.* **10**, 103 (1977).
*30.* Briggs, D., *J. Electron Spectrosc.* **9**, 487 (1976).
*31.* Brinen, J. S., and Schmitt, J. L., *J. Catal.* **45**, 274 (1976).
*32.* Reucroft, P. J., Bradley, E. B., DeAngelis, R. J., and Sargent, G. A., "Surface Structure and Mechanisms of Gasification Catalyst Deactivation," Quart. Rep. No. 5, Feb. 1, 1977 to April 30, 1977 and Quart. Rep. No. 9, Feb. 1, 1978 to April 30, 1978, DOE Contract No. EX-76-C-01-2229.
*33.* Shalvoy, R. B., Davis, B. H., and Reucroft, P. J., to be published.

# Particle Size Distribution Function of Supported Metal Catalysts by X-ray Diffraction

**P. Ganesan and H. K. Kuo**
Institute for Mining and Minerals Research
Kentucky Center for Energy Research Laboratory
Lexington, Kentucky 40583

**A. Saavedra**
Instituto Militar de Engenharia
Pca. Gen. Tiburcio, ZC 20,000, Urca
Rio de Janeiro, Brazil

and

**R. J. DeAngelis**
Department of Metallurgical Engineering and
Materials Science
College of Engineering
University of Kentucky
Lexington, Kentucky 40506

## ABSTRACT

An X-ray diffraction method which is capable of determining average particle size, microstrain, and the particle distribution function existing in crystalline materials is presented. The method is based on the analysis of a single X-ray diffraction profile. Results obtained on coprecipitated nickel oxide on alumina- and silica-supported catalytic materials indicate that appreciable strains exist. It is suggested that the strains present in NiO could be due to the pressure developed in the small particles to balance the surface tension forces and the distortion produced by the deformation of face-centered cubic structure into a rhombohedral form. The changes in particle size distributions observed during sintering determined from three catalytic materials provide evidence that particle growth takes place by atomic migration mechanism. In one material the particle growth during sintering appears to be controlled predominantly by crystallite migration and coalescence. The sintering behavior appears to be controlled by the extent of the bimodal character of the initial distribution function and the average particle size in the as-received condition.

## INTRODUCTION

There are a number of experimental techniques available to characterize the average crystallite size and crystallite size distributions of metal-supported catalysts (*1*). Selective gas adsorption techniques give only the average crystallite size and require prior knowledge of adsorbate–metal surface interaction (*2*). Small-angle X-ray scattering has the practical difficulty that the micropores present in the supports also act as scattering centers and interfere with

the scattering from metal crystallites. However, this difficulty has been effectively eliminated by filling the pores with a liquid of electron density equivalent to that of the support (*3*, *4*). Transmission electron microscopy is direct and therefore more reliable, but involves the tedious examination of many specimens in order to insure that the sample is a true representative of the bulk catalyst (*5*). Magnetic methods described in detail by Selwood (*6*) have been applied to some metals and alloys, e.g., Ni, CO, and Fe. X-Ray line-broadening investigations of supported catalysts have been limited to finding the average crystallite size from integral breadth or half-intensity breadth of a diffraction profile. A few investigations have been reported where the crystallite size distribution was determined; however in these studies the lattice strain contribution to the X-ray line broadening was neglected or assumed to be zero (*7–9*).

The major objective of this work is to develop a reliable method to measure the particle size distribution function of a supported metal catalyst using X-ray diffraction profile shape analysis. Distribution data of this type are required to test the existing catalyst sintering models (*10*, *11*). The existing method of analysis, following Warren and Averbach (*12*), requires two orders of the diffraction profile in order to separate the particle size and strain contributions to the broadening of the X-ray line. In the case of supported metal catalysts, due to the difficulty of making satisfactory intensity measurements on the higher order reflections, it is very difficult, if not impossible, to obtain two orders of a (hkl) profile. Having only one order of a profile necessitates use of the assumption that the lattice strains are zero in order to compute the particle size distribution function.

There has been considerable work reported on the structure and stability of small clusters of atoms which indicates that the most stable particle consists of tetrahedron units of atoms existing in a multiple twinned array (*13*, *14*). This concept finds some experimental support from electron microscope observations made on some face-centered cubic metals which show images containing internal strain contrast, which has been interpreted as being a result of the existence of multiply twinned structures (*15*, *16*). In view of this, it is clear that the strain contribution to X-ray line broadening could be significant if the particle sizes are reasonably large and the lattice strains are appreciable. Thus one has to be careful in making zero strain assumption when using X-ray diffraction profile shape analysis in investigations on small particles. In addition the measurements of strains are important if the correlation between the lattice strains and specific activity of nickel catalysts, which has been suggested to exist (*17*), is to be established.

In this paper an approximate method of determining the particle size distribution function from a single X-ray diffraction profile from a material containing strains is reported. In this method the zero strain assumption is not required. Results obtained on coprecipitated nickel oxide on alumina and silica indicate that the strains present are very significant and must be taken into account. This paper contains a description of the X-ray diffraction method developed for investigating catalyst-type materials along with preliminary results obtained on the unreduced catalysts. Previous work by Shephard (*8*) on the alumina-supported nickel–nickel oxide catalysts indicates that the crystallite size of the nickel in the reduced catalysts closely follows that of the corresponding oxide. Therefore it is expected that the results obtained on the unreduced catalysts will correlate with the

particle size distribution functions existing in the reduced catalysts. Investigations to confirm this are currently underway.

## THEORY

### Single Profile Analysis Technique

The single diffraction profile technique is based on the work of Gangulee (*18*) and Mignot and Rondot (*19*). The Stokes corrected cosine coefficients (*20*) from a (hkl) diffraction profile are composed of two components, a size coefficient $A_L^S$ and a microstrain or distortion coefficient $A_L^D$; their relationship can be expressed as:

$$A_L = A_L^S \cdot A_L^D, \tag{1}$$

where $A_L$ are the Stokes corrected cosine coefficients at a given $L$, and $L$ is $n\delta$. Here $n$ is the harmonic number and $\delta$ is a distance normal to the diffracting planes. Defining a variable $X = 1/D_e$, where $D_e$ is the effective diffracting particle size; for small values of $n$ and $\delta$ where the values of $L$ are small and such that the number of diffracting domains in the specimen with this dimension is insignificant, the particle size term of the Fourier coefficients can be expanded as:

$$A_L^S = (1 - LX). \tag{2}$$

The distortion coefficients can be expanded for small values of $n$, as:

$$A_L^D = (1 - KL^2\langle \epsilon_L^2 \rangle), \tag{3}$$

where $K$ is $2\pi^2/d^2$, $d$ is the (hkl) planar spacing, and $\langle \epsilon_L^2 \rangle$ is the mean square of the microstrain averaged over all distances in the diffracting specimen spaced $L$ apart.

Letting $Y_L = K\langle \epsilon_L^2 \rangle$, the small $L$ value cosine coefficient can be written as:

$$A_L = (1 - LX)(1 - Y_L L^2). \tag{4}$$

Equation (4) can be solved for $X$ if the functional form of $Y_L$ is known. In this way the particle size can be separated from the microstrain terms. The problem then resolves to determination of the most suitable forms of $Y_L$. Assuming the form of the strain function to be (*21*)

$$Y_L = (C/L)\delta K \tag{5}$$

leads to an expression for $A_L$ of

$$A_L = 1 - L(X + C\delta K) + L^2(XC\delta K). \tag{6}$$

The expression for $A_L$ has the form of a second-order polynomial in $L$. Now defining a polynomial of second degree:

$$R_L = a_0 + a_1 L + a_2 L^2, \tag{7}$$

the coefficients of which, by comparing with Eq. (6), are:

$$a_0 = 1; \quad a_1 = -(X + C\delta K); \quad \text{and} \quad a_2 = XC\delta K. \tag{8}$$

From these relations it follows that

$$\begin{aligned} X &= \tfrac{1}{2}(-a_1 \pm (a_1^2 - 4a_2)^{\frac{1}{2}}), \\ D_e &= 1/X, \\ C &= a_2/X\delta K, \\ \langle \epsilon_L^2 \rangle &= (C/L)\delta. \end{aligned} \tag{9}$$

The determination of the coefficients $a_0$, $a_1$, and $a_2$ can be made by solving the system of equations:

$$\begin{aligned} \sum_t A_L &= a_0 N + a_1 \sum_t L + a_2 \sum_t L^2, \\ \sum_t LA_L &= a_0 \sum_t L + a_1 \sum_t L^2 + a_2 \sum_t L^3, \\ \sum_t L^2 A_L &= a_0 \sum_t L^2 + a_1 \sum_t L^3 + a_2 \sum_t L^4, \end{aligned} \tag{10}$$

where $N$ is the number of coefficients used in the evaluation, $N \geq 4$; $t$ is an integer satisfying $t = (L_N - L_0)/(L_1 - L_0)$, where $L_0$ is the distance corresponding to the initial coefficient used in the computation of Eq. (10).

The best solutions to Eq. (10) are selected from four criteria: (i) $a_0 \approx 1$; (ii) $a_2 > 0$, since $a_2$ from Eqs. (6) and (7) can be

written as $d^2A_L/dL^2$ which must be positive; (iii) $\sum_i (R_L - A_L)/N$ is a minimum; (iv) $(dA_L/dL)_{L\to 0} = a_1 = -(X + C\delta K)$. After the best solution to Eq. (10) is determined it is a simple process to calculate the average coherent diffracting particle size $D_e$ and lattice mean square strain $\langle \epsilon_L^2 \rangle$ by employing Eq. (9).

### Particle Size Distribution Function

While single profile analysis provides a convenient method to calculate lattice microstrain it is important to note that the particle size distribution function cannot be obtained by this method alone, since from Eq. (2), $d^2A_L^S/dL^2$ reduces to zero. However by employing the usually accepted small $(L/d)$ approximation it is possible to obtain the particle size distribution function by combining both single profile and multiple order analysis as follows. Although this approach does contain limitations, it is a major improvement over the zero strain approximation.

The expression for the relationship between the particle size and distortion coefficients in the Warren–Averbach method (*12*) is given by

$$A_L = A_L^S \langle \cos 2\pi L/d\epsilon_L \rangle. \qquad (11)$$

For small values of $L/d$ the argument of the microstrain term is small and, using the approximations $\langle \cos X \rangle = 1 - \langle X^2 \rangle/2$ and $1 - X \simeq \exp(-X)$, Eq. (11) can be written as

$$A_L = A_L^S \exp -2\pi L^2/d^2 \langle \epsilon_L^2 \rangle. \qquad (12)$$

This method of separation of particle size and microstrain term makes no assumption of the nature of strains and Eq. (12) is good only for small values of $L/d$. However it can be shown (*22*) that Eq. (12) is exact for all values of $L/d$ if the microstrain distribution is Gaussian. The distribution of strains at a given $L$ has been shown to be close to Gaussian (*23–25*), but not the variation of $\langle \epsilon_L^2(\mathrm{hkl}) \rangle^{\frac{1}{2}}$ with $L$.

Now it is possible to obtain the particle size coefficient $A_L^S$ from Eq. (12) by substituting the values for mean square strain $\langle \epsilon_L^2 \rangle$ obtained from single profile analysis [Eq. (9)]. The particle size distribution function, $P(L)$, can then be obtained from the second derivative of $A_L^S$ with respect to $L$ (*22*), that is,

$$P(L) = \frac{d^2A_L^S}{dL^2} \cdot \mathrm{Dc}. \qquad (13)$$

The particle size distribution data can be employed to calculate the average particle size using two relationships:

$$\bar{D} = \sum_L LP(L)\Delta L \qquad (14a)$$

$$\bar{D}_1 = \left[ \sum_L \frac{1}{L} P(L)\Delta L \right]^{-1}, \qquad (14b)$$

where $P(L)$ is the value of the distribution function at the size $L$ normalized such that $\int P(L)dL = 1$. $\bar{D}$ is the volumetric mean particle size and $\bar{D}_1$ is the average value of the thickness of the particle normal to the (hkl) reflecting planes (*26*).

The complete X-ray diffraction profile shape analysis which involves the calculation of Stokes corrected coefficients $A_L$, particle size coefficients $A_L^S$, and particle size distribution function $P(L)$ has been computerized. Figure 1 contains a schematic of the computer program.

## EXPERIMENTAL PROCEDURE

The description of the catalytic materials used in this investigation, which were supplied by Catalysts and Chemicals Inc., is given in Table 1. Pellets of the four unreduced catalysts were ground into powders and were pressed at 40,000 psi into pellets of 1.25 in. diameter and approximately 0.25 in. thick.

A Picker diffractometer and a Cu-target x-ray tube were used for the dif-

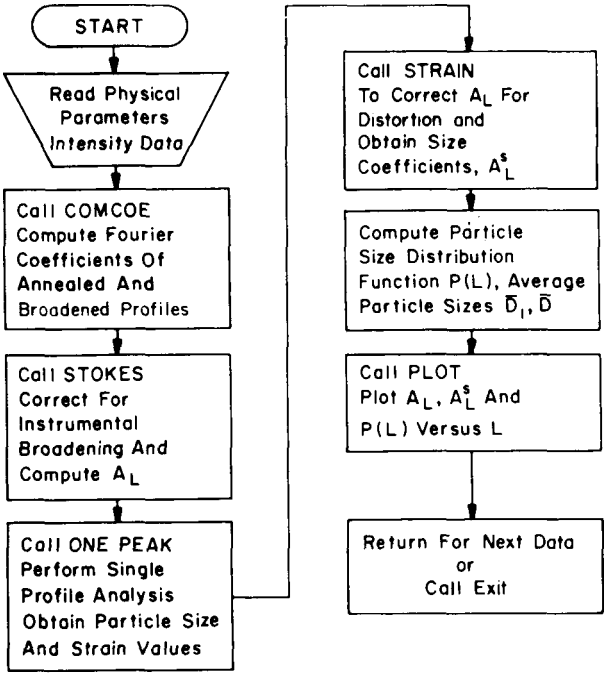


**Figure 1. Block diagram indicating major elements of the computer program.**

fraction runs. A diffracted beam monochromator was constructed employing a single bent grain oriented graphite monochromator crystal. This eliminated most of the background intensity outside the diffraction lines. A proportional detector with pulse height analyzer was used for the detection system.

X-Ray data describing the X-ray diffraction profile from the four unreduced catalysts were collected in the as-received condition and after sintering for 1 hr at 900 or 1000°C. Due to extremely small particle sizes of the catalysts in the as-received condition (25 to 40 Å) the tails of the (111), (200), (222), and (400) profiles of NiO overlapped with a neighboring profile. Hence data on the (220) profile from the unreduced catalysts were collected. In addition, NiO is rhombohedral at room temperature and the (220) line is a single line. The data were collected by step scanning in 1/30 degree steps counting 500 seconds per step. The standard used to correct the data for instrumental broadening was a pure chemical-grade NiO which was sintered in the pellet form for 4 hr at 1300°C.

**Table 1. Physical and Chemical Properties of Catalytic Materials.**

| | Catalyst No. | | | |
|---|---|---|---|---|
| | C-150-1-01 | C-150-1-02 | C-150-1-03 | C-150-4-03 |
| Ni (%) | 51.7 | 46.6 | 47.0 | 55.6 |
| C (%) | 2.94 | 2.13 | 5.84 | 2.70 |
| Cl (%) | – | – | 0.006 | 0.013 |
| S (%) | 0.06 | 0.04 | 0.09 | 0.09 |
| Surface area ($m^2/g$) | 211 | 301 | 202 | 177 |
| Pore volume ($cm^3/g$) | 0.34 | 0.58 | 0.328 | 0.514 |
| Density ($g/cm^3$) | 1.05 | 0.88 | 1.01 | 0.93 |

## RESULTS

There are several methods to characterize the crystallite size by X-ray diffraction. The simplest is the determination of the effective particle dimension from the half-breadth of the profile, $D_{\text{half-breadth}}$, by the Scherrer formula

$$D_{\text{half-breadth}} = K\lambda/\beta_D \cos\theta, \qquad (15)$$

where $\beta_D$ is the half-breadth of the profile corrected for instrumental broadening, $\lambda$ is the wavelength, $\theta$ is the diffraction angle, and $K$ is a constant close to 0.9.

The particle size can also be determined from the initial slope of the Stokes corrected coefficients (in this method the strains in the material are assumed to be zero). In this case the particle size is given by (*28*):

$$D_{\text{coefficient}} = [-(dA_L/dL)_{L\to 0}]^{-1}. \qquad (16)$$

The strain-corrected effective particle size obtained employing the single profile analysis technique [Eq. (9)] has been designated as $D_{\text{one peak}}$. The NiO particle sizes in catalytic materials determined by the above methods, together with the values of $\bar{D}_1$, $\bar{D}$, and $D_{\max}$ determined from particle size distribution as defined earlier, are reported in Table 2.

The particle sizes determined from the half-breadth of the diffraction profile are

Table 2. Particle Sizes and Microstrains of Nickel Oxide Catalyst Materials as Measured by Various X-Ray Diffraction Techniques.

| Catalyst No. | $D_{half\text{-}breadth}$[a] (Å) | $D_{coefficient}$[b] (Å) | $D_{one\ peak}$[c] (Å) | $\bar{D}_1$[d] (Å) | $\bar{D}$[e] (Å) | $D_{max}$[f] (Å) | Microstrain $[(\epsilon^2\ 20\ Å)^{1/2} \times 10^2]$ |
|---|---|---|---|---|---|---|---|
| C-150-1-01 Silica[g] | 28.8 | 20.8 | 20.4 | 17.6 | 18.3 | 18.0 | 0.40 |
| C-150-1-02 Silica[g] | 37.3 | 21.0 | 22.0 | 19.7 | 21.3 | 18.0 | 0.60 |
| C-150-1-03 Alumina[g] | 24.5 | 18.4 | 19.5 | 17.9 | 20.0 | 16.0 | 0.57 |
| C-150-4-03 Alumina[g] | 38.5 | 24.5 | 25.8 | 22.9 | 25.6 | 21.0 | 0.77 |
| C-150-1-01 (1000°C, 1 hr)[h] | 96.1 | 54.0 | 48.0 | 45.1 | 62.2 | 48.0 | 0.23 |
| C-150-1-02 (1000°C, 1 hr)[h] | 67.1 | 46.0 | 50.0 | 41.6 | 53.4 | 44.0 | 0.32 |
| C-150-1-03 (1000°C, 1 hr)[h] | 120.8 | 78.0 | 72.0 | 72.3 | 92.5 | 50.0 | 0.39 |
| C-150-4-03 (500°C, 1 hr)[h] | 39.8 | 26.0 | 26.0 | 25.9 | 27.6 | 26.0 | 0.72 |
| C-150-4-03 (900°C, 1 hr)[h] | 151.3 | 91.0 | 88.5 | 69.9 | 93.0 | 80.0 | 0.19 |
| C-150-4-03 (1000°C, 1 hr)[h] | 181.7 | 103.0 | 103.8 | 99.5 | 127.3 | 110.0 | 0.36 |

[a] Effective particle size from half-breadth of the profile by Scherrer formula [Eq. (15)].

[b] Particle size from the initial slope of the Stokes corrected coefficients [Eq. (16)].

[c] Effective particle size from single profile analysis technique [Eq. (9)].

[d] $\bar{D}_1 = [\Sigma_L (1/L) P(L)\ \Delta L]^{-1}$.

[e] $\bar{D} = \Sigma_L\ L\ P(L)\ \Delta L$.

[f] $D_{max}$ is the value of the crystallite size having maximum probability.

[g] Support.

[h] Heat treatment.

from 1.50 to 2.0 times greater than those obtained from the coefficients ($D$ coefficient), single-peak analysis, and $D$ one peak, and the distribution function ($\bar{D}_1$ and $\bar{D}$) reflects the extent of the approximations involved in the half-breadth approach. The accuracy with which the Scherrer equation can be applied is limited by the uncertainties in $K$ and the size distribution effects in modifying the breadth and shape of a diffraction line. For these reasons Klug and Alexander (*29*) point out that the effective diameter obtained by this method may have an absolute accuracy of only 50%. As expected the $\bar{D}_1$ particle size values are always smaller than $\bar{D}$ and the ratio of $\bar{D}_1/D$ decreases as the particle size distribution function becomes broader (*26*).

Attempts at the independent determination of the average particle size of the unreduced catalyst form by chemisorption are not possible because hydrogen does not adsorb on nickel oxide. However, the particle sizes obtained by the X-ray diffraction technique on reduced nickel catalysts were found to agree very well with those obtained from the surface area mea-

surements by hydrogen chemisorption (*27*).

The particle size distribution functions obtained from the C-150-4-03 (alumina supported) unreduced catalyst in the as-received and sintered conditions are shown in Fig. 2. These data indicate that sintering at 900 and 1000°C causes nickel oxide particles to grow rapidly and also produces a broadening of particle size distribution. The effect of sintering at 500°C in terms of particle growth is small but the particle size distribution becomes sharper. The same data are plotted in Fig. 3 with the particle size normalized by dividing it by $D_{max}$, the value of the crystallite size having maximum probability density. The evidence of the formation of particles smaller than the initial minimum particle size is more apparent in Fig. 3 as compared to Fig. 2. Figures 4–6 show similar plots for catalysts C-150-1-01, C-150-1-02, and C-150-1-03.

The values of the lattice microstrain existing in the unreduced catalysts in the as-received and sintered conditions, obtained by the single profile analysis method, are reported in Table 2. These results indicate that the strains present in the supported metal catalysts are of significant magnitude and the strains tend to decrease upon sintering.

The effect of zero strain assumption on the size distribution function was evaluated by determining the distribution functions from both $A_L$ and $A_L^S$. The difference between these are clearly demonstrated in Figs. 7 and 8. In the sintered condition, even though the strains are lower (see Table 2) when compared to the as-received sample, the effect of the microstrain on the X-ray line broadening and hence on the size distribution function is more pronounced.

## DISCUSSION

The particle size distribution functions obtained for these catalysts are comparable to those obtained for similar catalysts by others (*8*, *30*, *31*). The observed particle size distribution functions are generally consistent with both the atomic migration (*11*) and the particle coalescence models (*32*) of sintering. Because the two models predict many similar changes in the particle size distribution functions it has been difficult to obtain unambiguous data characteristic of one particular model. For in-

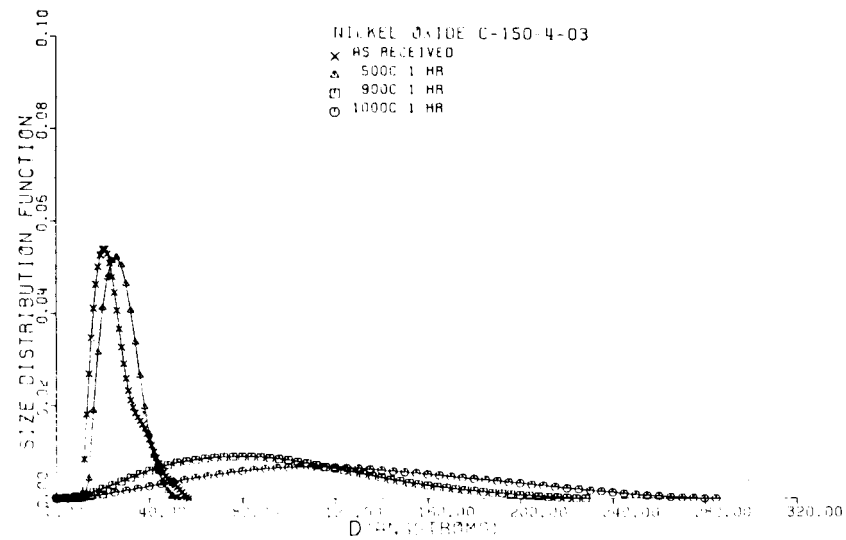


**Figure 2. Particle size distribution functions of as-received and sintered NiO catalyst C-150-4-03.**

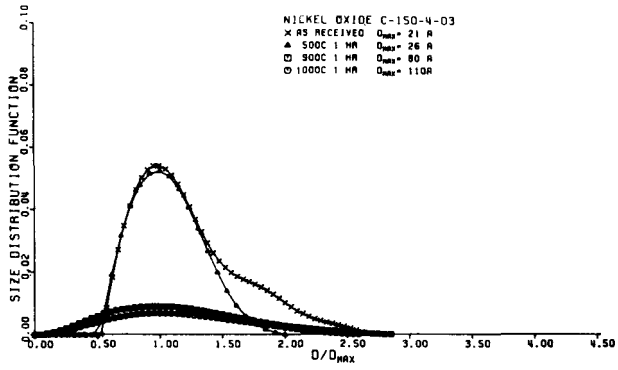


**Figure 3. Particle size distribution functions of as-received and sintered NiO catalyst C-150-4-03 normalized by dividing D by $D_{max}$. The values of $D_{max}$ are indicated.**

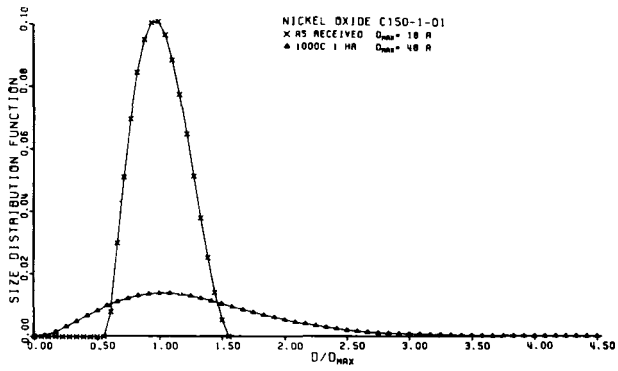


**Figure 4. Particle size distribution functions of as-received and sintered NiO catalyst C-150-1-01 normalized by dividing D by $D_{max}$. The values of $D_{max}$ are indicated.**

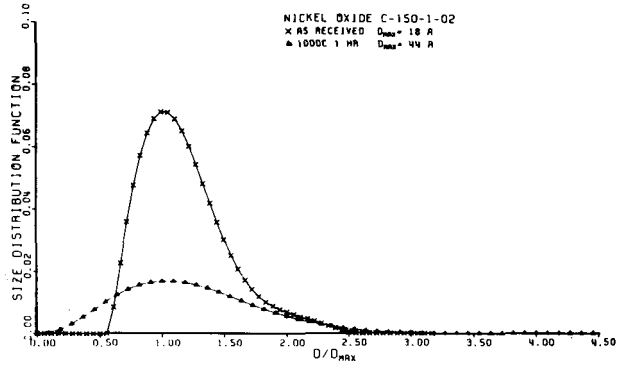


**Figure 5. Particle size distribution functions of as-received and sintered NiO catalyst C-150-1-02 normalized by dividing D by $D_{max}$. The values of $D_{max}$ are indicated.**

stance the development of the tails on the large diameter side of the distribution function can be reconciled with both models (*33*, *34*). However, the formation of a significant tail in the particle size distribution function in the small particle size range (e.g., see Figs. 3–5) suggests strongly that the atomic migration mechanism is operating (*11*). All of the changes in particle size distribution functions observed on all catalysts, except on C-150-1-03, provide evidence that the atomic migration mechanism is operative.

The behavior of the particle size distribution function in C-150-1-03 catalyst appears to indicate that a coalescence mechanism was operative. The pronounced bimodal character of the distribution function and the initial smaller particle size of the as-received material would tend to promote particle growth by coalescence as suggested by Wynblatt and Gjostein (*35*). This is also consistent with the behavior of alumina-supported nickel catalysts reported by Richardson and Desai (*30*). Assuming the particle growth by coalescence to predominate, the bimodal character would tend to be preserved during sintering as observed for this case.

In the case of C-150-4-03 catalyst the particle size is substantially larger in the as-received material. This would tend to inhibit coalescence and favor atomic migration. The sintering behavior of this catalyst has all the characteristics associated with the atomic migration mechanism. The fact that the low-temperature sintering of this material produces a sharper distribution is rather interesting and needs further investigation. If this phenomenon occurs generally, then low-temperature pretreatment of the catalyst prior to reduction could reduce the rate of sintering after the catalyst has been put into service in methanation.

The presence of large lattice strains in nickel oxide brings out the importance of

separating the strain component of X-ray line broadening because it could be an important consideration in catalysis activity and, by assuming the strains to be zero, could lead to as high as a 25% error in the estimation of average particle size. While it is difficult to pinpoint the reason for the presence of microstrains in these catalysts, several possibilities which could cause these strains will be given.

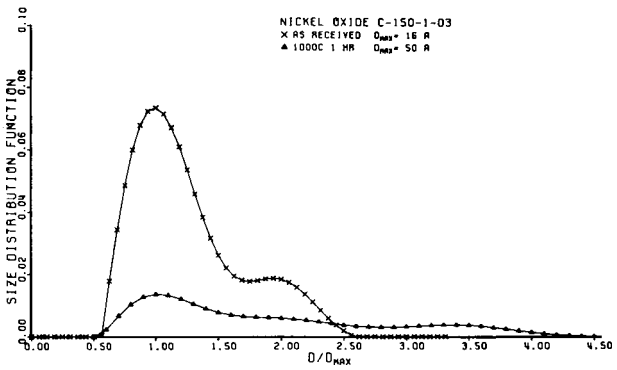


**Figure 6. Particle size distribution functions of as-received and sintered NiO catalyst C-150-1-03 normalized by dividing D by $D_{max}$. The values of $D_{max}$ are indicated.**

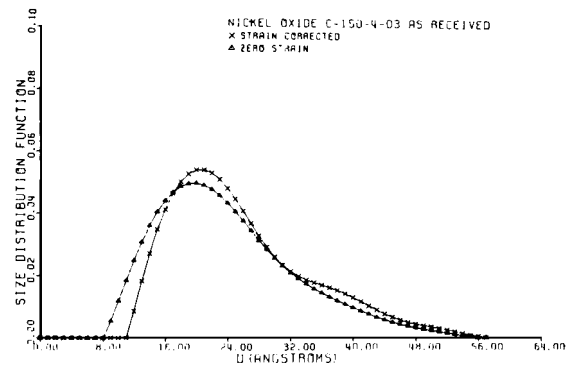


**Figure 7. Particle size distribution functions in the as-received NiO catalyst C-150-4-03 obtained using zero strain and strain-corrected conditions.**

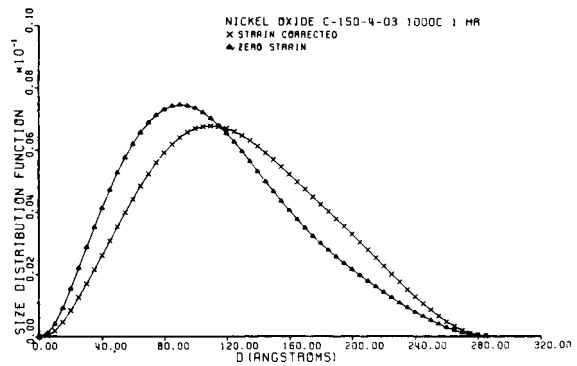


**Figure 8. Particle size distribution functions in the NiO catalyst C-150-4-03, sintered at 1000°C for one hour, obtained using zero strain and strain-corrected conditions.**

If the surface to volume ratio of small particles is very high, an internal pressure might develop in these particles which is inversely proportional to the particle radius. This pressure that develops to balance the surface tension forces would lead to the creation of internal strains. Based on a minimum energy configuration Hoare and Pal (*13*) have shown that certain nonlattice growth schemes showing tetrahedral, pentagonal, and icosahedral symmetry are appreciably more stable than microcrystallites based on face-centered cubic (fcc) structures. Allpress and Sanders (*14*) have shown that, if complex structures such as those mentioned above were formed from units of a regular tetrahedron with an undistorted fcc structure bounded by (111) faces, the complete particles would contain gaps due to misfit between adjoining units. Electron microscope images of small particles (*16*, *36*) reveal no dislocations or faults but do show some strain contrast. These observations would indicate that the misfit is distributed throughout the particle by a relaxation of the fcc structure of each unit (*14*). Allpress and Sanders (*14*) have shown that the deviation from ideal fcc structure is more pronounced for decreasing particle size. This is attributed to the proportionally higher number of the surface atoms in small crystallites which have less than the maximum number, 12, of nearest neighbors. This would explain the decrease of strains upon sintering, since as the crystallite size increases the structure would tend to be more toward ideal face-centered cubic.

The strains present in NiO could also be due to the deformation of the face-centered cubic structure into a rhombo-

hedral form as reported by Rooksby (*37*). At the present time we can only speculate that the strains present in these materials could be due to the pressure developed in the small particles to balance the surface tension forces and/or the distortion produced by rhombohedral deformation of face-centered cubic structure. The reduction of strains upon sintering and the presence of an appreciable amount of strains even after sintering are consistent with either of these possibilities.

## CONCLUSIONS

(i) By an extension of a diffraction method based on the analysis of a single X-ray line profile it is now possible to obtain the particle size distribution function corrected for strain broadening. (ii) The particle size distribution function of NiO-supported catalysts broadens upon sintering for 1 hr at 900 and 1000°C. The average particle size increases and there is evidence of formation of particles smaller than the initial minimum particle size. (iii) The mean square microstrains that exist in small NiO particles are appreciable and the strain correction has a greater effect on the particle size distribution function as the average particle size increases.

## ACKNOWLEDGEMENTS

This research was sponsored by the Institute for Mining and Minerals Research through Contract No. PD 18 and by the Energy Research and Development Agency through Contract No. E (49-18) 2229.

## REFERENCES

1. Whyte, Jr., T. E., *Catal. Rev.* **8**, 117 (1973).
2. Muller, J., *Rev. Pure Appl. Chem.* **19**, 151 (1969).
3. Gunn, E. L., *J. Phys. Chem.* **62**, 928 (1958).
4. Whyte, Jr., T. E., Kirklin, P. W., Gould, R. W., and Heinemann, H., *J. Catal.* **25**, 407 (1972).
5. Adams, C. R., Benesi, H. A., Curtis, R. M., and Meisenherimer, R. G., *J. Catal.* **1**, 336 (1962).
6. Selwood, P. W., "Adsorption and Collective Paramagnetism," p. 46. Academic Press, New York, 1962.
7. Pausescu, P., Manaila, R., and Popescu, M., *J. Appl. Crystallogr.*, 7, 281 (1974).
8. Shephard, F. E., *J. Catal.* **14**, 148 (1969).
9. Coenen, J. W. E., and Linsen, B. G., "Physical and Chemical Aspects of Adsorbents and Catalysts," (B. G. Linsen, Ed.), p. 471. Academic Press, London, 1970.
10. Ruckenstein, E., and Pulvermacher, B., *AIChE J.* **19**, 224, 356 (1973).
11. Flynn, P. C., and Wanke, S. E., *J. Catal.* **34**, 390, 400 (1974).
12. Warren, B. E., and Averbach, B. L., *J. Appl. Phys.* **21**, 595 (1950).
13. Hoare, M. R., and Pal, P., *Advan. Phys.* **20**, 161 (1971).
14. Allpress, J. G., and Sanders, J. V., *Aust. J. Phys.* **23**, 23 (1970).
15. Ino, S., *J. Phys. Soc. Japan* **21**, 346 (1966).
16. Kimoto, K., and Nishida, I., *J. Phys. Soc. Japan*, **22**, 940 (1967).
17. Kishimoto, S., *J. Phys. Chem.* **77**, 1719 (1973).
18. Gangulee, A., *J. Appl. Crystallogr.* **7**, 434 (1974).
19. Mignot, J., and Rondot, D., *Acta Met.* **23**, 1321 (1975).
20. Stokes, A. R., *Proc. Phys. Soc.* **61**, 382 (1948).
21. Rothman, R. L., and Cohen, J. B., *Advan. X-Ray Anal.* **12**, 208 (1969).
22. Warren, B. E., *Prog. Metal Phys.* **8**, 152 (1959).
23. McKeehan, M., and Warren, B. E., *J. Appl. Phys.* **24**, 52 (1953).
24. Evans, W. P., Ricklefs, R. E., and Millan, J. F., *in* "Local Atomic Arrangements Studied by X-ray Diffractions,"(J. B. Cohen and J. E. Hilliard, Eds.), p. 351. Gordon and Breach. New York, 1966.
25. De Angelis, R. J., *in* "Local Atomic Arrangements Studied by X-ray Diffraction" (J. B. Cohen and J. E. Hilliard, Eds.), p. 271. Gordon and Breach, New York, 1966.

26. Guinier, A., "X-ray Diffraction in Crystals, Imperfect Crystals and Amorphous Bodies," Freeman, San Francisco, 1963.
27. Lin, C. H., M. S. Thesis, University of Kentucky, May, 1977.
28. Bertaut, E., *in* "International Tables for X-ray Crystallography" (C. H. Macgillavry and G. D. Rieck, Eds.), Vol. 3, p. 318. The Kynoch Press, Birmingham, England, 1962.
29. Klug, H. P., and Alexander, L. E., "X-ray Diffraction Procedures." Wiley, New York, 1967.
30. Richardson, J. T., and Desai, P., *J. Catal.* 42, 294 (1976).
31. Sashital, S. R., Burwell, R. L., Jr., Butt, J. B., and Cohen, J. B., to be published.
32. Granquist, C. G., and Buhrman, R. A., *J. Catal.* 42, 477 (1976).
33. Wanke, S. E., *J. Catal.* 46, 234 (1977).
34. Granquist, C. G., and Burhman, R. A., *J. Catal.* 46, 238 (1977).
35. Wynblatt, P., and Gjostein, N. A., *Progr. Solid State Chem.* 9, 21 (1975).
36. Komoda, T., *Japan. J. Appl. Phys.* 7, 27 (1968).
37. Rooksby, H. P., *Acta Crystallogr.* 1, 226 (1948).

# Characterization of a Sulfur-Resistant Methanation Catalyst by XPS

**R. B. Shalvoy**
Institute for Mining and Minerals Research
Kentucky Center for Energy Research Laboratory
Lexington, Kentucky 40583

**P. J. Reucroft**
Department of Metallurgical Engineering and
Materials Science
University of Kentucky
Lexington, Kentucky 40506

## ABSTRACT

A Ni-Cr on $MgSiO_3$ catalyst has been developed by United Catalysts, Inc. This catalyst converts 60 percent of the input CO to $CH_4$ after a heavy presulfiding treatment that reduces the CO conversion of conventional catalysts to less than 10 percent. The unsulfided conversion rate is better than 95 percent. X-ray photoemission spectra obtained from a series of untreated, sulfided, and methanation-tested Ni and Ni-Cr on $MgSiO_3$ catalysts show the presence of nickel sulfide in catalysts which are deactivated by the sulfiding. Both nickel sulfide and nickel sulfate are found in the catalysts that retain appreciable methanation activity. The amount of sulfur in the active catalysts is also appreciably less than in the inactive catalysts. The relationship between the resistance to sulfur poisoning and the presence of Cr and $MgSiO_3$ is discussed.

## INTRODUCTION

Increased utilization of its coal resources is an important part of the American energy plan.[1] The production of substitute natural gas (SNG) offers a clean, easily transported, and desirable fuel.[2] Production of this fuel requires the catalytic methanation of the low BTU coal synthesis gas which is most often performed with nickel catalysts.[2,3] As nickel is readily poisoned by sulfur,[4] the gasification process must include a sulfur removal step. It would be desirable to develop a sulfur resistant catalyst which could be used in a simplified gasification process and with higher sulfur content coals.

X-ray photoelectron spectroscopy (XPS) has been applied to the study of poisons in catalysts with success.[5-7] Not only the presence, but also the chemical state of the poisons can be determined by XPS as a function of the sample's previous treatment. From this information the poisoning process and the effects of additives or promoters can be better understood.

United Catalysts, Inc. has developed a sulfur resistant methanation catalyst as the result of a screening program.[8] Samples were reduced in an $H_2$ gas stream with 0.6% $H_2S$ admixed to presulfide the catalysts. Conventional catalysts ($Ni/SiO_2$) were effectively deactivated by this treatment (Table I). It was found that Ni-Cr on $MgSiO_3$ (or $MgAl_2O_4$)

**Table I. The Basic Properties of the Coprecipitated Conventional and Sulfur-Resistant Methanation Catalysts Used in this Study.**

| Composition (wt. %) | 52 $Ni/SiO_2$ | 59 Ni/ $MgSiO_3$ | 39 Ni/17Cr/ $MgSiO_3$ |
|---|---|---|---|
| Surface Area ($m^2g^{-1}$) | 211 | 190 | 191 |
| Pore Volume ($cm^2g^{-1}$) | 0.34 | – | 0.40 |
| Activity (% CO conversion) | | | |
| Unsulfided | >95 | >95 | >95 |
| Sulfided | 7-12 | 7-12 | 60-80 |

catalysts retained good methanation activity (60%–80% CO conversion), when methanation tested at higher than normal temperatures (600°C as opposed to 300°C for $Ni/SiO_2$). At 300°C this activity was not observed, however. This behavior is promising and the Ni–Cr/$MgSiO_3$ catalyst has been studied by XPS after various reducing and sulfiding treatments with a particular interest in the chemical states of Ni, Cr, and S. The overall goal is to better understand the effects of Cr and the $MgSiO_3$ support on the performance of nickel-based catalysts.

## EXPERIMENTAL

The data were recorded using an AEI (Kratos) ES200B ESCA spectrometer with computer controlled data acquisition. Unmonochromatized Mg x rays were employed. System pressures were typically $10^{-8}$–$10^{-9}$ Torr ($10^{-6}$–$10^{-7}$ Pa) during data collection. The system was calibrated by setting the Cu $2p_{3/2}$–Cu $3p_{3/2}$ kinetic energy spacing to 857.6 eV and the Au $4f_{7/2}$ binding energy to 84.0 eV.[9] Charging (typically 3–4 eV) was measured by the shifting of the impurity C 1*s* line from a neutral value of approximately 285.0 eV. More complete details on experimental technique and calibration are given elsewhere.[10]

Samples were examined as cylindrical pellets. This was the form in which they were sulfided and methanation tested. They were etched with 1-keV Ar ions to obtain a depth profile of the sulfur poisoning. The etching program was moderated by the fact that NiO and NiS are reduced by the etching routine to Ni metal.[10,11]

## RESULTS AND DISCUSSION

The spectra, binding energies, and depth profiles of a Ni on $MgSiO_3$ and a Ni–Cr on $MgSiO_3$ catalyst are shown in Figs.

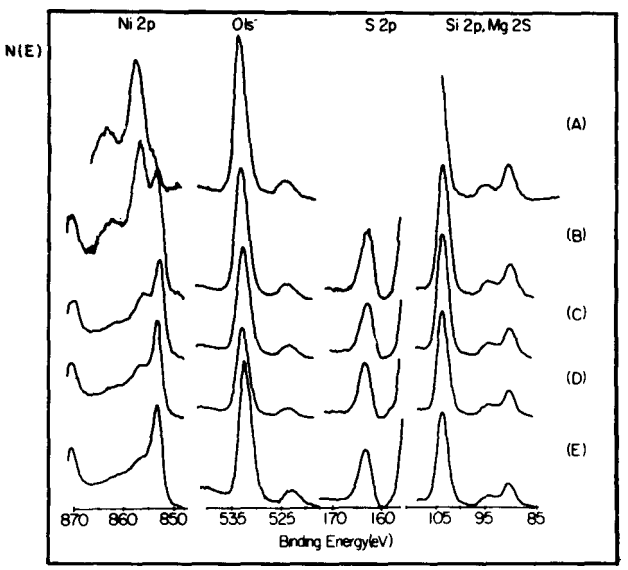


**Figure 1. XPS spectra of a sulfided Ni on $MgSiO_3$ catalyst sample etched with 1-keV Ar ions for a cumulative time of (a) unetched, (b) 2 minutes, (c) 7 minutes, (d) 15 minutes, (e) 37 minutes.**

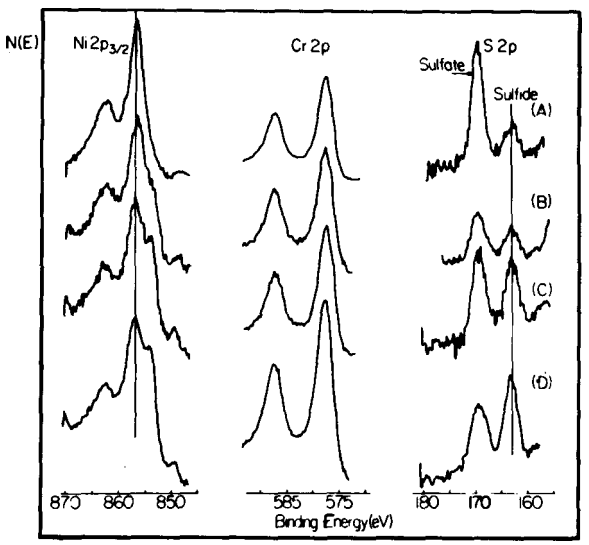


**Figure 2. XPS spectra of a sulfided Ni-Cr on $MgSiO_3$ catalyst etched with 1-keV Ar ions for a cumulative time of (a) unetched, (b) 5 minutes, (c) 15 minutes, (d) 45 minutes.**

1 and 2 and Table II. The Ni catalyst was sulfided and stored in air before study. It was inactive for methanation. The spectra showed a thin layer of NiO on the surface with NiS becoming predominant within 50 Å. Continued etching reduced the $Ni^{2+}$ to $Ni^0$, a reduction which has been observed to occur for pure NiS, but not for $NiSO_4$.[12] The Ni–Cr catalyst was sulfided, methanation tested (60% activity), and exposed to air before study (treatment no. 1 in Figs. 3 and 4). This sample had a mixed NiS, $NiSO_4$ surface region with the sulfate predominating. Etching deeply into the sample showed a significant sulfide spectrum with an appreciable sulfate signal. The spectra of the Cr levels and the support material components were not affected by the etching program (Fig. 2). The Cr appeared to be present as $Cr_2O_3$ in all the Ni–Cr catalysts tested. The spectra of the Mg, Si, and O levels corresponded to those of pure $MgSiO_3$.

This is the first observation of $NiSO_4$ in the methanation catalysts studied. Conventional, deactivated Ni catalysts formed only NiS regardless of the treatment or gas exposure.[12] All the $MgSiO_3$-supported catalysts showed both NiS and $NiSO_4$ to a greater or lesser extent (Figs. 3 and 4). The formation of $NiSO_4$ as opposed to NiS appears to be related to

**Table II. Binding Energies and Peak Widths (in eV) for Some Standard Samples and Sulfided Nickel Catalysts.**

| Material | Level | | |
|---|---|---|---|
| | Ni $2p_{3/2}$ | S 2p | |
| Ni | 852.8(1.6) | | |
| NiS | 853.0(4.5) | | 162.3(3.1) |
| $NiSO_4$ | 857.0(4.4) | 169.4(2.7) | |
| $Ni/MgSiO_3$ | 853.0(3.0) | | 162.4(3.2) |
| $Ni\text{-}Cr/MgSiO_3$ | 856.9(4.3) | 169.6(3.0) | 162.9(3.2) |
| | 854.0(-) | | |

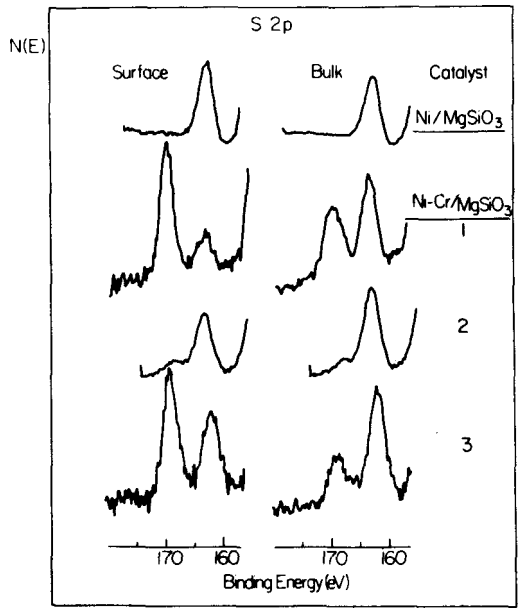


**Figure 3. XPS spectra of the S 2p levels for surface and bulk regions of the Ni on $MgSiO_3$ and Ni-Cr on $MgSiO_3$ catalysts with varying sample treatments (Nos. 1-3, described in text). The $NiSO_4$ peak is observed only in the Ni-Cr catalysts.**

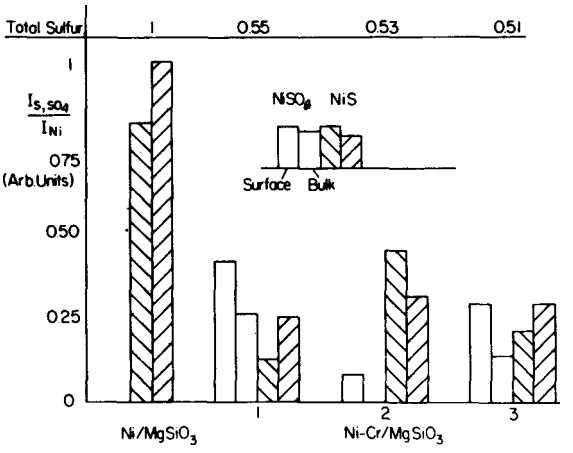


**Figure 4. The ratio of the XPS peak intensities between the S 2p and Ni $2p_{3/2}$ core levels in the $Ni/MgSiO_3$ and $Ni\text{-}Cr/MgSiO_3$ catalysts (sample treatments Nos. 1-3 are described in the text). The unshaded columns represent the $NiSO_4$ signal from the surface (left column) and the bulk (right column) of the sample. The shaded columns represent the surface (left column) and bulk (right column) NiS signals. The total sulfur signal (sulfide + sulfate) is also given.**

the increased methanation activity of the sulfided catalysts.

The intensity of the sulfur peaks in the active sulfided catalysts is about half that of the conventional catalysts (Fig. 4). Some variations in the sulfide to sulfate ratio, depending on the sample's handling, are also observed. The Ni on $MgSiO_3$ sample (reduced, sulfided, methanation tested, stored in air) shows somewhat less sulfur on the surface than in the bulk. This is most likely due to oxygen substitution for sulfur in surface NiS. This sample has an approximate concentration composition of $NiS_x$ with $x = 0.5$ to 0.7. A similarly treated Ni-Cr on $MgSiO_3$ catalyst (treatment no. 1) shows about half the sulfur on a per nickel atom basis observed in the Ni on $MgSiO_3$ catalyst. A Ni-Cr on $MgSiO_3$ catalyst which had been reduced, sulfided, *not* methanation tested and stored in $N_2$ before study (treatment no. 2) showed a low concentration of $NiSO_4$, particularly in the bulk. It also showed the same lower total sulfur content observed after treatment no. 1. The lower sulfur content in the bulk of this sample is most likely due to preferential etching or reduction of NiS to Ni by the Ar ion beam.

The effects of air exposure on the Ni-Cr catalysts were tested by exposing the catalyst stored in $N_2$ prior to study to air for a month and then reexamining this sample (treatment no. 3). A significant amount of $NiSO_4$ is again observed although the total amount of sulfate is much less than observed for treatment no. 1. Total sulfur remained low. As this sample was not methanation tested this result does not conclusively implicate the sulfate formation with either the air exposure or the methanation testing. Most likely both treatments lead to the formation of some $NiSO_4$. The study of a reduced, sulfided, methanation-tested, and inert gas stored Ni-Cr on $MgSiO_3$ catalyst should clear up this question. This sample is being prepared by United Catalysts.

It is possible that the $NiSO_4$ formation is due solely to the air exposure of the sulfided catalyst. This does not explain, however, why this form is not observed in any of the conventional methanation catalysts, even after long air exposures. $Cr_2O_3$ appears to be promoting the formation of the sulfate which is also a more active form of Ni than NiS.[13] This combined with the lower sulfur uptake appears to lead to an incompletely poisoned catalyst which retains appreciable activity. There is less interaction between the Ni and the support for $MgSiO_3$ as opposed to $SiO_2$.[14] This allows more Ni to be reduced and catalytically available (Ni particle sizes are comparable for these two supports[12]). As the reducing and methanation atmospheres are not conducive to the oxidation of NiS, this speculation on the role of $NiSO_4$ in the increased activity of the Ni-Cr catalyst and its formation during methanation must be confirmed by the observation of $NiSO_4$ in a methanation tested sample not exposed to air.

## CONCLUSION

A sulfided Ni-Cr on $MgSiO_3$ catalyst which retains appreciable methanation activity has been found. This catalyst takes up less sulfur and takes it up in a less noxious form than conventional Ni methanation catalysts which are deactivated by the sulfiding treatment. These improvements may be due to oxidation of the sulfur in the coal synthesis gas stream by the $Cr_2O_3$ in the catalyst, as evidenced by the presence of $NiSO_4$ in the sulfided catalyst. Further tests of this hypothesis are planned when the appropriately treated samples are received. These results suggest the possibilities inherent in binary

metal catalysts and the utility of XPS in analyzing complex catalysts.

## ACKNOWLEDGMENTS

Many helpful discussions with Arthur Hausberger, United Catalysts, Inc., and Burtron Davis, Institute for Mining and Minerals Research, aided in the preparation of this paper. Research support through DOE Contract No. EX-76-C-01-2229 and the Institute for Mining and Minerals Research is gratefully acknowledged.

## REFERENCES

1. S. S. Penner and L. Icerman, *Energy: Demands, Resources, Impact, Technology and Policy*, Addison Wesley, Reading, MA, 1974.

2. W. L. Lom and A. F. Williams, **Substitute Natural Gas**, Wiley, New York, 1976.

3. G. A. Mills and F. W. Steffgen, **Catal. Rev.**, Vol. 8, pp. 159, 1973.

4. Robert A. Meyers, **Coal Desulfurization**, Marcel Dekker, New York, 1977.

5. S. A. Best, R. G. Squires, and R. A. Walton, **Journal of Catalysis**, Vol. 47, pp. 292, 1977.

6. J. S. Brinen, **Journal of Electron Spectroscopy**, Vol. 5, pp. 377, 1975.

7. W. N. Delgass, T. R. Hughes, and C. S. Fadley, **Catal. Rev.**, Vol. 4, pp. 179, 1970.

8. Arthur L. Hausberger and William A. Kustes, *"Sulfur Resistant Methanation Catalyst,"* Final Report, DOE Contract No. EX-76-C-01-2032, January 1978.

9. W. P. Dianis and J. E. Lester, **Analytical Chemistry**, Vol. 45, pp. 1416, 1973.

10. R. B. Shalvoy and P. J. Reucroft, **Journal of Catalysis** (to be published).

11. K. S. Kim, W. E. Baitinger, J. W. Amy, and N. Winograd, **Journal of Electron Spectroscopy**, Vol. 5, pp. 351, 1975.

12. R. B. Shalvoy (unpublished results).

13. Bruce C. Gates, James R. Katzer, and G. C. A. Schuit, **Chemistry of Catalytic Processes**, McGraw-Hill, New York, p. 248, 1977.

14. P. J. Reucroft, E. B. Bradley, R. J. DeAngelis, and G. A. Sargent, *"Surface Structure and Mechanisms of Gasification Catalyst Deactivation,"* Second Annual Report, DOE Contract No. EX-76-C-01-2229, Feb. 1977 – Jan. 1978.

# Particle-Size Distribution of NiO in Coprecipitated $NiO-Al_2O_3$ Powders

A. Kidron
Physics Department
University of Alabama in Huntsville
Huntsville, Alabama 35800

R. J. De Angelis and P. J. Reucroft
Department of Metallurgical Engineering and Materials Science
University of Kentucky
Lexington, Kentucky 40506

## ABSTRACT

The particle-size distribution along the [100] and [111] directions of NiO catalyst particles coprecipitated with alumina were measured by x-ray diffraction profile analysis. The average particle size is about 20 Å in both directions. The distribution along the [111] direction shows three peaks, indicating an anisotropy in the shape of the particles, and supports the idea that the particles are platelets with the [111] direction normal to their surface. This study shows beyond doubt that careful x-ray diffraction profile analysis techniques employing least-squares analysis methods can be used to determine the distribution of particle sizes existing in metal supported catalyst materials.

## INTRODUCTION

Metal catalysts are generally employed in the form of metal dispersed as small crystallites on high surface area supports. In this form a high ratio of metal atoms exist on the surface of the small crystallites which leads to an active catalytic material. The support also serves the function of physically separating the small crystallites of metal, which tends to inhibit agglomeration of the small crystallites into larger crystallites. This agglomeration, known as sintering, occurs very rapidly in unsupported metal catalysts (e.g., very fine metallic powders).[1] Sintering also occurs at high temperatures in supported metal catalysts and has the very undesirable effect of reducing the activity of the catalyst. The process of sintering when referred to a supported metal catalyst indicates a process which leads to a change in particle-size distribution.[2] The sintering behavior of the catalyst depends on the initial particle-size distribution function and the mechanism of sintering.[3] Therefore, a reliable determination of the initial particle-size distribution function (PSD) and the changes occurring in the PSD during sintering become essential if the sintering process is to be understood and ultimately controlled.

Electron microscope techniques have been used to determine PSD in supported nickel catalysts with limited success.[4] The difficulties associated with this approach have been discussed by Flynn *et al.*[5] The technique has been used with more success to determine the PSD of platinum supported catalysts.[6–8]

There are two x-ray techniques which are capable of giving PSD data: small-angle scattering (< 5° of the incident beam) and analysis of the shape of the x-ray diffraction profile. These techniques have previously been applied to characterize platinum and palladium supported catalysts[9] and to precipitated pure nickel oxide[10] but not to supported nickel oxide catalytic material. To use small-angle scattering on supported metal catalysts requires the elimination of scattering due to the pores of the support material. One approach to accomplishing this is to fill the pores with a liquid having the same electron density as the support.[11,12] The analysis of the shape of x-ray diffraction profiles can be applied directly to the metal supported catalyst, but the shapes of the extremely broad lines associated with particle sizes less than 50 Å are difficult to record accurately, especially the long low-intensity tail portion of the profile.

Diffraction profiles from materials of extremely small particle size also overlap because of the long tails which makes accurate determination of background intensity most difficult. This problem introduces errors into Fourier coefficients which lead to coefficient oscillations and produce oscillations in the PSD functions. Oscillations in the Fourier coefficients do not occur if the background intensity is taken too low and the coefficients are calculated using a least-squares analysis method.[13] However, a renormalization for the incorrect area may be required. It has also been shown that it is not necessary to have a complete experimental definition of the profile function to calculate Fourier coefficients.[13] This becomes important when diffraction

lines merge into one another because it allows a small section of unreliable data to be dropped without affecting the coefficient values. Although numerous studies in the past have employed diffraction methods to study catalysts and extract particle-size information, the least-squares method of line profile analysis has not been employed.

This investigation was undertaken with the main objective of demonstrating that the least-squares method of x-ray diffraction line profile analysis can be used to determine the distribution of sizes of particles existing in supported metal catalytic materials. A coprecipitated nickel oxide—alumina catalyst material containing 55% nickel and having a specific surface area of 177 $m^2/g$ [14] was chosen for this investigation because in its reduced state it is typical of the catalysts used in methanation processes. In addition, it is known that the nickel oxide precipitates in the particle-size range of 20 to 50 Å, which in the past has been considered to be beyond the resolution of the wide-angle x-ray technique.[15]

## EXPERIMENTAL PROCEDURES

A Picker diffractometer and a Cu-target x-ray tube were used for the diffraction runs. A homemade diffracted beam monochromator equipped with a doubly-bent graphite crystal eliminated most of the background intensity outside the diffraction lines, and specially took care of the unwanted fluorescence from the Ni atoms in the sample. A proportional counter with subsequent pulse-height analysis was used for the detection system.

Great care was taken to obtain a good alignment of the diffractometer. This is important in the measurement of line profiles,[16] especially in the present study where some merging of neighboring diffraction lines was expected due to the small particle sizes involved. The resulting alignment was checked by running a diffraction pattern of a Si standard sample. With a divergence slit of 0.4°, a receiving slit of 0.01°, and a goniometer speed of $\frac{1}{4}$°/min, the (220) line of Si showed a clear $K_\alpha$ doublet resolution with a minimum between the $K_{\alpha 1}$ and $K_{\alpha 2}$ components being at a height of 40% of the $K_{\alpha 1}$ peak.

To obtain a NiO sample with a very large particle size which could be used to measure the instrumental broadening of the diffraction lines some reagent-grade NiO powder was pressed under 40 000 psi pressure into briquets $1\frac{1}{4}$ in. in diameter and about $\frac{1}{16}$ in. thick. One of these briquets was then sintered at 1350 °C for about 10 h. It shrank somewhat during this sintering and changed color from dark grey to dark green as expected. A diffraction run taken from this sample showed a characteristic fcc structure. The splitting of the Cu-$K_\alpha$ doublet into $K_{\alpha 1}$ and $K_{\alpha 2}$ components was similar to the splitting obtained by the Si standard sample run under the same setup of the goniometer.

The NiO sample to be analyzed for particle-size distribution was prepared from an alumina supported catalyst containing 55% metallic nickel by pressing the powder into the shape of a briquet. The sample was not subsequently sintered. The diffraction pattern obtained from this sample was also of a typical fcc structure except that the diffraction lines were now much broader than in the case of the annealed sample and some of the lines merged one into another.

The merging of the (111) and (200) lines was very small and could be handled by simple extrapolation. On the other hand, the second-order lines (222) and (400) were too broad and merged too much into neighboring lines to allow even a rough estimate of the peak breadth. The analysis was then confined to the (111) and (200) profiles only. The intensity of the profiles of the instrumental and broadened lines were measured by step scanning along the profiles in steps of $\frac{1}{60}$° in $2\theta$ where $\theta$ is the Bragg angle.

## THE ANALYSIS AND CALCULATIONS

The analysis of the particle-size distributions was performed using the Warren-Averbach[17] and Bertaut[18] procedures. The actual calculation was carried out using a computer program developed for such a purpose.[13,19] As a first step this program subtracts the background intensity along the profiles. Then corrections are made for the decrease of the scattering factor with the Bragg angle, for polarization, and for the Debye-Waller temperature factor. The program then calculates the Fourier coefficients of the diffraction lines either by a least-squares method[13] or by a simple Fourier transformation. These coefficients are normalized so that the total intensity under the profile is unity.

In the Warren-Averbach-Bertaut procedure, one writes the intensity of the diffraction profile as a Fourier series. In terms of

$$S = (2\pi \sin\theta/\lambda) \tag{1}$$

and

$$S_0 = (2\pi \sin\theta_0/\lambda), \tag{2}$$

where $\lambda$ is the wavelength of the radiation, $\theta$ is the Bragg angle along the profile, and $\theta_0$ is the Bragg angle of the centroid of the profile; this series takes the form[19]

$$I(S-S_0) = A_0 + \sum_{n=1}^{m} \left[ 2A_n \cos\left(\frac{2\pi n(S-S_0)}{\Delta S}\right) + 2B_n \sin\left(\frac{2\pi n(S-S_\theta)}{\Delta S}\right)\right]. \tag{3}$$

Such a series holds for the "instrumental" profile taken from the annealed (with practically "infinite" particle size) sample of NiO, as well as for the "broadened" profile taken from the sample to be analyzed. This "broadened" profile is actually a convolution of the "true" profile from this sample and the "instrumental" profile[20] so that a deconvolution yields the Fourier coefficients $A_n$ and $B_n$ of the "true" profile.

In actual practice one calculates $A(L)$ and $B(L)$, i.e., $A_n$ and $B_n$ as a function of $L$, where $L$ is a distance in real space and is given by $L = n/\Delta S$ where $n$ is the harmonic number and $\Delta S$ is the span of the diffraction line in $S = (2\pi \sin\theta/\lambda)$.

The Fourier cosine coefficients $A(L)$ of the "true" profile have actually two components given by

$$A(L)=A_S(L)A_D(L), \tag{4}$$

where $A_S(L)$ are the "particle size" coefficients and $A_D(L)$ are the "strain" coefficients. The latter measure the microstrains in the material, and to separate them from $A_S(L)$ one needs to measure the same diffraction profiles at least for two different orders, i.e., (111), (222), etc.

In our present study, as explained above, there was no possibility to measure the second-order lines (222) and (400) with any accuracy. The assumption was then made that there is no appreciable strain broadening of the diffraction profiles. Consequently, the values of $A(L)$ of the "true" profiles were taken as the values of $A_S(L)$.

This assumption is actually well justified in the present work. A simple calculation from the breadth of the profiles shows that the particle sizes in question should be around 20 Å. In a detailed transmission electron microscope study of the structural features of NiO particles, Larkins *et al.* found no indication of the existence of dislocations in the structure.[21] One cannot expect many vacancies or dislocations, etc., to exist in such small particles and consequently there is no reason to assume the existence of any strains in them. Furthermore, with particle sizes in the range of 20 Å the behavior of the cosine coefficients is controlled by particle-size effects. Even if the strains were of significant magnitude, they would have little to no effect on the form of the PSD function; the reliable determination of which is the objective of this work.

The particle-size distribution is given by the second derivative of $A_S(L)$ by the relation[18]

$$\frac{d^2A_S(L)}{dL^2}=\frac{p(L)}{\overline{D}}, \tag{5}$$

where $p(L)$ is actually the density of the distribution of the length of columns of unit cells perpendicular to the diffracting plane. $\overline{D}$ is the average length of these columns, i.e., it is the average particle size in the direction perpendicular to the diffracting plane.

Similarly, the first derivative of $A_S(L)$ will be given by

$$\frac{dA_S(L)}{dL}=\frac{1}{\overline{D}}\int_L^{\infty}p(L)\,dL=-\frac{1}{\overline{D}}+\frac{1}{\overline{D}}\int_0^{L}p(L)\,dL, \tag{6}$$

so that at the limit $L\to 0$ we have

$$\left(\frac{dA_S(L)}{dL}\right)_{L\to 0}=-\frac{1}{\overline{D}}, \tag{7}$$

which gives a way to measure the average particle size not directly from the distribution.

## RESULTS

One of the critical points of the experimental measurements was the exact assessment of the background intensity for the broadened lines. Indeed, the background intensity of the (111) line had to be taken about 1% less than the value measured in order to avoid a negative curvature of $A_S(L)$ for $L\to 0$ which would give "negative particle sizes" at this region. Similarly, for the (200) line we had to reduce the background by 4% to avoid a negative curvature for $L\to 0$.

These numbers (i.e., 1 and 4%), though, were of the order of magnitude of the standard deviation (about 1%) of the background intensity as calculated from the number of counts measured. They were initially determined from the first plots of $A_S(L)$ versus $L$ by extrapolating $A_S(L)$ to $L=0$ and then changing the background so that $A_S(0)=1.0$, which is its true value by definition. An independent check of this procedure was to see if the average particle size as calculated from the distribution is the same (or at least close to) the average particle size as calculated from the initial slope of $A_S(L)$ versus $L$.

Errors are also expected in $A_S(L)$ due to the finite summation in the Fourier transforms,[22] especially when the lines are broad and secondary diffraction maxima outside the main peak can be relatively large. For this reason, the Fourier coefficients of the broadened lines were calculated by a least-squares method,[13] whereas for the "annealed" lines a simple Fourier transformation was used.

The first and second derivatives of the $A_S(L)$ resulting from the procedure given above were calculated by using an IBM computer subroutine (DET5) which uses a Lagrangian interpolation polynomial of degree 4. These derivatives are given in Figs. 1–4.

The most interesting aspect of these results is that while the particle-size distribution in the [100] direc-

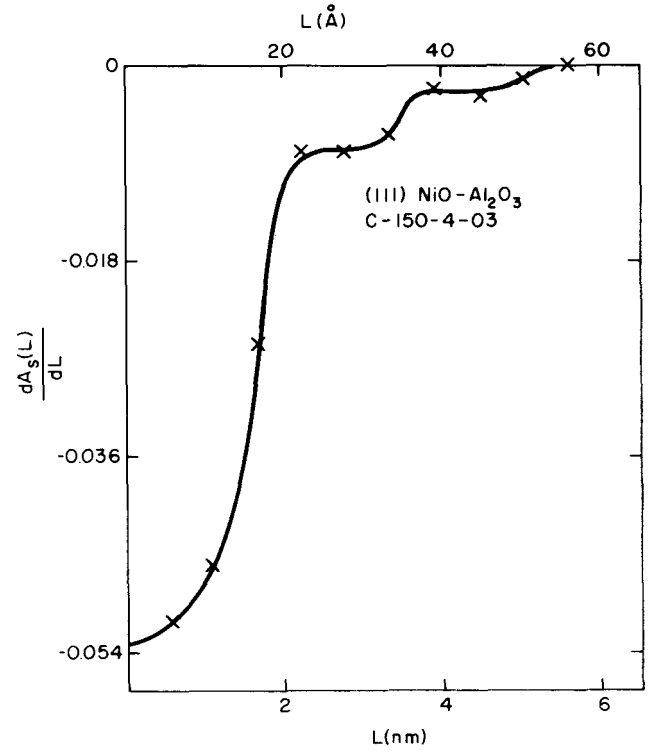


**Fig. 1. First derivatives of the particle-size coefficient for the (111) line.**

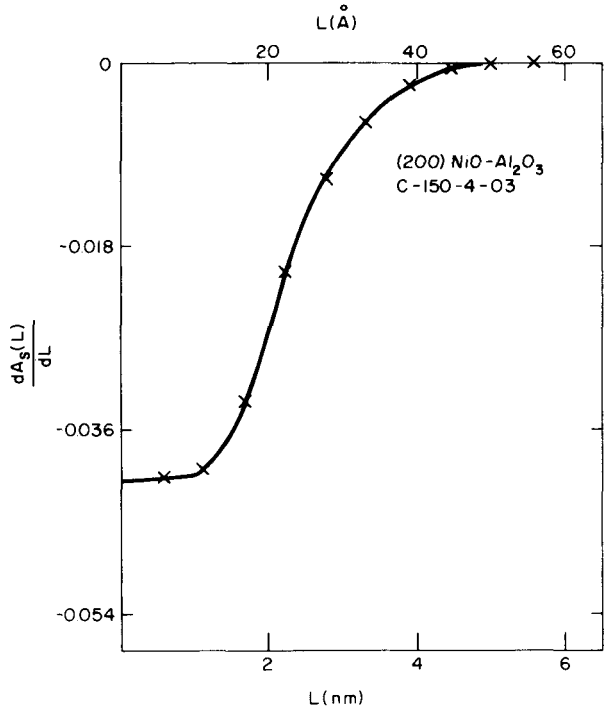


**Fig. 2. First derivatives of the particle-size coefficients for the (200) line.**

tion is continuous (Fig. 4), the particle-size distribution in the [111] direction seems to be made of three distinct distributions (Fig. 3). One can see this behavior already in Fig. 1 which gives the first derivatives of $A_S(L)$ for the [111] direction. In Fig. 1 one can distinguish very clearly three consecutive S-shaped figures typical of (normal or similar) cumulative distribution functions, one for $L=0$ to around 30 Å, the

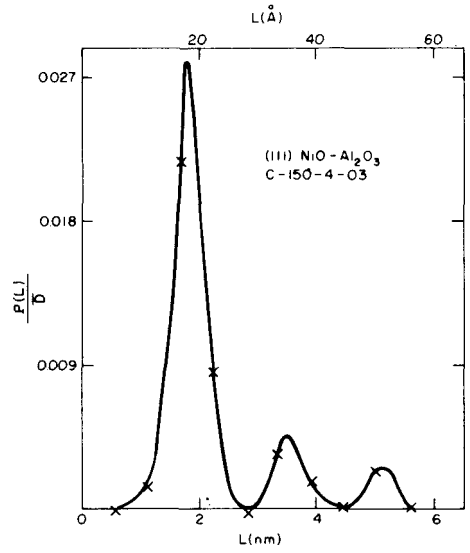


**Fig. 3. Second derivatives of the particle-size coefficients (i.e., $[d^2A_S(L)/dL^2] = p(L)/\bar{D}$ where p(L) is the distribution of the column sizes and $\bar{D}$ is the average column size) for the (111) line.**

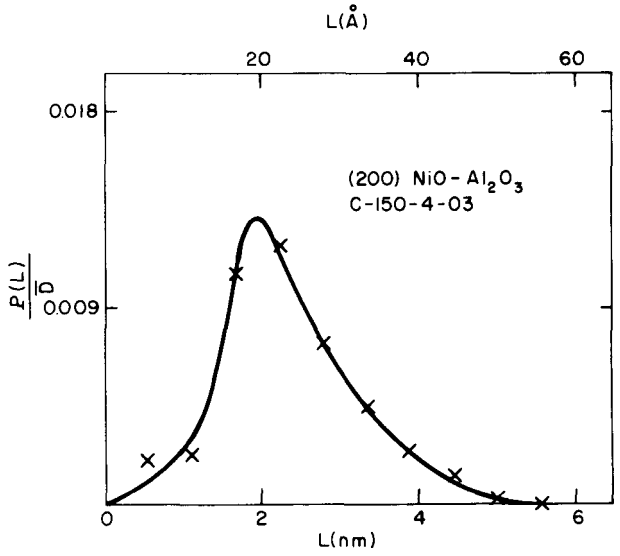


**Fig. 4. Second derivatives of the particle-size coefficients (i.e., $[d^2A_S(L)/dL^2] = p(L)/\bar{D}$ where p(L) is the distribution of the column sizes and $\bar{D}$ is the average column size) for the (200) line.**

second for $L=30$ Å to around 45 Å, and a third one for $L=45$ Å to around 60 Å. For the [100] direction one can see only one S-shaped curve (in Fig. 2) for the first derivatives of $A_S(L)$. This latter result indicates that the oscillations observed in the PSD in the [111] direction are real and not due to computational errors or procedures.

In Table I we give the average particle sizes as calculated from the initial slopes of $A_S(L)$ (i.e., from Figs. 1 and 2 for $L \to 0$), and also the average particle sizes as calculated from the distributions themselves (i.e., from Figs. 3 and 4). The average particle sizes calculated from the distributions of the (111) and (200) lines seem to be similar. Also, the values of $\bar{D}$ for the [100] direction as caculated from the initial slope of $A_S(L)$ and from the distribution itself seem to be close (24.4 and 23.54 Å, respectively). On the other hand, for the [111] direction the values of the same parameters are 18.9 and 22.5 Å, respectively, and seem to disagree. But a calculation of the value of $\bar{D}$ from the first distribution (the first maximum) in Fig. 3 gives $\bar{D}=18.1$ Å, and this value agrees quite well with $\bar{D}=18.9$ Å obtained from the initial slope.

**Table I. Values of the average particle size $\bar{D}$.**

| Direction | From initial slope | From the distribution |
|---|---|---|
| [111] | 18.9 Å | 22.5 Å |
| [100] | 24.4 Å | 23.5 Å |

## DISCUSSION

The primary objective of this investigation was to demonstrate that x-ray diffraction profile shape analysis techniques could be employed to describe the particle-size distribution function existing in supported metal catalysts. A method employing the least-squares analysis computation method to determine Fourier coefficients has been presented along with a description of the technique that is required to determine the proper level of background intensity.

It is believed that the particles being characterized in this study are of an individual character rather than a measure of the subgrain size existing in a larger particle. This interpretation is supported by the direct observation transmission electron microscopy results obtained on supported nickel catalysts by Shephard.[23] He also showed that a good empirical relationship exists between the metal surface area measured by hydrogen chemisorption and the x-ray determined average crystallite size. The almost complete absence of twins in supported platinum, palladium, and gold catalysts[24] also provides support to the idea that the particle size measured is the actual particle dimension. It is generally observed that the average nickel particle size obtained after reducing NiO is only slightly greater than the particle size of the prereduced NiO. This strongly indicates that defects of the type associated with subgrains do not exist in the nickel oxide.

The difference between the shape of particle-size distribution functions measured for the [111] and [100] directions can be accounted for in terms of a growth process during precipitation. Electron microscope observations by Larkins *et al.*[21] and Shephard[23] show that a number of thin platelet particles exist with three fold symmetry. This would correspond to a platelet with [111] direction normal to the surface or in the growth direction. This type of growth morphology of NiO on $Al_2O_3$ has been suggested by Coenen and Linsen.[25] Assuming the growth process involved the formation of steps on the surface normal to the growth direction as this step migrated across the surface, the crystal would increase its dimension by the step height. For a process of this type, the PSD as measured in the growth direction would be expected to have a multimodal character as observed in the PSD for the [111] direction. This proposed explanation needs further substantiation. Additional work on the mechanisms and kinetics of the precipitation process is required to elucidate these points.

The average particle-size data ostensibly does not support this model of particle shape. However, it must be noted that particle size averaging occurs over all crystallographic orientations and particle orientations with respect to the x-ray beam. Therefore, it is not suprising that the average particle size along the [111] and [100] are approximately equal. This same effect has been noted previously on unsupported NiO.[10]

## REFERENCES


1. J. R. Anderson, **Structure of Metallic Catalysts**, Academic Press, New York, p. 221, 1975.
2. S. E. Wanke and P. C. Flynn, **Catal. Rev.**, Vol. 12, pp. 93, 1975.
3. P. Wynblatt and N. A. G. Jostein, **Acta Metallurgica**, Vol. 24, pp. 1165, 1976.
4. R. van Hardeveld and A. van Montfoort, **Surface Science**, Vol. 4, pp. 396, 1966.
5. P. C. Flynn, S. E. Wanke, and P. S. Turner, **Journal of Catalysis**, Vol. 33, pp. 233, 1974.
6. T. A. Dorling, M. J. Eastlake, and R. L. Moss, **Journal of Catalysis**, Vol. 14, pp. 23, 1967.
7. R. L. Moss, **Platinum Met. Rev.**, Vol. 11, pp. 1, 1967.
8. C. R. Adams, H. A. Benesi, R. M. Curtis, and R. G. Meisenheimer, **Journal of Catalysis**, Vol. 1, pp. 336, 1962.
9. W. L. Smith, **Journal of Applied Crystallography**, Vol. 5, pp. 127, 1972.
10. B. Moraweck, A. J. Renouprez, and B. Imelik, **Journal Chimica Physica**, Vol. 70, pp. 594, 1973.
11. T. E. Whyte, P. W. Kirklin, R. W. Gould, and H. Heinemann, **Journal of Catalysis**, Vol. 25, pp. 407, 1972.
12. E. L. Gunn, **Journal of Physical Chemistry**, Vol. 62, pp. 928, 1958.
13. A. Kidron and R. J. De Angelis, *SMD Symposium on Computer Aided Engineering*, Waterloo Press, Waterloo, Ontario, pp. 285-298, 1971.
14. Catalyst type C150-4-03, supplied by Catalysts and Chemicals Inc., Louisville, Ky.
15. J. R. Anderson, **Structure of Metallic Catalysts**, Academic Press, New York, p. 365, 1975.
16. A. Kidron and J. B. Cohen, **Journal of Applied Crystallography**, Vol. 6, pp. 8, 1973.
17. B. E. Warren and B. L. Averbach, **Journal of Applied Physics**, Vol. 21, pp. 595, 1950.
18. E. F. Bertaut, **Acta Crystallography**, Vol. 3, pp. 14, 1950.
19. A. Kidron and J. B. Cohen, Technical Report 7, ONR-NR-031-733, Unpublished, 1973.
20. A. R. Stokes, **Proceedings of the Royal Society**, Vol. 61, pp. 382, London, 1948.

21. F. P. Larkins, P. J. Fensham and J. V. Sanders, **Transactions of the Faraday Society**, Vol. 66, pp. 1748, 1970.

22. E. F. Bertaut, **Acta Crystallography**, Vol. 5, pp. 117, 1952.

23. F. E. Shephard, **Journal of Catalysis**, Vol. 14, pp. 148, 1969.

24. N. R. Avery and J. V. Sanders, **Journal of Catalysis**, Vol. 18, pp. 129, 1970.

25. J. W. E. Coenen and B. S. Linsen, **Physical and Chemical Aspects of Adsorbents and Catalysts**, edited by B. S. Linsen, Academic Press, London, p. 471, 1970.

ABSTRACT OF THESIS

# A Study of Metal Surface Area in Supported Nickel Catalysts by Hydrogen Chemisorption

A thesis submitted in partial fulfillment of the
requirements for the degree of Master of Science
at The University of Kentucky

by
Ching-Huei Lin
Taipei, Taiwan, R.O.C.

Director

Dr. P. J. Reucroft
Professor of Materials Science
University of Kentucky
Lexington, Kentucky
1977

In order to measure surface area and total pore surface area of supported coprecipitated nickel catalysts, a volumetric gas adsorption system was constructed and tested. The nickel metal surface areas of typical methanation catalysts were determined by hydrogen chemisorption measurements and the total BET surface areas were determined by nitrogen adsorption. Values of the average particle size can be estimated from these measurements.

The Ni metal surface areas of the reduced alumina supported catalysts were found to be 31.6 $m^2/g$ and 28.0 $m^2/g$ for 47.0 and 55.6 percent Ni content, respectively. For silica supported catalysts, the Ni metal surface areas were found to be 84.8 $m^2/g$ and 42.6 $m^2/g$ for 51.7 and 46.6 percent Ni content, respectively. A slight decrease in the total BET surface area was observed for the reduced catalysts compared to the unreduced catalysts. The total BET surface areas of the unreduced alumina supported catalysts were found to be 146 $m^2/g$ and 171 $m^2/g$ for 47.0 and 55.6 percent Ni content, respectively. The total BET surface areas for silica supported catalysts were found to be 184 $m^2/g$ and 235 $m^2/g$ for 51.7 and 46.6 percent Ni content, respectively. These total BET surface areas are in good agreement with the results reported recently from Catalysts and Chemicals, Inc.

## ABSTRACT OF THESIS

# Structural Characteristics of Catalytic Materials Containing Nickel Supported on Alumina or Silica

A thesis submitted in partial fulfillment of the
requirements for the degree of Master of Science
in Metallurgical Engineering and Material Science
at The University of Kentucky

by
Hai-Ku James Kuo
Lexington, Kentucky

Co-Directors

Dr. P. J. Reucroft, Professor
Dr. R. J. DeAngelis, Professor
Metallurgical Engineering and Materials Science
University of Kentucky
Lexington, Kentucky
1977

X-ray diffraction and transmission electron microscopy (TEM) were employed to determine the average particle sizes and particle size distribution functions for coprecipitated support nickel catalysts. The average particle sizes of four supported nickel catalysts in the unreduced form were determined from the half breadth and the Stokes corrected coefficients of the (220) x-ray diffracting profiles. Particle size distribution functions for these catalysts, in the as-received condition, and after sintering, were also determined. The formation of nickel aluminate during calcining at 900 and 1000°C was observed in the alumina supported catalysts. The average particle size and particle size distribution curve of the supported nickel catalyst C150-1-01 were determined directly from the TEM micrograph. The difficulty of measuring the particle size below 45 Å, and limitations of the TEM for examining highly dispersed supported nickel catalysts, make this technique qualitative rather than quantitative.

ABSTRACT OF THESIS

# Surface Area Studies on Variable Composition Nickel–Alumina Methanation Catalysts

A thesis submitted in partial fulfillment of the
requirements for the degree of Master of Science
at The University of Kentucky

by
Kwung-Hong Ho
Taipei, Taiwan R.O.C.

Director

Dr. P. J. Reucroft
Professor of Materials Science
University of Kentucky
Lexington, Kentucky
1977

A volumetric gas adsorption system was used to measure the total surface area and metal surface area of alumina supported coprecipitated nickel catalysts. The nickel metal surface area of typical methanation catalysts was determined by hydrogen chemisorption measurement and the total BET surface area was determined by nitrogen adsorption. Values of the average nickel particle size can be estimated from these measurements. It was found that the total surface area for both unreduced and reduced catalysts is almost the same. At constant nickel content, the hydrogen chemisorption on reduced catalysts increases with increasing reducing temperature, up to 450°C. At a constant reducing temperature, the hydrogen chemisorption increases with increasing nickel content in the catalyst.

ABSTRACT OF THESIS

# Effect of Reduction Temperature and Time on the Surface Area of Nickel Methanation Catalysts

A thesis submitted in partial fulfillment of the
requirements for the degree of Master of Science
in Metallurgical Engineering and Materials Science
at The University of Kentucky

by
Jong-Wan Park
Lexington, Kentucky

Director

Dr. P. J. Reucroft
Professor of Materials Science
University of Kentucky
Lexington, Kentucky
1979

The effects of reduction temperature and time on the surface area of nickel methanation catalysts supported on alumina and silica were studied. The nickel metal surface area was determined by hydrogen chemisorption measurements and total BET surface area was measured by nitrogen adsorption. The BET surface areas of all catalysts decreased with increasing reduction temperature and time, indicating the occurrence of agglomeration of pores in supports. Upon reducing at 600°C for 16 hours, the nickel surface areas of the C150-1-01 and C150-4-03 catalysts were 107.8 and 65.1 $m^2/g$ of Ni, respectively. The hydrogen chemisorption data showed that silica supported catalysts yielded easier reduction of NiO than alumina supported catalysts. The interaction between metal oxide and support seems to play a significant role in the reduction kinetics. This effect was most pronounced for the lowest nickel content catalyst supported on alumina, *i.e.*, the L141 catalyst (23.4 percent reduction). The degree of sintering increased generally with increasing nickel content in the alumina supported catalysts. It appears that, with adequate nickel concentrations, the use of silica supported catalysts is more desirable than alumina supported catalysts for maximum metal surface area.

# Raman Spectra of CO, $H_2$ and $O_2$ Adsorbed on Ni(111)

**John M. Stencel**
**Eugene B. Bradley**
Department of Electrical Engineering
University of Kentucky
Lexington, Kentucky 40506

## Abstract

Experimental results are discussed for laser Raman spectra which are obtained from Ni(111) after this surface is exposed to CO, $H_2$ and $O_2$ in the 300°C temperature region. A major Raman band is observed at 80 $cm^{-1}$. Intensity variations in this band are shown with respect to CO, $H_2$ and $O_2$ exposure and evacuation. The discussion describes possible surface species which could produce the observed spectra and compares them with graphitic chemilayers which have been observed in similar adsorption studies.

## Introduction

Laser Raman spectroscopy has not been used to study adsorption properties of gases on smooth metallic surfaces. The difficulty of such an investigation can be appreciated by recognizing the effort needed to obtain a usable signal/noise ratio for $H_2SO_4$/KI on a smooth Pt electrode.[1] Increasing the density of the Raman scatterers, as in high-surface area adsorbents (700 $m^2/g$), decreases the difficulty of spectral acquisition in terms of the adsorbate, but may also increase fluorescence due to the adsorbent which can obscure the Raman spectrum.[2,3] Nevertheless, adsorption on high-surface area silica has allowed the Raman detection of $CCl_4$ down to four percent of a monolayer.[4] The first Raman spectrum due to the adsorption of CO + $H_2$ on a smooth crystalline Ni surface is reported in this paper. The intensity changes of the Raman bands due to adsorption of CO, $H_2$ and $O_2$ are also shown and discussed in relation to possible adsorbed species.

## Experimental

The design of the experimental ultrahigh-vacuum system used for this study has been presented.[5] A nickel crystal was obtained from Materials Research Corporation and was cut with a diamond saw. It was then mechanically polished in a water-alumina slurry which had successive alumina particle sizes of 1.0, 0.3 and 0.05 microns. After chemical etching in a solution of $HNO_3$:$H_3PO_4$:$HCH_3COO$, the x-ray diffraction pattern showed well-defined Laue spots indicative of having the (111) plane to within ±1.0 degree of the sample surface.

The nickel crystal was mounted in an adsorption chamber evacuated to 5 x $10^{-8}$ torr with the nickel crystal at 300°C. Hydrogen ($H_2$) (Matheson, research grade) was then admitted into the chamber to a pressure of 0.5 torr, followed by evacuation with a sample temperature of 500°C. This $H_2$ exposure and evacuation was repeated and then CO (Matheson, research grade) was admitted with the sample at 350°C. A Raman spectrum was obtained from 40 to 4400 $cm^{-1}$ after each of these exposures, but no Raman bands were observed. After reduction of the CO pressure to 1 torr, and admission of $H_2$ to a total of CO + $H_2$ pressure of 4 torr, a Raman band was located which was centered at 80 $cm^{-1}$.

## Discussion

Figure 1 shows the results of scans at 1.5 $cm^{-1}$ resolution over a spectrum of 50 to 110 $cm^{-1}$.

The effect of $O_2$ (Matheson, research grade) on the band intensity at 80 $cm^{-1}$ is shown in Figure 2(a). The band

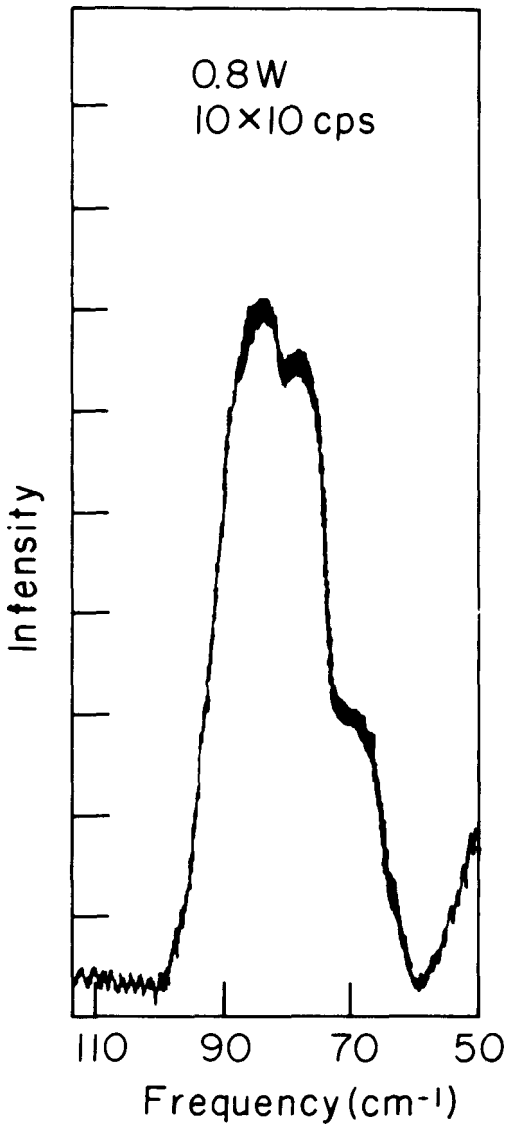


**Figure 1. The Raman bands observed after CO + $H_2$ adsorption onto Ni(111) at 350°C. The instrumental resolution was 1.5 $cm^{-1}$.**

intensity started to decrease at an $O_2$ pressure of $5 \times 10^{-3}$ torr with the nickel crystal at 350°C. However, heating the sample above 440°C caused the intensity to increase to within 92 percent of its original value. Evacuation and readmission of $O_2$ at a temperature of 350°C would not produce further intensity changes. Subsequent admission of $H_2$ into the evacuated chamber ($10^{-6}$ torr) with the same sample temperature continued to increase the intensity at 80 $cm^{-1}$ (Figure 2(b)). Then evacuation decreased this intensity by 15 percent while $O_2$ exposure continued to decrease the intensity at 80 $cm^{-1}$.

Figure 3 shows the intensity changes at 80 $cm^{-1}$ for the adsorption of CO on Ni(111) at 360°C after $O_2$ exposure and evacuation ($10^{-6}$ torr). Initially, the intensity decreased, but began to increase at approximately 1.2 torr CO pressure, and then decreased with evacuation. These results were repeatable, but the resultant intensity at 80 $cm^{-1}$ after each $H_2$ exposure was less than that in the preceding cycle if the sample temperature was kept below 400°C.

The monatomic FCC unit cell of nickel (space group Fm3m) should not possess Raman-active modes. Identification of the adsorbed species by characteristic vibrational frequencies was difficult due to the absence of other Raman modes which have similar intensity variations as that at 80 $cm^{-1}$. If modes other than the 80 $cm^{-1}$ exist, they would be on the order of $10^2$ less intense. It is possible that the band in the 80 $cm^{-1}$ region is due to a forbidden or defect-actuated Ni mode. In this case, the intensity decrease during $O_2$ exposure would be due to the formation of NiO, and subsequent $H_2$ or CO exposure would reduce the oxidized nickel surface. However, the appearance of this band coincided with $H_2$ + CO exposure, and hence it was assumed to result from the adsorption of these gases. Also, the effect of CO was not always an increase in intensity at 80 $cm^{-1}$; if CO was adsorbed after $H_2$, the intensity at 80 $cm^{-1}$ decreased.

It is known from LEED and Auger spectra that CO dissociates over Ni(111) at temperatures near 100°C, and in the process, forms a carbonaceous adlayer.[6] Auger studies have shown that such a carbon adlayer has bonding characteristics of metal carbides, and that a graphitic surface residue is formed during high-temperature treatment of this surface.[7] The oxidation of such a graphitic surface on Pt, which has the same crystal structure as Ni, produces $CO_2$ with high-temperature desorption (>400°C).[8] However, not all of the oxygen is removed with this treatment because CO is desorbed at 700°C. Such results indicate that the intensity decrease with $O_2$ exposure, as shown in Figure 2, is due to the addition of an $O_2$ layer on the adsorbed surface species. This reactivity to $O_2$ is limited to the 200 to 440°C temperature region because temperatures below 200°C have no effect on the intensity at 80 $cm^{-1}$, while above 440°C the oxygen is desorbed. That the intensity after 440°C heating is less than the initial value could be the result of the removal of surface carbon, partial destruction of the chemilayer symmetry and retention of oxygen. The inactivity of the resulting surface to $O_2$ does indicate that symmetry alterations have occurred. Similarly, after $H_2$ exposure, which increases the intensity at 80 $cm^{-1}$, the 40 to 110 $cm^{-1}$ region shows increased structural features, as in Figure 1, whereas after $O_2$ exposure the remaining Raman band is nearly symmetrical about 80 $cm^{-1}$.

After $O_2$ exposure, CO exposure is expected to reduce the oxygen adlayer.[9] The initial decrease of intensity (Figure 3) could result from random carbon deposition, or possibly from hydrogen removal. The latter possibility is considered because the adsorption of CO after $H_2$ causes a decrease in the intensity at 80 $cm^{-1}$. It is not definite that the chemilayer does not have bound hydrogen. Raman measurements of low-frequency modes for cyclic hydrocarbons (C/H from 1.25 to 2.0) show intense bands in the 40 to 120

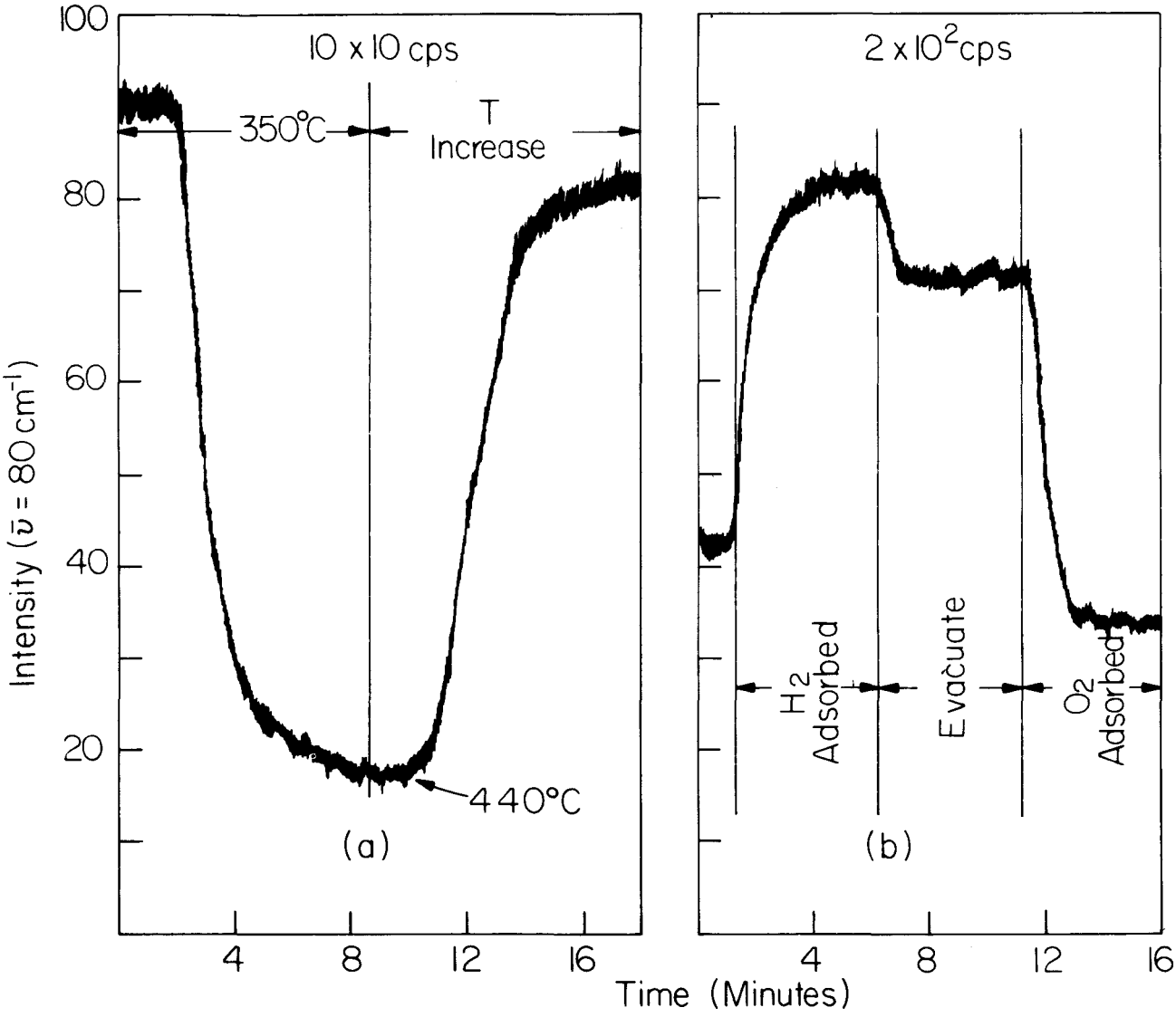


**Figure 2. (a) Effects of $O_2$ exposure on the intensity of the Raman band at 80 cm$^{-1}$. (b) Effects of $H_2$ exposure, evacuation and subsequent $O_2$ exposure on the intensity of the Raman band at 80 cm$^{-1}$. The sample temperature was 350°C.**

cm$^{-1}$ region. Such bands have been assigned to librational modes for $C_{10}H_8$ and $C_{14}H_{10}$.[10] The polarization characteristics of these modes are identical to what is observed for the 80 cm$^{-1}$ region in our spectra.

## Acknowledgment

We wish to thank the Institute for Mining and Minerals Research for the argon ion laser used in this work.

## References

1. R. P. Cooney, P. J. Hendra and M. Fleischmann, *J. Raman Spec.*, Vol. 6, 264 (1977).
2. G. Karagounis and R. Issa, *Nature* (Lond), Vol. 195, 1196 (1962), *Z. Electrochem*, Vol. 66, 874 (1962).
3. P. J. Hendra and E. J. Loader, *Trans. Faraday Soc.*, Vol. 67, 828 (1971).
4. M. L. Howe, K. L. Watters and R. G. Greenler, *J. Phys. Chem.*, Vol. 80, 382 (1976).
5. J. M. Stencel, D. M. Noland, E. B. Bradley and C. A. Frenzel, *Rev. Sci. Instr.*, in press.
6. G. A. Sargent, unpublished results.
7. R. J. Madix, *Catal. Rev.-Sci. Eng.*, Vol. 15, 293 (1977).

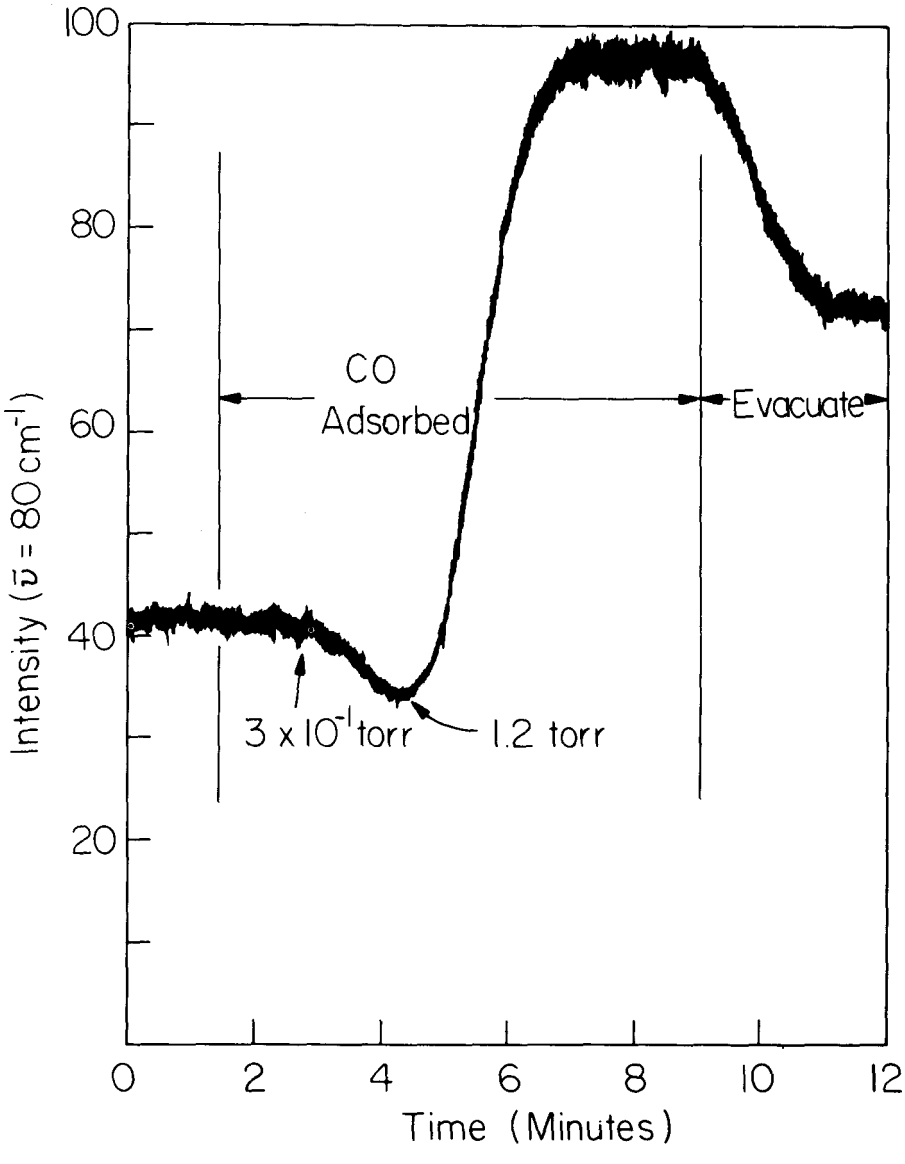


**Figure 3. Effects of CO exposure after $O_2$ exposure on the intensity of the Raman band at 80 cm$^{-1}$. The sample temperature was 360°C.**


8. F. P. Netzer and R. A. Willie, *J. Catalysis*, Vol. 51, 18 (1978).

9. F. A. Cotton and G. Wilkinson, *Advanced Inorganic Chemistry*, (Interscience, 1972), p. 890.

10. M. Suzuki, T. Yokoyama and M. Ito, *Spectrochim. Acta*, Vol. 24A, 1091 (1968).

# Ultrahigh Vacuum Chamber for Raman Studies of Gases Adsorbed on Metals

J. M. Stencel, D. M. Noland, E. B. Bradley
Department of Electrical Engineering
University of Kentucky
Lexington, Kentucky 40506

C. A. Frenzel
Coastal Sciences Associates
6900 Canal Blvd.
New Orleans, Louisiana 70124

## ABSTRACT

The ultrahigh vacuum chamber described is being used to study laser Raman spectra associated with gas adsorption on clean metal surfaces. The system enables sample temperatures from -85° to 600°C to be obtained, and besides surface cleaning capabilities associated with high-temperature oxidation or reduction, it incorporates an $Ar^+$ sputter gun for surface cleaning. Initial experiments of CO + $H_2$ adsorption of crystalline Ni surfaces are described and the effects of $H_2$ and $O_2$ exposure shown for the 80 $cm^{-1}$ band which results from CO + $H_2$ adsorption.

## INTRODUCTION

Analysis of the characteristics of adsorbed monolayers on smooth metal surfaces has been accomplished mainly by using LEED, ESCA, Auger, and infrared reflectance spectroscopy. Recently the first Raman spectrum of monomolecular layers adsorbed on smooth electrode surfaces has been reported.[1] Such studies show that the Raman effect can be very useful in determining adsorbate–adsorbent interactions and that it could be valuable for describing adsorbed surface species associated with catalyzed reactions. We describe an experimental chamber which was designed and built to study adsorbed surface species associated with catalyzed reactions which produce methane.

The intensity of Raman scattered radiation is inherently low and hence measurements of adsorbed monolayers are difficult to acquire. As early as 1962 Raman spectra were reported for hydrocarbons sorbed to silica,[2] while more recently, various experimenters have used Raman spectroscopy for studying adsorbed species on high-area adsorbents.[3–5] Similar studies on a 700-$m^2/g$ adsorbent have shown detectable Raman bands for 4% of a monolayer of $CCl_4$ while a 50-Å polystyrene film on Ag has also been investigated.[6] These studies indicate that monomolecular layers on smooth metal surfaces should be detectable if a maximum amount of the Raman scattered radiation is collected and efficiently transferred to the Raman spectrometer.

Raman data can provide identification and structural information of adsorbed species of any molecular weight, which can then be correlated with the complementary information obtained from infrared analysis. However, a complete description of the surface interaction relies on knowing the condition of the adsorbent surface before exposure to any adsorbate. This is usually complicated by surface contamination which can occur during sample preparation. Usually contaminants can be removed by high-temperature oxidation or reduc-

tion but this treatment may result in surface restructuring or monolayer formation of some unwanted species. Thus, a Raman sample chamber with traditional gas-surface cleaning and ultrahigh vacuum capabilities are minimal requirements for studying chosen adsorbate–adsorbent reactions. Extensions of these systems which can provide more complete data are low-temperature capabilities for studying physadsorbed states and alternate surface cleaning methods such as $Ar^+$ bombardment.[7] It is also advantageous to have information on the same surface from different research areas, such as Auger spectroscopy, which is specifically a surface analysis tool and typically can monitor fractions of monolayer coverages.

## I. DESIGN

In Fig. 1 is shown an overall view of the adsorption chamber with the associated gas handling section. All tubing and valves in this system are stainless steel which contain Cu gaskets in the joints of the ultrahigh vacuum portion (1) and Teflon ferrules in the high-vacuum portion (2). The system is mounted on a movable cart to allow transportation between Raman and infrared spectrometers while the adsorption chamber C with associated vacuum pumps and gauges is fastened to a vertically adjustable arm on the cart.

During adsorption experiments gases of interest are admitted to the mixing manifold A which has been evacuated to $10^{-4}$ Torr with the sorption pump B. The mixer is then flushed with the gas to be adsorbed, repumped to $10^{-4}$ Torr, and refilled to a known pressure to ensure that only high-purity gases will enter the adsorption chamber C. The sorption pump is also used to rough-pump C after which the ion pump D is used to obtain pressures below $10^{-4}$ Torr. Gases in A are then leaked into C through a variable leak valve E while the gas pressure in the chamber is continually monitored by ion and thermocouple gauges. The sample onto which these gases are adsorbed is held in a stainless steel holder which is attached via a tungsten rod to a rotary motion feedthrough F. Rotating the sample from the position in which the $Ar^+$ sputter gun I is used to clean the surface, to the position between the viewports G-G′, places the sample in the laser beam for spectral acquisition. Alternately, the sample can be reduced or oxidized to eliminate surface contaminants while being heated by a resistive element which is connected to the electrical feedthrough H. Iron/Constantan thermocouples are used to monitor the sample temperature and are also connected to the electrical feedthrough *H*.

In Fig. 2 is shown an enlarged view of the adsorption chamber when the sample is in position for data acquisition. The chamber is 18 cm long and has a diameter of 15 cm. Both end plates of the cell, shown in Fig. 3, are removable to enable sample handling and adjustments of the various experimental feedthroughs. Cu gaskets are used for sealing each end and the feedthroughs and allow bakeout of the chamber to 250°C. Two glass viewports G and G″ of 3.8 cm diameter allow impingement of the $Ar^+$ laser radiation normal or near-parallel to the sample surface K. Raman scattered radiation is collected by a Cassegrain aluminized spherical mirror L which has a diameter of 5 cm and a focal length of 14 cm. This radiation then exits through viewport G′ and enters a Jarrell–Ash 25–300 spectrometer.

The stainless-steel sample holder is made as small as possible to accommodate cylindrical samples of approximately 0.8 cm diameter. Thermocouple and the heating

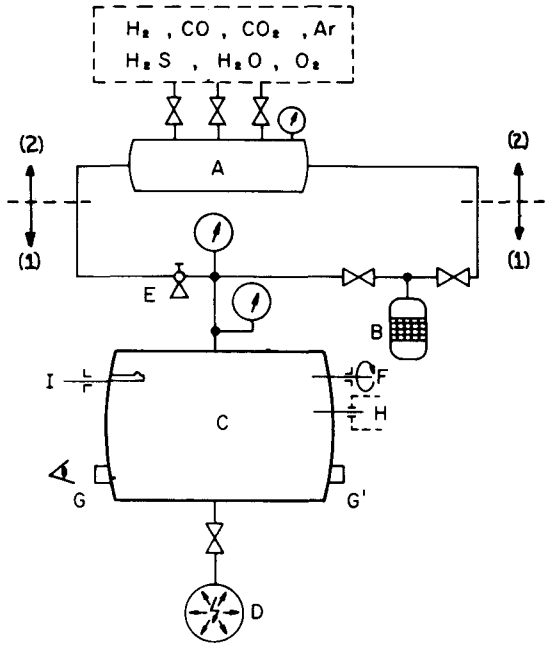


**Fig. 1. Overall view of the gas handling and adsorption system used for laser Raman studies of adsorbed gases on metal surfaces.**

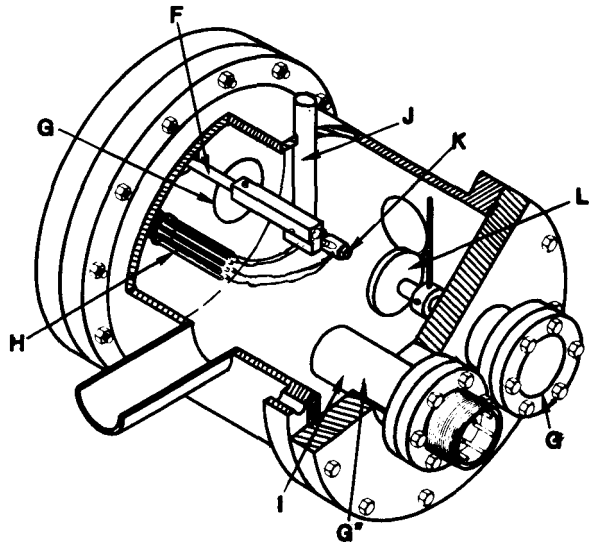


**Fig. 2. Detailed view of the adsorption chamber. The functions of the labeled parts are described in the text.**

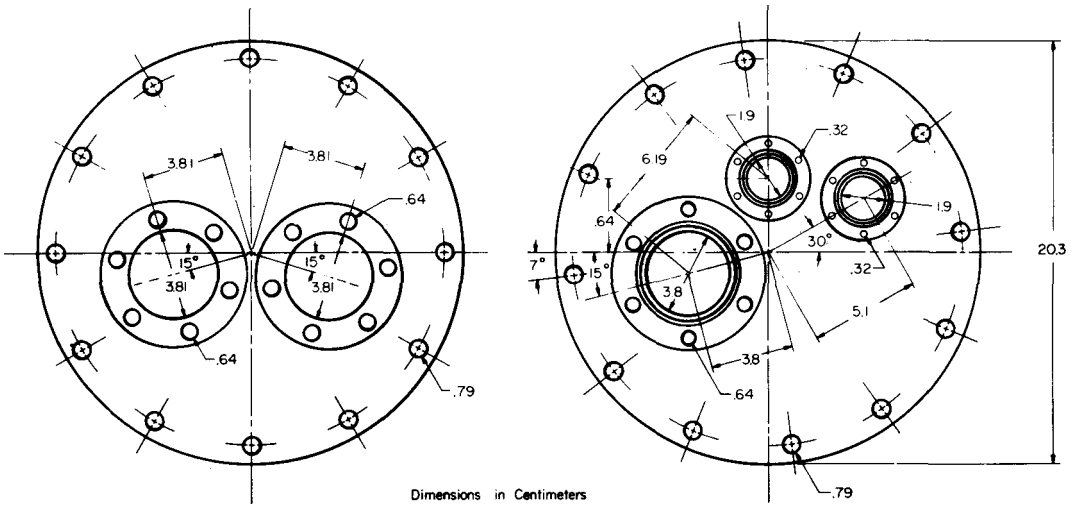


**Fig. 3. Detailed exterior view of the end plates which are attached onto the adsorption chamber.**

element leads lie close to the front and back, respectively (front being toward the mirror), of a 0.32-cm-diam tungsten rod which connects the sample holder to the rotary motion feedthrough F. In the sample position this tungsten rod is forced against the surface of the stainless-steel "cold-finger" J. The length of the cold-finger within the cell is such that it does not interfere with collection or transfer of the Raman scattered radiation as is shown in Fig. 4. This system is still being used for preliminary investigations and hence the chamber bakeout has not been completed. However, a pressure of $7 \times 10^{-9}$ Torr has been achieved and sample

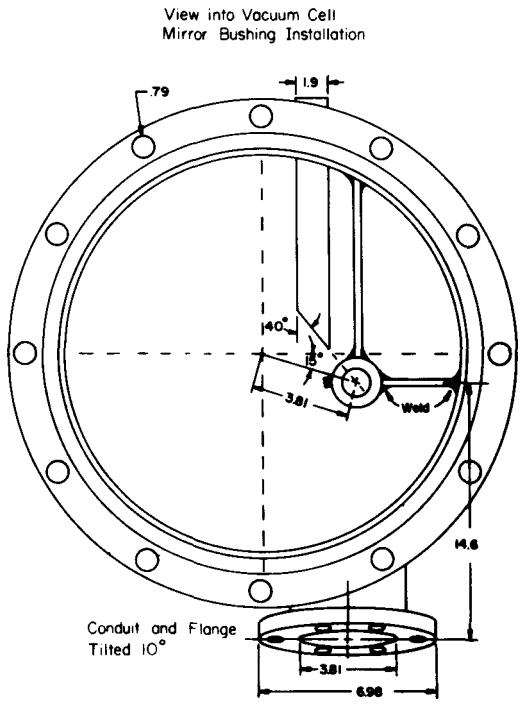


**Fig. 4. View looking into the adsorption chamber showing the cold-finger and Cassegrain mirror support.**

temperatures from −85° to 600°C have been obtained at $5 \times 10^{-8}$ Torr with 800 mW power incident on the sample.

## II. EXPERIMENTAL RESULTS

A single-crystal Ni sample which had been cut and polished to within ±1° of its (111) plane was placed in the sample holder of the chamber. The chamber was evacuated to $5 \times 10^{-8}$ Torr for a 2-day period while the sample was heated at 300°C. $H_2$ (Matheson, Research Grade) was admitted and kept in the chamber at 0.5 Torr for 1 h while the sample temperature remained at 300°C. The chamber was evacuated to $8.5 \times 10^{-8}$ Torr, and $H_2$ readmitted to 0.5 Torr with the Ni sample at 500°C. After 1 h the chamber was evacuated to $9 \times 10^{-8}$ Torr and a spectral scan was run from 40 to 4000 $cm^{-1}$ using 800 mW of unfocused $Ar^+$ laser light at 4880 and 5145 Å. No Raman bands were observed.

After this $H_2$ treatment, CO (Matheson, Research Grade) was admitted to 1 atm with the sample at 350°C. A spectrum was obtained from 40 to 4000 $cm^{-1}$ but no Raman bands were observed. The chamber was evacuated to a CO pressure of 1 Torr, $H_2$ admitted to increase the pressure to 4 Torr, and a spectrum was recorded using the 4880-Å line with the sample at 30°C. An intense Raman band appeared at 80 $cm^{-1}$ which had a bandwidth at ½ height of approximately 25 $cm^{-1}$. The adsorbed species which causes this band is not known, but it is very stable since heating to 500°C with evacuation to $5 \times 10^{-8}$ Torr over a 2-day period decreased the band intensity by only 30%.

After this evacuation $H_2$ was admitted into the chamber to 0.3 Torr with the sample at 300°C. In Fig. 5(a) is shown the intensity changes of the 80 $cm^{-1}$ band as a function of time which result from this $H_2$ exposure. $H_2$ has increased its intensity by 225% and the intensity then decreases by 10% as a result of evacuation. After the chamber had been evacuated to $5 \times 10^{-7}$ Torr, $O_2$ (Matheson, Research Grade) was admitted to 0.3 Torr

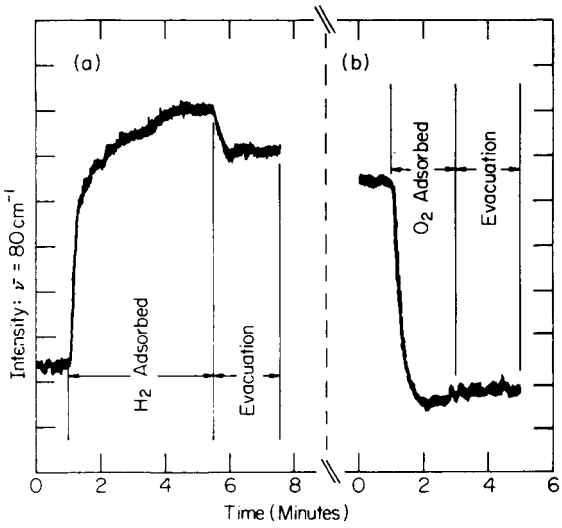


**Fig. 5. Raman intensity changes observed for (a) $H_2$ adsorption at 300°C, and (b) $O_2$ adsorption at 300°C, for the (111) Ni plane.**

with the sample at 300°C. As noted in Fig. 5(b) the 80 $cm^{-1}$ band intensity decreased by 72% as a result of $O_2$ exposure. At this time it is impossible to describe the adsorbed species which is responsible for this Raman band. The $H_2$ and $O_2$ adsorption experiments indicate, however, that the effects of less than $1.0 \times 10^{-9}$ mol $H_2$ and $5.0 \times 10^{-11}$ mol $O_2$ can be readily detected. Experiments are continuing in which the effects of $Ar^+$ bombardment and adsorption of other gases are being monitored to describe more fully gas adsorption onto clean Ni surfaces.

## ACKNOWLEDGEMENT

We wish to thank the Institute of Mining and Minerals Research, University of Kentucky, for the Argon ion laser used in this work. This work was supported by ERDA Contract No. Ex-76-C-01-2229.

## REFERENCES

1. R. P. Cooney, P. J. Hendra, and M. Fleischmann, **Journal of Raman Spectroscopy**, Vol. 6, pp. 264, 1977.

2. G. Karagounis and R. Issa, **Nature**, Vol. 195, pp. 1196, London, 1962; **Z. Electrochem.**, Vol. 66, pp. 874, 1962.

3. P. J. Hendra and E. J. Loader, **Transactions of the Faraday Society**, Vol. 67, pp. 828, 1971.

4. E. Buechler and J. Turkevich, **Journal of Physical Chemistry**, Vol. 76, pp. 2325, 1972.

5. I. D. M. Turner, S. O. Paul, E. Reid, and P. J. Hendra, **J. C. S. Faraday Transactions**, Vol. I 72, pp. 2829, 1976.

6. M. L. Howe, K. L. Watters, and R. G. Greenler, **Journal of Physical Chemistry**, Vol. 80, pp. 382, 1976.

7. C. Brucker and T. Rhodin, **Journal of Catalysis**, Vol. 47, pp. 214, 1977.

# Structural Changes in a Sulfur-Resistant Methanation Catalyst as Determined from Infrared Spectra

J. M. Stencel, R. E. Heinz, and E. B. Bradley
Department of Electrical Engineering
University of Kentucky
Lexington, Kentucky 40506

## ABSTRACT

The infrared spectrum of a sulfur-resistant $NiO/Cr_2O_3/MgAl_2O_4$ methanation catalyst is presented and compared to the spectra of the catalyst after it was reduced, sulfided, and tested for methanation activity. The molecular structure of the catalyst is shown to be represented by NiO and MgO dispersed in a quasitridimensional Cr—O—Al network. Reduction and sulfiding reorders this network and alters the $AlO_n$ coordination while reducing $Cr^{6+}$ to $Cr^{3+}$ or $Cr^{2+}$. The sulfided and methanation-tested catalyst has intense sulfate absorption indicative of sulfur which is coordinated with NiCr and/or NiMg sites.

## INTRODUCTION

This work is part of a research program to characterize the structure of methanation catalysts and relate structural features to methanation activity. Infrared studies are used to characterize molecular bonding in the catalyst from the as-prepared form to the deactivated condition.[1]

The use of coal to produce high-grade methane via catalytic conversion relies on the retention of high (>70%) conversion rates of $CO + 3H_2 \rightarrow CH_4 + H_2O$ over extended time periods. However, sulfur from the coal which is transferred to the catalyst bed in the form of $SO_2$ or $H_2S$ and adsorbed on methanation sites in sulfide form causes irreversible catalyst deactivation. For example, methanation tests have shown that although $NiO/SiO_2$ and $NiO/Al_2O_3$ catalysts produce over 90% conversion of CO to $CH_4$, less than 20% conversion occurs after sulfiding these catalysts.[2] This poisoning, which is related to a decrease in the number of active sites per unit volume, occurs also during the long-term deactivation mechanism, sintering.[3] Such poisoning reconstructs the active catalytic surface, as does adsorption of sulfur on Pt surfaces.[4] If we assume negligible interactions between the active metal surface and the support material, such reconstruction should not affect appreciably the coordination of the support. However, it is shown that reduction, sulfiding, and methanation testing alter the infrared vibrational frequencies of the support material.

We report the infrared spectra of a coal methanation catalyst which has been shown to have a suitable methanation conversion rate (≈70%) even after sulfur poisoning.[2] The manufacturer represents the catalyst as $NiO/Cr_2O_3/MgAlO_4$, but the spectra of the as-prepared, nonreduced catalyst is not just the spectra of these components; rather, other molecular bonding is present also. The spectrum of the as-prepared catalyst is compared to that obtained after this catalyst had been subjected to temperatures (350°C), pressures (30 atm) and gas compositions typical of the Lurgi coal gasification process and after being exposed to sulfur. It is shown that molecular reordering of the support material occurs during reduction of the catalyst and during the methanation reaction. Effects of sulfur adsorption are also compared for the sulfided and metanation-tested catalysts which indicate sites and coordination of sulfur adsorption.

## I. EXPERIMENTAL

The $NiO/Cr_2O_3/MgAl_2O_4$ catalyst was supplied by United Catalysts, Inc., Louisville, KY. The catalyst is commercially available and so the exact preparation methods are proprietary. However, the preparation does include precipitation of Ni, Cr, and Mg salts with subsequent washing and calcination at 300°C. In Table I are shown some physical properties of this catalyst.

Catalyst samples were obtained in pellet form. They consisted of: (1) the as-prepared $NiO/Cr_2O_3/MgAl_2O_4$ catalyst, (2) the reduced catalyst which had been sulfided in a laboratory methanator, and (3) the reduced catalyst which had been sulfided and subsequently tested for its methanation activity. The second sample was removed from the testing chamber after being cooled with dry $N_2$ and it was sealed in a container under positive $N_2$ pressure. Sample (3) was also cooled in the laboratory methanator with a dry $N_2$ purge, but it was sealed in a container under normal room atmosphere conditions.

Table I. Composition and Surface Area of the NiO/$Cr_2O_3$/$MgAl_2O_4$ Methanation Catalyst.

| Surface Area of Catalyst ($m^2$/g) | | Weight Percents of Constituents | |
|---|---|---|---|
| New | 191 | NiO | 49.7 |
| Sulfided; methanation tested | 96 | $Cr_2O_3$ | 25.3 |
| | | $MgAl_2O_4$ | 25.0 |

Each catalyst sample was powdered with mortar and pestle in a glove box purged with dry $N_2$. This powder was then mixed with KBr to concentrations of approximately 1% by weight and translucent pellets were pressed under 20 000 psi with a $N_2$ purge at all times. The resulting transmission pellet was placed in a sample holder which had KRS-5 windows, and the pellet was purged with $N_2$ during spectral acquisition. Perkin-Elmer 621 and 337 spectrophotometers were used to obtain infrared spectra from 4000 to 400 $cm^{-1}$. The instrumental resolution was approximately 6 $cm^{-1}$ in the 1300 to 400 $cm^{-1}$ region while larger slit widths were used for samples (2) and (3) from 4000 to 1300 $cm^{-1}$ to compensate for their decreased transmission in this region.

Reference spectra of various substances were obtained to facilitate assignments of the absorption bands which were observed. These reference spectra included the spectra of spectrophotometric grade NiO and $Al_2O_3$ and technical grade $NiSO_4 \cdot 6H_2O$, $NiAl_2O_4$, $MgAl_2O_4$, $K_2Cr_2O_7$, $Cr(OH)_3$, $Cr_2(SO_4)_3 \cdot 15H_2O$, and $Cr_2O_3$. Mixtures of some compounds were made in approximately a 1:1 weight ratio to allow spectral acquisition of NiO/$Al_2O_3$, NiO/$MgAl_2O_4$, and NiO/$NiAl_2O_4$. Spectra were also obtained for a NiO/$Cr_2O_3$/$MgAl_2O_4$-Nujol oil slurry which had poor transmission characteristics due to scattering effects of the catalyst.

## II. ANALYSIS

In Fig. 1(a) is shown the 1300 to 400 $cm^{-1}$ spectral region of the as-prepared NiO/$Cr_2O_3$/$MgAl_2O_4$ catalyst. Absorption from 850 to 500 $cm^{-1}$ is similar to that seen

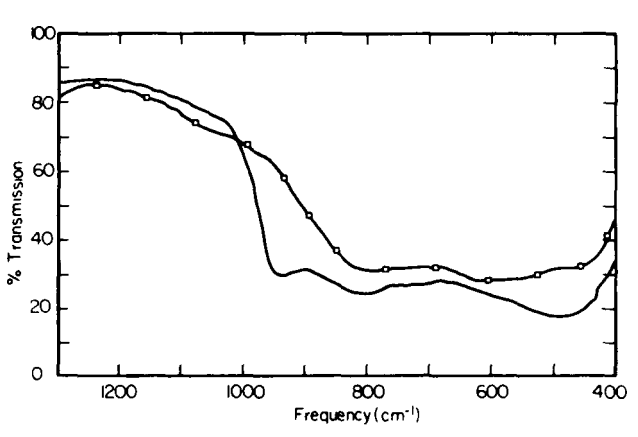


Fig. 1. (a) ——, infrared spectra of the as-prepared NiO/$Cr_2O_3$/$MgAl_2O_4$ catalyst in KBr (2.1 mg/$cm^2$); (b) □—□, infrared spectra of NiO/$Al_2O_3$ (2.0 mg/$cm^2$).

for amorphous $Al_2O_3$,[5] but the broad unstructured bands do not coincide with what is expected for the spinel $MgAl_2O_4$.[6,7] The absorption characteristics of NiO/$Al_2O_3$ do, however, closely approximate that which is observed for the catalyst in this region [Fig. 1(b)]. The increased relative absorption which is evident for the catalyst near 470 $cm^{-1}$ implies that modes other than Al—O and Ni—O vibrational modes contribute to the band intensity in this region. The Cr—O vibrational modes associated with $Cr_2O_3$ would provide absorption intensities mainly in the 700 to 500 $cm^{-1}$ region.[8] Dichromates have intense bands from 950 to 900 $cm^{-1}$ due to Cr—O stretching modes and have similarly intense modes from 800 to 700 $cm^{-1}$ which are the result of the antisymmetric Cr—O—Cr stretching mode.[9,10] The absence of this enhanced absorption from 800 to 700 $cm^{-1}$ in Fig. 1(a), the similarities of the absorption seen in Fig. 1, (a) and (b), and the enhanced relative absorption which is observed from 550 to 400 $cm^{-1}$ for NiO/$MgAl_2O_4$ indicate that Ni—O, Mg—O, and Al—O vibrational modes can describe the infrared spectra of the catalyst from 850 to 400 $cm^{-1}$.[11,12]

The infrared band centered at 930 $cm^{-1}$ is associated with Cr—O vibrational modes. It is believed that the oxygen is tetrahedrally coordinated to the Cr, as in $CrO_4^{=}$; such symmetry should not contribute appreciable infrared absorption due to Cr—O vibrational modes in the 850 to 500 $cm^{-1}$ region. Far infrared data which we have obtained on a RIIC FS-520 interferometer from catalyst/CsI pellets and catalyst/Nujol mulls on polyethylene show no major bands from 350 to 150 $cm^{-1}$. The absence of distinct bands within this region is similar to that observed for $Al_2(CrO_4)_3$.[9] However, the relatively high Cr—O stretching frequency, 20 to 40 $cm^{-1}$ larger than that observed for $MgCrO_4$ or $Al_2(CrO_4)_3$, could be the result of Cr—O and Al—O interactions which increase slightly the Cr—O stretching frequency. Condensed $CrO_4$ and $AlO_4$ units would be expected to cause increased Cr—O stretching frequencies.[7] Such an interpretation would indicate a quasi-tridimensional chromate or possibly Cr—O—Al network. The broad absorption bands in this region defy definite conclusions as to these possibilities.

In Fig. 2, (a) and (b), are shown the infrared spectra from 1300 to 400 $cm^{-1}$ of the catalyst in the as-prepared form and after it was reduced at 300°C and then exposed to $H_2S$ at 300°C. Band intensity differences of the two spectra from 800 to 400 $cm^{-1}$ are due to the reduced concentration needed for the sulfided catalyst to enable sufficient transparency of the sample in the 4000 to 2000 $cm^{-1}$ region. However, it is immediately apparent that the sulfided catalyst has been altered appreciably in terms of the chromate absorption at 930 $cm^{-1}$. Electron spectroscopy for chemical analysis (ESCA) data shows that sulfur has been adsorbed, but infrared bands due to sulfide species are not observable in this frequency region. When the sulfided catalyst is exposed to atmosphere a band does appear at 1120 $cm^{-1}$, as is shown in Fig. 2(c). This band results from the oxidation of the adsorbed sulfur and its frequency is characteristic of a sulfate species. The intensity and shape of the 1120 $cm^{-1}$ band does not change during extended atmospheric exposure of the catalyst at a temperature of 25°C. However, as shown in Fig. 2(d), heating of the catalyst in air at 250°C increases the multiplicity and intensity of the infrared absorption in the 1100 $cm^{-1}$ region. The bands which appear at 1180, 1120, and 1070 $cm^{-1}$ are expected to result from temperature-dependent oxidation effects on sulfur

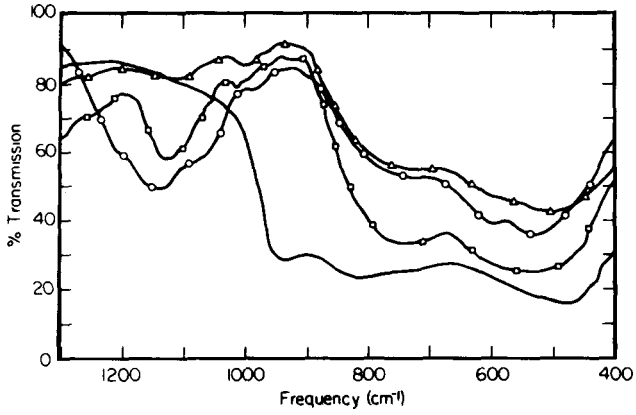


**Fig. 2. Infrared spectra of: (a) ——, the as-prepared $NiO/Cr_2O_3/MgAl_2O_4$ catalyst in KBr (2.1 mg/cm$^2$); (b) Δ——Δ, the reduced and sulfided catalyst obtained under $N_2$ atmosphere (1.5 mg/cm$^2$); (c) □——□, the reduced and sulfided catalyst after exposure of the catalyst to atmosphere at 25°C (1.6 mg/cm$^2$); (d) ○——○, the reduced and sulfided catalyst after heating the catalyst to 250°C (1.9 mg/cm$^2$).**

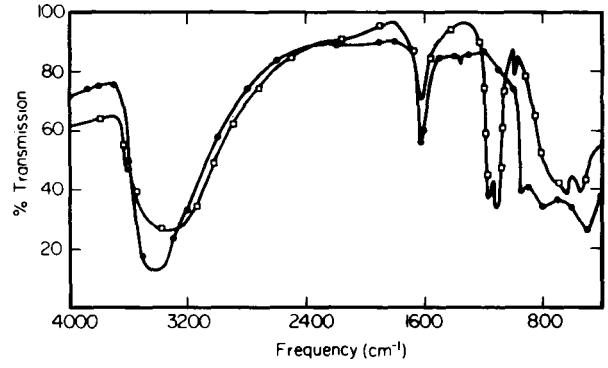


**Fig. 3. The infrared spectra of: (a) ●——●, the as-prepared $NiO/Cr_2O_3/MgAl_2O_4$ catalyst in KBr (2.1 mg/cm$^2$); (b) □——□, the reduced, sulfided and methanation tested catalyst (2.0 mg/cm$^2$).**

sites which have different coordination, site symmetry, or metal-sulfur bond strengths. The absorption near 600 $cm^{-1}$ is more intense relative to that at 800 $cm^{-1}$ in Fig. 2(d) and this, along with the band multiplicity in the 1100 $cm^{-1}$ region, indicates species of the form $X_2(SO_4)_3$ as in $Cr_2(SO_4)_3$. These spectral results also show that the sulfur species associated with the 1120 $cm^{-1}$ absorption is the most readily oxidized.

In Fig. 3 are shown the infrared spectra from 4000 to 400 $cm^{-1}$ of the unused and the sulfided, methanation-tested catalyst. The pre-sulfiding included 6% $H_2S$ in a $H_2$ stream which flowed through the catalyst bed for approximately 1 h while subsequent methanation tests were run for up to 16 h. Bands which are observed from 3600 to 3000 $cm^{-1}$ and at 1640 $cm^{-1}$ are due to adsorbed $H_2O$. It is expected that the $H_2O$ was adsorbed during the exposure to air and is not directly related to the methanation reaction. However, the shoulder at 3620 $cm^{-1}$, which is due to an $OH^-$ vibrational mode, is only observed in the methanation-tested catalysts. By comparison with previous infrared spectra, which were obtained in this laboratory on methanation-tested silica and alumina-supported catalysts containing Ni, it is thought that the 3620 $cm^{-1}$ band is due to a terminal hydroxyl attached to a Ni site. The 1135 and 1100 $cm^{-1}$ bands are due to sulfate vibrational modes but are at different frequencies than those observed for the sulfided sample in Fig. 2. It is not completely evident, upon comparison of Fig. 2, (c) and (d), with Fig. 3(b), that oxidation effects at 25°C after removal of the cooled catalyst from the methanation test bed could cause the multiplicity and the intensity of the 1135 and 1100 $cm^{-1}$ absorption. The concentration of sulfide and sulfate species on a catalyst surface relative to that in the bulk of the catalyst can be obtained with ESCA as the surface atoms are sputtered (milled) away during $Ar^+$ sputtering. Analysis of ESCA spectra obtained as a function of $Ar^+$ milling time show that the ratio of sulfur/oxygen is less at the surface as compared to the bulk in the sulfided catalyst even after exposure to air. However, the sulfided and methanation-tested catalyst has an approximate equal sulfur/oxygen ratio throughout the catalyst and the ESCA sulfur signal indicates two distinct sulfur species. This information coincides with the doublet nature of the infrared sulfate bands in Fig. 3(b). Also, the narrow absorption at 990 $cm^{-1}$, and the small absorption peak at 630 $cm^{-1}$, which has to be caused by a very narrow band in order to be seen within the background absorption, are further evidence of two distinct sulfur sites. Such infrared bands are characteristic of $XY(SO_4)_2$ compounds.[9]

The chromate absorption at 930 $cm^{-1}$ for the as-prepared catalyst is absent for the methanation-tested sample in Fig. 3(b), as was observed for the reduced and sulfided catalyst of Fig. 2. Band intensities in the 820 $cm^{-1}$ region are also decreased, as was observed to a lesser degree in Fig. 2. This change is thought to be due to the destruction of the condensed $AlO_4$ and $CrO_4$ units along with the corresponding creation of isolated $AlO_4$ and/or $AlO_6$ units. Simultaneously, the decrease in band intensity from 520 to 400 $cm^{-1}$ in Fig. 3(b), which is not observed in Fig. 2, indicates that the amount of NiO and MgO has decreased. This decrease in the metal oxides would then enable the creation of $NiMg(SO_4)_2$ or $NiCr(SO_4)_2$ coordination during the sulfide/methanation tests. The spectra of the catalyst which had been reduced and sulfided does not show this type of sulfate coordination. Thus, it is expected that the methanation reaction promotes the oxidation of the sulfided NiCr or NiMg sites. If a cooperative effect is operational between the active metal Ni and the support metals Cr and Mg in which the oxidation of the adsorbed sulfur allows the Ni orbitals to redistribute in an active methanation symmetry, then the methanation reaction would continue even though the concentration of sulfur would be great enough in many catalysts to poison the reaction completely. Oxidation of the sulfur would decrease the Ni—S bond strength; this decrease could explain the evolution of sulfur from the catalyst bed during the methanation testing.[2] It is fair to note that this hypothesis is dependent upon whether the intense sulfate bands in Fig. 3(b) are due to the methanation reaction and not due to the oxidation effects of atmospheric exposure. Presently the experimental data do support this hypothesis.

The role of the support material in heterogeneous

catalysis has not been studied thoroughly but can be investigated by infrared spectroscopy.[13] The present results show that the support material is not an inert substance; it can play an important role in catalytic activity and stability. The ability to synthesize catalysts with long-term activity is indicated in the fact that a sulfided $NiO/MgAl_2O_4$ catalyst had very poor methanation activity compared to that observed for the $NiO/Cr_2O_3/MgAl_2O_4$ catalyst which had similar sulfide treatment.[2] However, the complete description of the molecular constituents and coordination is important in understanding the role of the support.

## III. CONCLUSIONS

We have shown that initially the chromium is in the $Cr^{VI}$ state which is reduced to $Cr^{3+}$ or $Cr^{2+}$ during normal methanation use. The fact that sulfur does not completely poison the active metal sites could be associated with a cooperative effect in which the Ni, Cr, and Mg are associated to create stable methanation sites. Such reordering occurs not only during the reduction of the catalyst, but also during the catalytic run.

## ACKNOWLEDGMENTS

This work was supported by ERDA Contract EX-76-C-01-2229. The authors wish to thank P. J. Reucroft and R. B. Shalvoy for their valuable discussion on the ESCA spectra of these catalysts. Thanks are also extended to A. Hausberger of United Catalysts, Inc., for the methanation activity data of these catalysts.

## REFERENCES

1. J. Stencel and E. Bradley, **Applied Spectroscopy**, Vol. 32, pp. 496, 1978.
2. A. Hausberger, United Catalysts, Inc., Louisville, KY, private communication.
3. M. A. Vannice, **Catal. Rev. Sci. Eng.**, Vol. 14, pp. 153, 1976.
4. G. A. Somorjai, **Journal of Catalysis**, Vol. 27, pp. 453, 1972.
5. I. I. Plyusnia, **Journal of Applied Spectroscopy**, Vol. 20, pp. 212, 1974.
6. S. D. Ross, **Inorganic Infrared and Raman Spectra**, McGraw-Hill, New York, p. 116, 1972.
7. P. Tarte, **Spectrochimica Acta**, Vol. 23A, pp. 2127, 1966.
8. R. Marshall, S. S. Mitra, P. J. Gielisse, J. N. Plendl, and L. C. Mansur, **Journal of Chemical Physics**, Vol. 43, pp. 2893, 1965.
9. R. A. Nyquist and O. Kagel, **Infrared Spectra of Inorganic Compounds**, Academic Press, New York, pp. 293-297, 319-329, 1971.
10. H. Stammreich, D. Bassi, O. Sala, and H. Siebert, **Spectrochimica Acta**, Vol. 13, pp. 192, 1958.
11. O. Kammori, K. Sato, and N. Yamaguchi, **Jpn. Anal.**, Vol. 16, pp. 1050, 1967.
12. N. T. McDevitt and W. L. Baun, **Spectrochimica Acta**, Vol. 20, pp. 799, 1964.
13. L. H. Little, **Infrared Spectra of Adsorbed Species**, Academic Press, New York, pp. 205-210, 1966.

# Infrared Spectra of Some Nonreduced Methanation Catalysts

**Eugene B. Bradley and John M. Stencel**
Department of Electrical Engineering and
Institute for Mining and Minerals Research
University of Kentucky
Lexington, Kentucky 40506

## ABSTRACT

The infrared spectra (4000 to 400 $cm^{-1}$) of two commercial, nonreduced methanation catalysts are recorded and interpreted. The catalysts were prepared as mixtures of (a) nickel in a silica support, and (b) nickel in an alumina support. Graphite was added to these mixtures as a binder to facilitate pressing of catalyst pellets for commercial use. It is revealed in the spectra of the catalysts that although (a) is prepared to have a simple NiO/$SiO_2$ composition, the silica support is not of the form $SiO_2$; rather, the spectral characteristics are similar to those found for linear chain silicates. In (b) the Al—O vibrations are characteristic of amorphous $Al_2O_3$, and $H_2O$ is tightly bound in the pellet. The $CO_3^=$ ion is present in both (a) and (b). It is not bound to Ni in either (a) or (b), but is bound in the silicate structure of (a) and associated with Al in (b). The presence of the ion cannot be explained by only *in situ* generation from atmospheric $CO_2$ and $H_2O$, but its presence must be due to residual $CO_3^=$ from the catalyst preparation.

## INTRODUCTION

A research program to characterize the surface structure of methanation catalysts and relate structural features to catalytic activity is being carried out using surface characterization techniques such as electron spectroscopy for chemical analysis, LEED, Auger spectroscopy, laser Raman and infrared spectroscopy, and x-ray diffraction. As part of the first phase of this program infrared absorption studies are being made in order to characterize the structure of methanation catalysts before reduction, after reduction, after exposure to CO and $H_2$ in a methanation reactor, and after exposure to sulfur in a methanation reactor.

We report the infrared spectrum (4000 to 400 $cm^{-1}$) of two commercial nonreduced methanation catalysts. These spectra are necessary for correlation later in the program with reduced catalysts which have been exposed in a methanation reactor and reduced catalysts which have been poisoned by sulfur in the synthesis gas stream. Interestingly, the infrared spectra of these catalysts are not just the spectra of the components of the catalyst as stated by the manufacturer; rather, other compounds are present in the mixture which are discussed in relation to the catalyst preparation method.

## I. EXPERIMENTAL

The methanation catalysts used in this investigation were supplied by United Catalysts, Inc., Louisville, KY. The alumina support catalyst is prepared by precipitation of nickel and aluminum salts with sodium carbonate. The precipitate is washed to eliminate Na and calcined 8 to 16 h at 500°F. The resulting material is finely ground and mixed with $H_2O$ and graphite is added. Pellets of this mixture are then pressed and calcined at 500°F. A similar technique is employed to produce the silica support catalyst. The chemical and physical properties of these catalysts, along with the measured methanation activity, are shown in Table I.

To obtain infrared spectra of the nonreduced catalyst pellets we powdered them with a mortar and pestle and a small quantity of the powder was mixed with KBr and

**Table I. Composition of the Coprecipitated Methanation Catalysts.**

| Manufacturer's Designation | C150-1-01 ($NiO-SiO_2$) | C150-4-03 ($NiO-Al_2O_3$) |
|---|---|---|
| Weight percent of Ni | 51.7 | 55.6 |
| Weight percent of C | 2.9 | 2.7 |
| Weight percent of support | 45.4 ($SiO_2$) | 41.7 ($Al_2O_3$) |
| $m^2/g$[a] | 211 | 177 |
| NiO crystal size (Å) | 30 | 40 |
| Methanation activity[b] | 90% | 95% |

[a]Total pore surface area.

[b]Weight percent of CO converted to $CH_4$ (in the absence of sulfur poisoning).

ground in a "Wig-L-Bug." The ground mixture was then compressed under 20,000 lb./in.$^2$ to a translucent pellet. Spectra which are reported were obtained in transmission from these pellets using Perkin Elmer 621 and 337 spectrophotometers. Heating of these samples was done in a high temperature furnace placed inside a glove box which was purged with dry $N_2$. The heated samples were then mounted in a sample holder which allowed the $N_2$ purge to be continued throughout the spectral scan. Spectra which were obtained from the powdered catalysts in Nujol oil were identical to those reported except for absorption due to the Nujol.

For the purpose of comparison, the infrared spectra of NiO, $SiO_2$, $Al_2O_3$, $NiSiO_3$, and $Na(OH)_2AlCO_3$ were obtained. The sample of NiO was obtained from Apache and it is given as 99.999% pure with respect to other metals. An electron spectroscopy for chemical analysis scan showed it to consist of trivalent and divalent Ni; thus, it was a mixture of NiO and $Ni_2O_3$. The samples of $SiO_2$ and $Al_2O_3$ were obtained from Johnson Matthey Chemicals, Ltd., London. These compounds were "grade one" which corresponds to an impurity level of less than 10 parts in $10^6$ of Ca, Cu, Mg, Ag, and Fe. The $NiSiO_3$ was a precipitate which was prepared from a solution of $NiNO_3$ and "water glass" (which is commercially named and is a caustic solution of $SiO_2$ and NaOH). The precipitate was collected and dried at 600°C for 10 h. The sample of $Na(OH)_2AlCO_3$ was obtained from a local supply store and its purity was unknown.

## II. DISCUSSION OF RESULTS

The infrared absorption spectra of these catalysts indicate that they are not just the superposition of the spectra of the constituents listed in Table I. The catalyst spectra are interpreted by comparison with known group frequencies in the literature and by comparison with the infrared spectra of NiO, $SiO_2$, $NiSiO_3$, $Al_2O_3$, and $Na(OH)_2AlCO_3$.

**A. C150-1-01.** The bands at 3475 and 1640 $cm^{-1}$ in Fig. 1a are due to the stretching and bending modes of adsorbed $H_2O$. The intensities of these bands are indic-

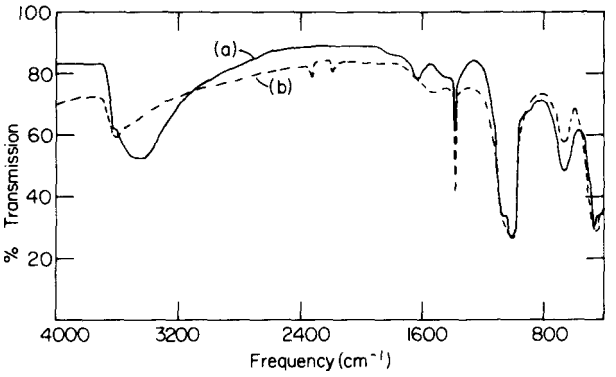


**Fig. 1. Infrared spectra of 1% by weight nickel oxide-silica methanation catalyst in KBr. (a) nonreduced, as-received form; (b) after 300°C heating for one hour in an $N_2$ atmosphere.**

ative of the hygroscopic nature of these high surface area catalysts; $H_2O$ absorption due to KBr was found to be insignificant compared to that shown, even for pure KBr pellets which had been exposed to air for 24 h. Heating the KBr-catalyst pellets in dry $N_2$ atmosphere at 300°C for periods ranging from 10 min to 24 h decreases the $H_2O$ absorption while producing a more pronounced $OH^-$ absorption at 3620 $cm^{-1}$ (Fig. 1b). However, continued heating at 300° would not remove the 3620 $cm^{-1}$ band; evidently the $OH^-$ is tightly bound within the silicate structure. The 1060 and 1000 $cm^{-1}$ bands are expected to be due to SiO vibrational modes. Their relatively low frequencies coincide with that of $SiO_n$ groups which have coordination number n greater than 2.

In general, increasing the value of n in $SiO_n$ groups does decrease the SiO stretching frequency.[1] Other factors which are important in describing the $SiO_n$ coordination and symmetry are the deformation or distortion of the coordinated groups and whether the silica groups are isolated or condensed. Isolated $SiO_2$ groups are evident only for crystalline quartz and they have Si—O stretching frequencies in the 1210 to 1110 $cm^{-1}$ region.[2,3] Matrix isolation studies of silicon monoxide show that SiO absorbs at 1225 $cm^{-1}$.[4] Increasing the coordination number n decreases this Si—O stretching frequency as seen in isolated $SiO_4$ groups[5,6] or in condensed tridimensional silicate networks.[5] The absence of an 800 $cm^{-1}$ band, which is characteristic of the O—Si—O bending mode in $SiO_2$, is also a primary indication that isolated $SiO_2$ groups do not exist in the C150-1-01 catalyst. The 470 $cm^{-1}$ band, which is relatively insensitive to $SiO_n$ coordination, is due to the Si—O—Si bending mode of the silicate groups and it is broadened by NiO absorption at 440 $cm^{-1}$.[7] These facts, along with the 670 $cm^{-1}$ absorption and the multiple 1060 to 1000 $cm^{-1}$ Si—O stretching modes indicate that the catalyst can be described more completely in terms of NiO—$Si_2O_7$ groups with coordinated $OH^-$ than simply NiO with a $SiO_2$ support. Evidently the coprecipitation technique and the high temperature calcination used in catalyst preparation promote the growth of $SiO_n$ groups with coordination number greater than that in $SiO_2$.

The narrow absorption band at 1380 $cm^{-1}$, along with the weak shoulder at 1470 $cm^{-1}$, which shifts to 1510 $cm^{-1}$ with heating, indicates that a carbonate species is present in the C150-1-01 catalyst. This interpretation is

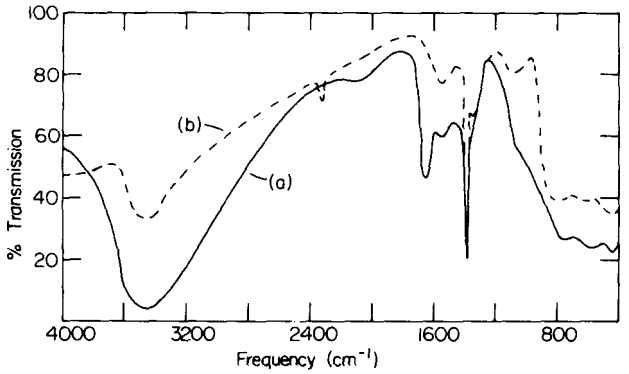


**Fig. 2. Infrared spectra of 1% by weight nickel oxide-alumina catalyst in KBr. (a) nonreduced, as-received form; (b) after 300°C heating for one hour in an $N_2$ atmosphere.**

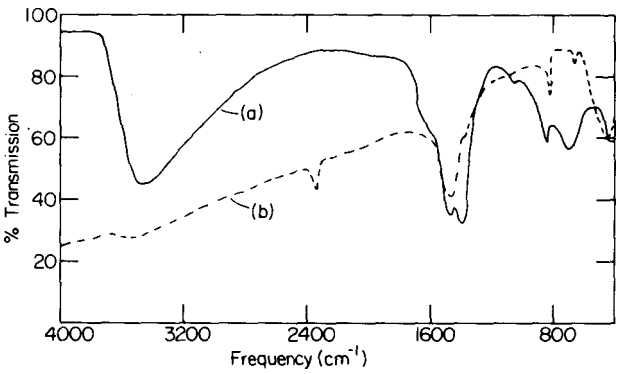


**Fig. 3. Infrared spectra of 1% by weight $NiCO_3$ in KBr. (a) as-prepared form; (b) after 300°C heating for one hour in an $N_2$ atmosphere.**

strengthened by the appearance of the linear $CO_2$ stretching vibration at 2340 $cm^{-1}$ in the heated sample which could occur as a result of $CO_3^=$ decomposition. A possible origin of this absorption band was discussed by McConnell,[8] who has shown that such infrared bands may arise from the bicarbonate ion generated *in situ* from atmospheric $CO_2$ and $H_2O$ during the grinding and pressing of the KBr pellet. His data show such an absorption in $K_2TeO_4$ in KBr without heat treatment. When NiO and $SiO_2$ are mixed in 50:50 wt% and 2% by weight of this mixture is added to KBr and pressed in a pellet, a very weak band appears at 1380 $cm^{-1}$. However, the catalyst in KBr shows a much stronger absorption at 1380 $cm^{-1}$ than that obtained by mixing the constituents in KBr. Thus, it is unlikely that the 1380 and 3620 $cm^{-1}$ bands are associated with *in situ* generated $HCO_3^-$ because of their large intensities. Also, the $OH^-$ band is not observed in the alumina support catalyst while the narrow intense 1380 $cm^{-1}$ band remains essentially unchanged which implies that $HCO_3^-$ does not cause these bands (see below). It is possible that the carbon binder was oxidized during the 500°C calcination used for catalyst preparation and/or that the calcination was insufficient in removing $CO_3^=$ which was introduced during the catalyst preparation. Other weak bands at 2185 and 900 $cm^{-1}$ are thought to be due to Si—H vibrations.[9, 10]

**B. C150-4-03.** This catalyst contains the largest percentage of Ni of the alumina support catalysts which were examined. Its spectrum is shown in Fig. 2a. The region 4000 to 1600 $cm^{-1}$ shows $H_2O$ absorption centered at 3475 and 1650 $cm^{-1}$. Heating the sample pellet in a $N_2$ atmosphere decreases the $H_2O$ band intensities, but similar to what was found in the spectra of $Al_2O_3$, continued heating at 300°C would not eliminate the adsorbed $H_2O$ (Fig. 2b). The Al—O stretching frequencies are centered at 800 and 600 $cm^{-1}$ as in $Al_2O_3$. Such broad absorption can be defined in terms of amorphous $Al_2O_3$ which is essentially a mixture of condensed and isolated $AlO_6$ and $AlO_4$ units.[1, 11, 12] The 440 $cm^{-1}$ absorption is due to NiO.

The 1530 and 1390 $cm^{-1}$ bands are thought to be associated with asymmetric and symmetric vibrations of a carbonate-like species. A number of tests were performed to clarify the origin of these bands.

First, the intensities of the 1390 and 1530 $cm^{-1}$ bands vs percent C150-4-03 in a KBr pellet were plotted, both for normally pressed pellets and for pellets which have been pressed only after flushing with $CO_2$ for 15 min. The admission of $CO_2$ increased the intensity of these bands for all concentrations of C150-4-03 while the peak absorption frequencies and band shapes were unchanged. These results indicate that nonlinear $CO_2$ and/or $CO_3$ is held within the catalyst, being associated with either the Ni or Al.

Second, the infrared spectrum of $NiCO_3$ (technical grade) shown in Fig. 3a was obtained to determine whether a carbonate ion attached to Ni could generate the 1530 and 1390 $cm^{-1}$ bands. Our conclusion is no and we arrive at this conclusion from the following argument. As seen from Fig. 3b, large spectral changes result from the heating of the $NiCO_3$ sample. If the 1475 and the 1395 $cm^{-1}$ bands are due to $CO_3^=$, it must be attached to the Ni as a unidentated ligand depicted below.

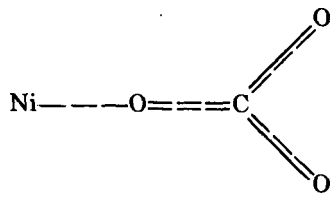


I

The $D_{3h}$ symmetry of $CO_3^=$ attached to the Ni as shown below would be expected to have absorption bands in the 1420, 860 and 680 $cm^{-1}$ regions.[13]

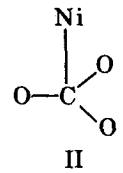


II

The 1395 $cm^{-1}$ band which could be associated with a symmetric CO vibration for I, as depicted by IIIa, would be infrared inactive in IIIb.

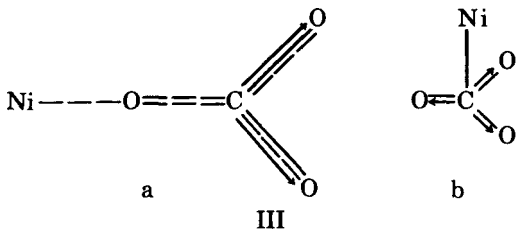


III

Then the 1475 $cm^{-1}$ $NiCO_3$ band would be the asymmetric CO vibration of species I while the weak 1070 $cm^{-1}$ absorption would be the O===C stretching vibration and 870 $cm^{-1}$ the out-of-plane bend of species I.

As shown in Fig. 3b the unidentate $CO_3^=$ ligand attached to Ni is unstable when heated to 300°C. The appearance of the 2340 $cm^{-1}$ band shows that linear $CO_2$ is formed as $NiCO_3$ decomposes. The bending mode of $CO_2$ would absorb at 670 $cm^{-1}$, but this band could also have contributions from the $CO_3^=$ bonded to the Ni. The remaining bands at 1475 and 820 $cm^{-1}$ indicate that species II is formed, but only as an intermediate state to the total decomposition of the $NiCO_3$ which occurs with continued heating. This transitional molecule also shows characteristic Ni—C vibrations by the broadening of the 440 $cm^{-1}$ band. Thus, the absorption frequencies of $NiCO_3$ do not coincide with those of the catalyst and $NiCO_3$ decomposes quite readily with heating.[14]

Third, the spectrum of $Na(OH)_2AlCO_3$ was obtained in order to compare the absorption frequencies in the 1400 $cm^{-1}$ region. This spectrum is shown in Fig. 4a, and it is to be compared with curves b and c in this figure. The following characteristics are evident when comparing the heated and unheated catalyst samples: (1) a shift of approximately 50 $cm^{-1}$ to 1570 $cm^{-1}$ for the 1520 $cm^{-1}$ band as a result of heating; (2) no frequency shift for the 1390 $cm^{-1}$ band; (3) an initial decrease in the intensity of the 1390 $cm^{-1}$ band, but continued heating at 300°C would not cause its disappearance; and (4) the appearance of a significant shoulder at 1350 $cm^{-1}$ with heating.

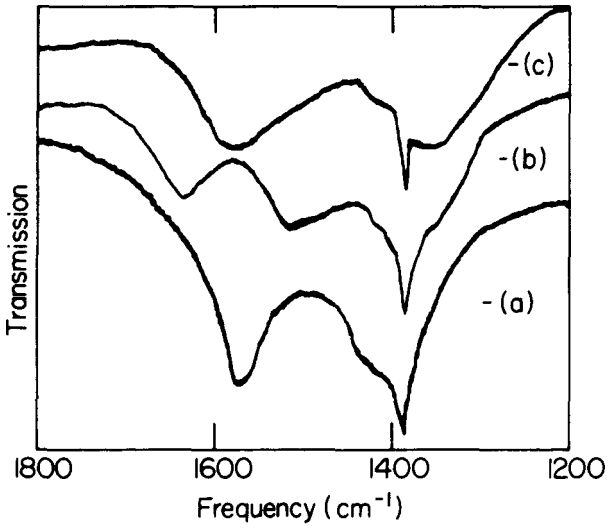


**Fig. 4. Infrared spectra of 1% by weight of (a) $Na(OH)_2AlCO_3$ in KBr; (b) nickel oxide-alumina methanation catalyst in KBr; and (c) after heating the catalyst at 300°C for one hour in an $N_2$ atmosphere.**

Curve a shows very good correspondence with curve c. The shift of the 1520 $cm^{-1}$ band with heating could be explained by a restructuring of the $CO_3^=$ with respect to the Al while the 1350 $cm^{-1}$ shoulder could be due to the formation of $K_2[Al(CO_3)_2]Br \cdot xH_2O$ or $Al_2(CO_3)_3$.[14] That the sharp 1390 $cm^{-1}$ band is associated with the symmetric stretch of $CO_3^=$ is further strengthened by previous research and by the spectra of C150-4-03 in CsI pellets. KBr forms a face-centered cubic lattice while CsI has a body-centered cubic lattice. The body-centered cubic lattice broadens absorption bands due to free ions in solid solution.[15] We find that the 1390 $cm^{-1}$ band spreads to approximately 50 $cm^{-1}$ half-width in CsI while it has a 10 $cm^{-1}$ half-width in KBr.

Fourth, we obtained the spectra of an alumina catalyst prepared by United Catalysts, Inc. which had only 10% Ni. The band at 1390 $cm^{-1}$ was 3.2 times more intense, and the 1520 $cm^{-1}$ band was 1.2 times more intense than the corresponding absorptions for C150-4-03. The discrepancy between these intensity increases for the asymmetric and symmetric stretching vibrations of $CO_3^=$ is not fully understood. These intensity changes indicate that the $CO_3^=$ species is not bonded to the Ni within the catalyst; however, the Ni does perturb the $CO_3^=$ vibrational modes.

## III. SUMMARY

It was shown that infrared spectra can describe the molecular coordination state of the support material which is used in commercial heterogeneous catalysts. Similar infrared studies on catalysts before and after methanation tests could provide useful information on the molecular reordering of the active sites and support material which occurs during the methanation reaction. Such information would provide a better understanding of catalyst deactivation associated with the sintering mechanism. For the commercial catalysts which were investigated it was shown that they cannot be described as simply NiO on $SiO_2$ or $Al_2O_3$ supports. Detailed knowledge of the chemical and physical properties of catalysts could lead to different preparation methods which provide active site dispersion resistant to sintering and sulfur poisoning.

## ACKNOWLEDGMENTS

This work was supported by ERDA Contract EX-72-C-01-2229.

We wish to thank United Catalysts, Inc., Louisville, KY, for supplying the catalysts used in this research. Also we thank Dr. Forrest F. Cleveland for his comments and suggestions on this work.

## REFERENCES

1. P. Tarte, Spectrochimica Acta, Vol. 23A, pp. 2127, 1967.

2. D. M. Karpinos and S. P. Listovnichaya, **V. Ya. Aivazov Porash, Met.**, Vol. 12, pp. 71, 1972.

3. C. H. Perry and J. D. Wrigley, **Journal of Applied Optics**, Vol. 6, pp. 586, 1967.

4. J. S. Anderson and J. S. Ogden, **Journal of Chemical Physics**, Vol. 51, pp. 4189, 1969.

5. P. H. Gaskell, **Physics and Chemistry of Glasses**, Vol. 8, pp. 69, 1967.

6. B. D. Saksena, **Transactions of the Faraday Society**, Vol. 57, pp. 242, 1961.

7. O. Kammori, K. Sato, and N. Yamaguchi, **Japan Anal.**, Vol. 16, pp. 1050, 1967.

8. R. L. McConnell, Ph.D. Dissertation, University of Kentucky, 1976.

9. C. H. Tindal, J. W. Straley, and H. H. Nielsen, **Physics Reviews**, Vol. 62, pp. 151, 1942.

10. G. E. Becker and G. W. Gobelli, **Journal of Chemical Physics**, Vol. 38, pp. 2942, 1963.

11. I. I. Plyusnia, **Applied Spectroscopy**, Vol. 20, pp. 214, 1970.

12. V. A. Kolesova, **Optical Spectroscopy**, Vol. 6, pp. 20, 1959.

13. H. W. Morgan and P. A. Staats, **Journal of Applied Physics**, Vol. 33, pp. 364, 1962.

14. B. M. Gatehouse, S. E. Livingstone, and R. S. Nyholm, **Journal of the Chemical Society**, London, pp. 3137, 1958.

15. H. Bonadeo and E. Silberman, **Journal of Molecular Spectroscopy**, Vol. 32, pp. 214, 1969.

# Raman Spectra of Carbon Monoxide Adsorbed on Oriented Crystalline Nickel Surfaces

by

**J. M. Stencel**
**E. B. Bradley**
Electrical Engineering Department
University of Kentucky
Lexington, Kentucky 40506

## Abstract

Raman spectral results for CO adsorbed at high pressures on Ni(100), Ni(110) and Ni(111) are presented. The bands near 2020 $cm^{-1}$ due to chemisorbed CO are discussed in relation to site of adsorption and surface cleanliness. Raman spectra of temperature and pressure-dependent CO adsorption on Ni(100) are also presented.

## Introduction

Raman spectra which were reported recently for CO adsorbed on Raney Ni and Ni-$SiO_2$,[1] and other Raman investigations have shown the utility of using Raman spectroscopy as a probe for the bonding and structure of adsorbed species.[2-4] However, little information can be found in the literature on Raman spectroscopy of adsorbed species on single-crystal surfaces. Perhaps this is the result of sampling problems[1] and the weak signal which is obtained from some adsorbate-adsorbent systems.[4] In other Raman investigations of adsorbed species, large enhancement of band intensities and relative intensity changes have been observed and described in terms of surface polarization.[5-7] Increasing the surface area of the adsorbent will increase the number of scattering centers, and hence, enhance the observed signal. This will also increase the difficulty of band assignments by introducing active sites of various adsorption energy and crystallographic orientation.

Therefore, investigations of the adsorption of CO on oriented planes of single-crystal Ni, including Ni(100), Ni(111) and Ni(110), were conducted with Raman spectroscopy. The spectra of chemisorbed and physically adsorbed CO were obtained with the oriented Ni crystals at temperatures from 100 to 210°K for near-grazing incidence of the laser excitation.

Chemisorbed CO was observed to have similar Raman frequencies on the various Ni surfaces at 5 x $10^4$ Pa CO pressure and 210°K. These results are discussed in relation to the cleanliness of the Ni surfaces prior to CO adsorption. A Raman band at 2141 $cm^{-1}$ was also observed for the Ni(100) surface with 5 x $10^4$ Pa CO pressure at 205°K; this band is related to physically adsorbed CO.

## Experimental Procedure

Nickel crystals purchased from Materials Research Corporation were oriented and cut to dimension with an abrasive wheel or diamond-edged saw. These samples were mechanically polished in a water-alumina slurry which had successive particle sizes of 1.0, 0.3 and 0.05 $\mu$. After chemical etching in a solution of $HNO_3$:$H_3PO_4$:$HCH_3COO$, the x-ray diffraction patterns showed well-defined Laue spots indicative of having the (111), (110) and (100) planes to within ±1.5 degrees of the sample surface. These samples were mounted in adsorption chambers for Raman spectral acquisition.

Two adsorption chambers were used. One of these chambers, a UHV adsorption system, has been described.[8] The other chamber was attached to a C.T.I. He cryogenic cooler. While this unit allowed the sample temperature to be varied from 90 to 400 °K, vacuums to only 1.3 x $10^{-3}$ Pa could be obtained. Each chamber was placed in the

sampling compartment of a Jarrell-Ash Model 25-300 Raman spectrometer for spectral acquisition. The 5145 Å line from a Spectra-Physics Model 171 $Ar^+$ laser was the excitation source with an angle of incidence at the Ni surfaces of 10 to 15 degrees. During CO (Matheson, research grade) adsorption and spectral acquisition, the laser power at the sample was estimated to be 40 mW. Raman scattered radiation was collected normal to the respective surfaces, even though, theoretically, this geometry is not an optimal choice for collection of radiation from a dipole near a metal surface.[9]

Treatment of the Ni catalysts prior to CO adsorption varied with respect to the particular adsorption chamber being used. In the UHV chamber, after the pressure became less than $2.7 \times 10^{-6}$ Pa, the temperature of the Ni crystal was raised to 750°K and maintained for one minute. The temperature was then decreased to 625°K, $H_2$ (Matheson, research grade) was admitted to $1.3 \times 10^3$ Pa and allowed to flow through the chamber for five minutes. Evacuation followed this reduction and when the system pressure reached $6.7 \times 10^{-6}$ Pa, the sample was cooled to 100°K and CO was admitted. After spectral acquisition, the UHV chamber was evacuated and the sample was allowed to cool to 575°K. When pressures near $2.7 \times 10^{-6}$ Pa were obtained, the sample surface was $Ar^+$ sputtered for approximately 10 minutes at 2 kV and 10 mA with $4 \times 10^{-2}$ Pa Ar pressure. Finally, annealing to 750°K was performed, and $H_2$ reduction then preceded another CO adsorption experiment.

In the C.T.I. adsorption chamber, $H_2$ was allowed to flow through at $1.3 \times 10^3$ Pa while the Ni sample was heated to 400°K. After a five-minute $H_2$ exposure, the chamber was evacuated to approximately $1.3 \times 10^{-3}$ Pa. Then the sample was cooled to 90°K, CO was admitted, and spectra were obtained using near-grazing incident laser irradiation with the scattered light collected normal to the surface.

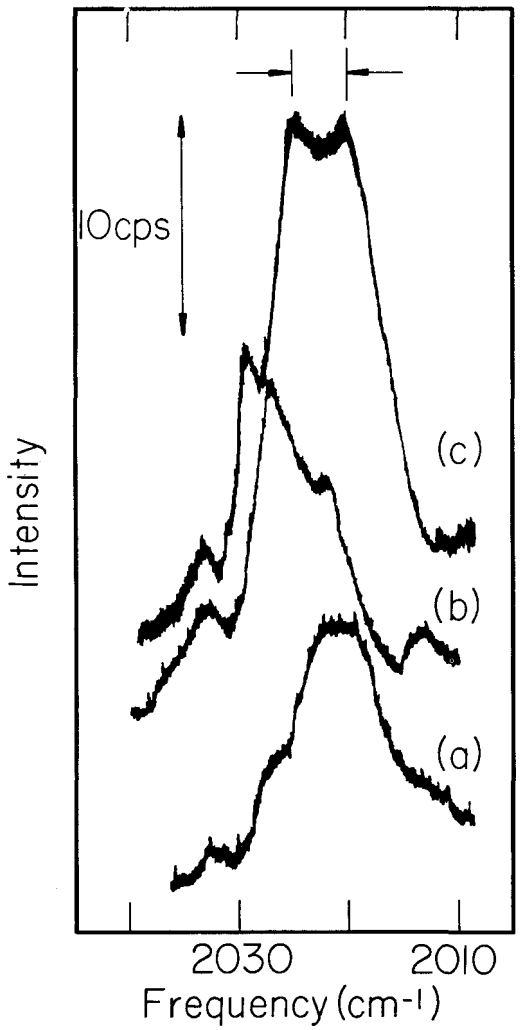


**Figure 1. Raman spectra of CO adsorbed on single-crystal Ni surfaces: (a) Ni(100), (b) Ni(111), and (c) Ni(110). Bulk crystal temperature was 205°K. The spectra are displaced vertically for clarity of presentation.**

## Experimental Results

Figure 1 shows the average of two spectral scans for CO adsorbed on Ni(100), Ni(111) and Ni(110) at 205°K, as obtained during use of the C.T.I. adsorption chamber. Spectral results from the Ni(111) and Ni(100) surfaces in the UHV chamber were identical to those depicted in this figure. The CO was admitted to $5.2 \times 10^4$ Pa with the samples at 125°K. This pressure increased the sample temperatures to approximately 170°K, during a five-minute interval, as a result of convection losses. However, the temperature was stable above 180°K and could be increased by resistive heating.

Table 1 lists the observed frequencies of the CO bands. No Raman bands were found in the 1940 to 2060 $cm^{-1}$ or 2050 to 1090 $cm^{-1}$ regions during this phase of the investigation.

**Table 1. Frequencies of the Raman Bands for CO on Crystalline Ni at 200°K.**

| Ni(111) $\upsilon(cm^{-1})$ | Ni(110) $\upsilon(cm^{-1})$ | Ni(100) $\upsilon(cm^{-1})$ |
|---|---|---|
| 2023 | 2020 | 2021 |
| 2027 | 2025 | 2027 |
| | 2029 | |
| 2033 | 2033 | 2033 |

Figure 2 shows spectra of CO adsorbed on Ni(100) at three different temperatures during adsorption in the UHV chamber. The temperature of the Ni crystal was held at 95°K before exposure, then the temperature was increased to 125°K with admission of $1.3 \times 10^2$ Pa CO. The resulting spectrum is shown in Figure 2a, which shows the average of three spectral scans. Subsequent admission of CO, to increase the pressure to $5.9 \times 10^2$ Pa, also increased the temperature of the sample. A 0.5°K per minute increase above 180°K allowed the acquisition of the spectrum in Figure 2b. The Ni temperature stabilized near 205°K. Figure 2c shows the average of two spectral scans at 205°K.

During this adsorption experiment, spectral scans from 2125 to 2160 $cm^{-1}$ revealed the band at 2141 $cm^{-1}$, as shown in Figure 3. The disappearance of the 2141 $cm^{-1}$ band coincided with that at 2020 $cm^{-1}$, and occurred over a 15-minute interval with the sample temperature held at approximately 210°K. However, no Raman bands were found during scans of the 950 to 1350 $cm^{-1}$ and 1700 to 2000 $cm^{-1}$ regions during this phase of the investigation. Other than the spectra reported earlier, the low-frequency region was not investigated in this work.[10]

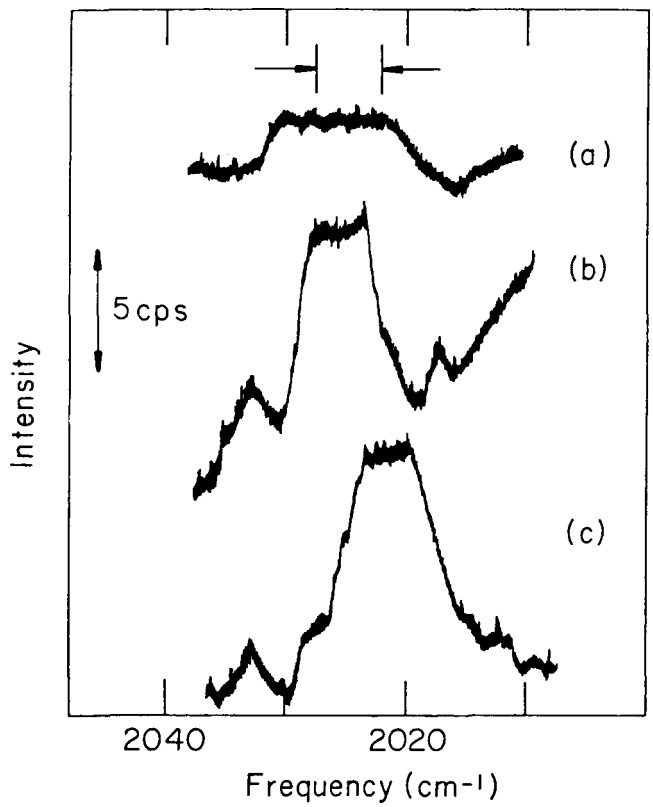


**Figure 2. Raman spectra of CO on Ni(100) at: (a) 125°K, (b) 185°K, and (c) 205°K. The spectra are displaced vertically for clarity of presentation, but the stray-background radiation for spectrum (a) was approximately 100 percent more than for (b) or (c).**

## Discussion

The preparation of the Ni surfaces in the UHV chamber is expected to be sufficient to obtain a clean, well-defined surface. However, during evacuation and cooling after $H_2$ reduction or $Ar^+$ sputtering, ambient CO and/or $O_2$ could contaminate the prepared surface. This contamination is possible when considering that the one-to-two minute cooling time for the samples before CO admission presents an exposure of approximately one to two liters of ambient gases to the Ni surfaces. Without additional surface analysis equipment within the UHV chamber, e.g., Auger, it is impossible to fully describe the cleanliness of the Ni surfaces before CO adsorption. It is also expected that the reduction temperatures, as well as the relatively poor vacuum in the C.T.I. chamber, do not allow preparation of a clean surface. Thus, surface oxide or carbon contamination could be the cause for the identical spectral results which were obtained from the two adsorption chambers for the 2000 to 2050 $cm^{-1}$ region.

It has been shown that CO adsorbed on incompletely reduced surfaces produces infrared bands above 2100 $cm^{-1}$.[11] Similarly, CO adsorbed to an oxide layer would be expected to produce bands in the 950 to 1360 $cm^{-1}$ or 1700 to 2000 $cm^{-1}$ regions. The absence of bands in these regions, except for the 2141 $cm^{-1}$ band, which coincides with gaseous CO, indicates that the adsorbed CO is bonded to the Ni surface and not to an oxide layer. The frequency of the CO bands shown in Figures 1 and 2 does coincide with a Raman CO mode found by Krasser, *et al.*, on Raney Ni.[1] They proposed that their 2020 $cm^{-1}$ and 2050 $cm^{-1}$

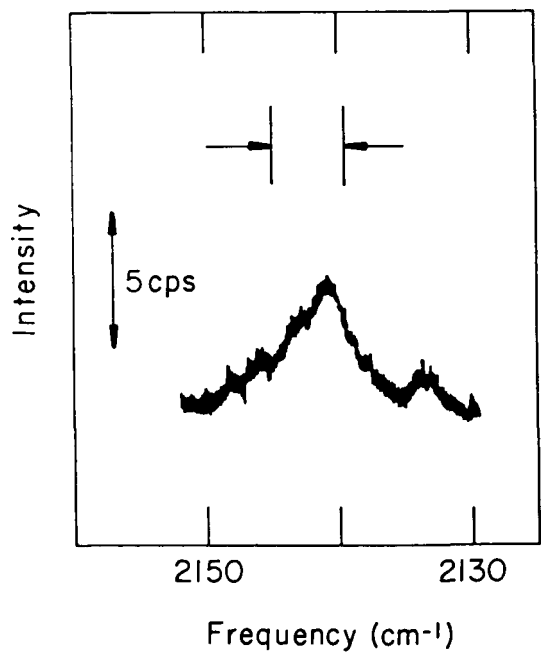


**Figure 3. A Raman spectrum of physadsorbed CO on Ni(100) at 205°K.**

bands were due to CO stretching modes of $Ni(CO)_4$. These frequencies are close to those expected for $Ni(CO)_4$,[12, 13] but low-energy electric diffraction (LEED) and electron energy loss (ELS) studies of CO on Ni(100) have shown that bands near 2060 $cm^{-1}$ are not due to $Ni(CO)_4$.[14] Eischens, *et al.*,[15] have also shown that bands due to CO on $Ni/SiO_2$ at 2041 $cm^{-1}$ are not caused by $Ni(CO)_4$. Thus, while it is possible that the Raman bands shown in Figures 1 and 2 are due to $Ni(CO)_4$, such a conclusion could be reached only after comparison of CO in relation to $Ni(CO)_4$ on the different crystalline surfaces.

An oxide layer on Ni(111) does block some CO adsorption sites and causes $O_{ad} - CO_{ad}$ interactions which reduce the amount of CO adsorbed.[16] This could explain the relatively large CO pressures ($5.2 \times 10^4$ Pa) which are needed to observe the Raman modes. The low temperature at which the Raman bands disappear (~210°K) also corresponds with the weakly bonded CO species expected for CO on a partially oxidized surface.[16] However, in general, comparisons between the present Raman results and previous ELS, LEED and thermal desorption data have to be examined carefully before conclusions are made.[14, 16, 17] This is necessitated by a number of factors. First, the mechanism producing Raman activity is different than that for ELS. In fact, Raman results for adsorption of CO on Ag films show numerous bands which do not coincide with what is seen by other techniques.[18] Second, ELS and LEED experiments are performed generally under UHV conditions and small exposures. This is not the case for the present results. Third, the cleanliness of the surface is known for most ELS and LEED experiments; the Raman results shown in Figures 1-3 are expected to be indicative of an oxygen or carbon contaminated surface. However, the degree of this contamination is not known.

The alterations in geometry for the UHV cell, which will allow variation of the incident and collected light directions, are near completion. Also, extra surface-analysis equipment that will more fully describe surface cleanliness before adsorption experiments are initiated is being installed. It is hoped that these additions will provide more exact interpretation from the Raman experiments.

## Acknowledgment

We wish to thank the Institute for Mining and Minerals Research, University of Kentucky, for the $Ar^+$ laser used in this work. This research was supported by DOE Contract No. EX-76-C-01-2229.

## References

1. W. Krasser, A. Ranade and E. Koglin, *J. Raman Spectrosc*, Vol. 6, 209 (1977).
2. P. J. Hendra and E. J. Loader, *Trans. Faraday Soc.*, Vol. 67, 828 (1971).
3. M. L. Howe, K. L. Watters and R. G. Greenler, *J. Phys. Chem.*, Vol. 80, 382 (1976).
4. R. P. Cooney, M. Fleischman and P. J. Hendra, *J. C. S. Chem. Comm.*, 235 (1977).
5. H. Jeziorowski and H. Knözinger, *Chem. Phys. Lett.*, Vol. 43, 37 (1976).
6. D. L. Jeanmaire and R. P. Van Duyne, *J. Electroanal. Chem.*, Vol. 84, 1 (1977).
7. R. P. Van Duyne, *J. Phys.* (Paris), Vol. C5, 239 (1977).
8. J. M. Stencel, D. M. Noland, E. B. Bradley and C. A. Frenzel, *Rev. Sci. Instrum.*, Vol. 49, 1163 (1978).
9. R. Greenler, *Surf. Sci.*, Vol. 69, 647 (1977).
10. J. M. Stencel and E. B. Bradley, *Spec. Lett.*, Vol. 11, 563 (1978).
11. J. B. Peri, *Disc. Faraday Soc.*, Vol. 41, 121 (1966).
12. L. H. Jones, *J. Chem. Phys.*, Vol. 28, 1215 (1958).
13. L. H. Jones, *Spectrochim. Acta*, Vol. 19, 1899 (1963).
14. S. Andersson, *Solid State Comm.*, Vol. 21, 75 (1977).
15. R. P. Eischens, S. A. Francis and W. A. Pliskin, *J. Phys. Chem.*, Vol. 60, 194 (1956).
16. H. Conrad, G. Ertl, J. Küppers and E. F. Latta, *Surf. Sci.*, Vol. 57, 475 (1976).
17. J. C. Bertolini, G. Dalmai-Imelik and J. Rousseau, *Surf. Sci.*, Vol. 68, 539 (1977).
18. T. H. Wood and M. V. Klein, paper presented at 25th National Symposium of the American Vacuum Society, Nov. 1978.

ABSTRACT OF THESIS

# Far-Infrared Investigation of Aluminate and Silicate Support Nickel Methanation Catalysts

A thesis submitted in partial fulfillment of the requirements
for the degree of Master of Science in Electrical Engineering
at The University of Kentucky

by
Gene Daniel Noland
Lexington, Kentucky

Director

Dr. Eugene B. Bradley
Professor of Electrical Engineering
Lexington, Kentucky
1979

The theory of infrared spectroscopy is introduced by briefly explaining crystal lattice vibrations and dispersive-type infrared spectrophotometry. The disadvantages of the dispersive-type instrument for obtaining far-infrared spectra are mentioned. Fourier transform spectroscopy is then introduced and discussed in some detail. The basic integral is derived and determination of interferogram sampling rates are explained. Fourier transform spectroscopy is also shown to be analogous to an electrical engineering communications problem by showing that the function of the spectrometer is to autocorrelate the infrared signal radiated from the source. The far-infrared spectra of silicate and aluminate support materials, and of Ni catalysts, are discussed and correlated with previously done medium infrared results.

# A Method to Study Sintering of a Supported Metal Catalyst

by

**H. K. Kuo, P. Ganesan and R. J. De Angelis**
Department of Metallurgical Engineering and
Institute for Mining and Minerals Research
University of Kentucky, Lexington 40506

## Abstract

An x-ray single-profile analysis method has been used to monitor the changes in the average nickel particle sizes and particle size distributions during sintering of a silica-supported nickel catalyst. Sintering was carried out in nitrogen and hydrogen atmospheres at temperatures from 500 to 800°C for times varying from 5 to 100 hours. The particle size distribution functions determined both by the x-ray single order line profile analysis and by transmission electron microscopy were in excellent agreement. The sintering process occurred very rapidly initially and then proceeded more slowly at longer times at the higher temperatures. The effects of sintering temperature on the changes of PSD were found to be much more pronounced than the effects of sintering time. As sintering progressed, the particle size distributions developed long tails to the large diameter side. The changes in the particle size distributions tend to indicate that the probable sintering mechanism for the silica-supported nickel catalyst is one associated with particle migration.

## Introduction

Metal catalysts are generally employed in the form of small metal particles of crystallites, dispersed on high surface area supports. In this form, a high ratio of metal atoms exists on the surface and an active catalyst results. The support also serves the function of physically separating the small metal particles, which in-turn tends to inhibit agglomeration of the small particles into larger particles. Strong interaction between the support and the metal particle also inhibits agglomeration. This agglomeration, known as sintering, occurs very rapidly in unsupported metal catalysts and leads to fewer metal atoms at the surface of the particle with consequent loss of catalyst activity. Sintering also occurs at high temperatures in supported metal catalysts and is the main source of catalyst thermal deactivation.

The process of sintering, by definition, requires changes to occur in the particle size distribution. The sintering behavior of a metal catalyst depends on the initial particle size distribution and knowledge of the progressive changes in the particle size distribution during sintering can assist in elucidating the mechanism of sintering in metal supported catalysts.[1] Therefore, a reliable determination of the initial particle size distribution function and the changes occuring in the PSD during sintering becomes essential if the sintering process is to be understood and ultimately controlled.

The purpose of this paper is to present an x-ray diffraction method based on a single-profile analysis technique which gives the diffracting particle size, lattice microstrains and particle size distribution function, and to present comparisons between particle size distributions determined by x-ray diffraction and electron microscopy. This comparison will be made on catalytic materials containing metallic nickel particles in the range of 30 to 100Å. The lower part of this range has until

recently been considered to be a particle-size range which could not be completely investigated using x-ray diffraction techniques.[2]

## Theory

### Single Profile Analysis Technique

The single diffraction profile technique is based on the work of Gangulee, and Mignot.[3,4] The Stokes corrected cosine coefficients from a (hkl) diffraction profile are composed of two components, a size coefficient $A_L^S$ and a microstrain or distortion coefficient $A_L^D$.[5] Their relationship can be expressed as

$$A_L = A_L^S \times A_L^D, \tag{1}$$

where $A_L$ are the Stokes corrected cosine coefficients at a given L, where L is $n\delta$. Here n is the harmonic number and $\delta$ is a distance normal to the diffracting planes. Defining a variable $X = 1/D_e$; where $D_e$ is the effective diffracting particle size, for small values of n and $\delta$ where the values of L are small and such that the number of diffracting domains in the specimen with this dimension is insignificant, the particle size term of the Fourier coefficients can be expanded as

$$A_L^S = (1 - LX). \tag{2}$$

The distortion coefficients can be expanded for small values of n, as

$$A_L^D = (1 - KL^2 < \epsilon_L^2 >), \tag{3}$$

where K is $2\pi^2/d^2$, d is the (hkl) planar spacing and $<\epsilon_L^2>$ is the mean square of the microstrain, averaged over all distance in the diffracting specimen spaced L apart.

Letting $Y_L = K <\epsilon_L^2>$, the small L value cosine coefficient can be written as

$$A_L = (1 - LX)(1 - Y_L L^2). \tag{4}$$

Equation (4) can be solved for X if the functional form of $Y_L$ is known. In this way the particle size can be separated from the microstrain terms. The problem then resolves to determination of the most suitable forms of $Y_L$. Assuming the form of the strain function to be[6]

$$Y_L = (C/L)\delta K, \tag{5}$$

leads to an expression for $A_L$ of

$$A_L = 1 - L(X + C\delta K) + L^2 (XC\delta K). \tag{6}$$

The expression for $A_L$ has the form of a second order polynomial in L. Now, defining a polynomial of second degree

$$R_L = a_0 + a_1 L + a_2 L^2, \tag{7}$$

whose coefficients by comparing with Eqn. (6) are

$$a_0 = 1,\ a_1 = -(X + c\delta K) \text{ and } a_2 = XC\delta K. \tag{8}$$

From these relations it follows that

$$X = 1/2\ (-a_1 \pm (a_1^2 - 4a_2)^{1/2}),$$

$$D_e = 1/X,$$

$$C = a_2/X\delta K, \text{ and} \tag{9}$$

$$\langle \epsilon_L^2 \rangle = (C/L)\delta.$$

The determination of the coefficients $a_0$, $a_1$ and $a_2$ can be made by solving the system of equations

$$\sum_t A_L = a_0 N + a_1 \sum_t L + a_2 \sum_t L^2,$$

$$\sum_t L A_L = a_0 \sum_t L + a_1 \sum_t L^2 + a_2 \sum_t L^3, \text{ and} \tag{10}$$

$$\sum_t L^2 A_L = a_0 \sum_t L^2 + a_1 \sum_t L^3 + a_2 \sum_t L^4,$$

where N is the number of coefficients used in the evaluation, $N \geq 4$; t is an integer satisfying $t = (L_N - L_0)/(L_1 - L_0)$, where $L_0$ is the distance corresponding to the initial coefficient used in the computation of Eqns. (10).

The best solution to Eqns. (10) are selected from four criteria:

(1) $a_0 \approx 1$,

(2) $a_2 > 0$, since $a_2$ from Eqns. (6) and (7) can be written as $d^2 A_L/dL^2$ which must be positive,

(3) $\sum_t (R_L - A_L)^2/N$ is a minimum, and

(4) $(dA_L/dL)_{L \to 0} = a_1 = -(X + C\delta K)$.

After the best solution to Eqn. (10) is determined, it is a simple process to calculate the average coherent diffracting particle size $D_e$ and lattice mean square strain $\langle \epsilon_L^2 \rangle$ by employing Eqn. (9).

### Particle-Size Distribution Function

While single-profile analysis is a convenient method to use when calculating lattice microstrain, it is important to note that the particle-size distribution function cannot be obtained by this method alone, since from Eqn. (2), $d^2 A_L^S/dL^2$ reduces to zero. However, by employing the usually accepted small (L/d) approximation it is possible to obtain the particle-size distribution function by combining results from both the single-profile and multiple-order analysis methods. Although this approach does contain limitations, it is a major improvement over the zero strain approximation.

The expression for the relationship between the particle size and distortion coefficients in the Warren-Averbach double order method is given by[7]

$$A_L = A_L^S \langle \cos 2\pi \, L/d \, \epsilon_L \rangle. \tag{11}$$

For small values of L/d the argument of the microstrain term is small and using the approximations $\langle \cos X \rangle = 1 - \langle X^2 \rangle/2$ and $(1 - X) \cong \exp(-X)$, Eqn. (11) can be written as

$$A_L = A_L^S \exp(-2\pi^2 \, L^2/d^2 \, \langle \epsilon_L^2 \rangle). \tag{12}$$

This method of separation of particle size and microstrain term makes no assumption of the nature of strains; however, Eqn. (12) is most exact at small values of L/d. It is easily shown that Eqn. (12) is exact for all values of L/d if the microstrain distribution is Gaussian.[8] The distribution of strains at a given L has been shown to be close to Gaussian, but the variation of $\langle \epsilon_L^2 (hkl) \rangle^{1/2}$ with L is not Gaussian.[9-11]

Now it is possible to obtain the particle size coefficient $A_L^S$ from Eqn. (12) by substituting the values for mean square strain $\langle \epsilon_L^2 \rangle$ obtained from the single profile analysis (Eqn. 9). The particle size distribution function, P(L), can then be

obtained from the second derivative of $A_L^S$ with respect to L;[8] that is

$$P(L) = \frac{d^2 A_L^S}{dL^2} \times D_e . \tag{13}$$

The particle size distribution data can be employed to calculate the average particle size using two relationships

$$\bar{D} = \sum_L L\, P(L)\, \Delta L, \text{ and} \tag{14a}$$

$$\bar{D} = [\sum_L \frac{1}{L} P(L)\, \Delta L]^{-1}, \tag{14b}$$

where P(L) is the value of the distribution function at the size L normalized such that $\int P(L)\, dL = 1$; $\bar{D}$ is the volumetric mean particle size, and $\bar{D}_1$ is the average value of the thickness of the particle normal to the (hkl) reflecting planes.[12]

The complete x-ray diffraction profile shape analysis, which involves the calculation of Stokes corrected coefficients $A_L$, particle size coefficients $A_L^S$ and the particle size distribution function P(L), has been computerized.[13]

## Results and Discussion

The silica supported catalytic material (C150-1-01) used in this investigation (supplied by United Catalysts Inc., Louisville, Kentucky), contained 51.7 percent nickel, 2.94 percent carbon, and 0.06 percent silica. It had a surface area of 211 square meters per gram, a pore volume of 0.34 cubic centimeters per gram, and a density of 1.05 grams per cubic centimeter. The catalytic materials $NiO/SiO_2$ were produced by a coprecipitation process. This is one of the four catalysts reported in a previous investigation.[13]

The particle size distribution functions obtained by the x-ray diffraction technique for the silica supported nickel catalyst C150-1-01, after sintering for up to 20 hours at temperatures between 500 and 800°C in a hydrogen atmosphere, are shown as isochronal plots in Figs. 1 through 4. The sintering behavior observed in a nitrogen atmosphere was very similar to the

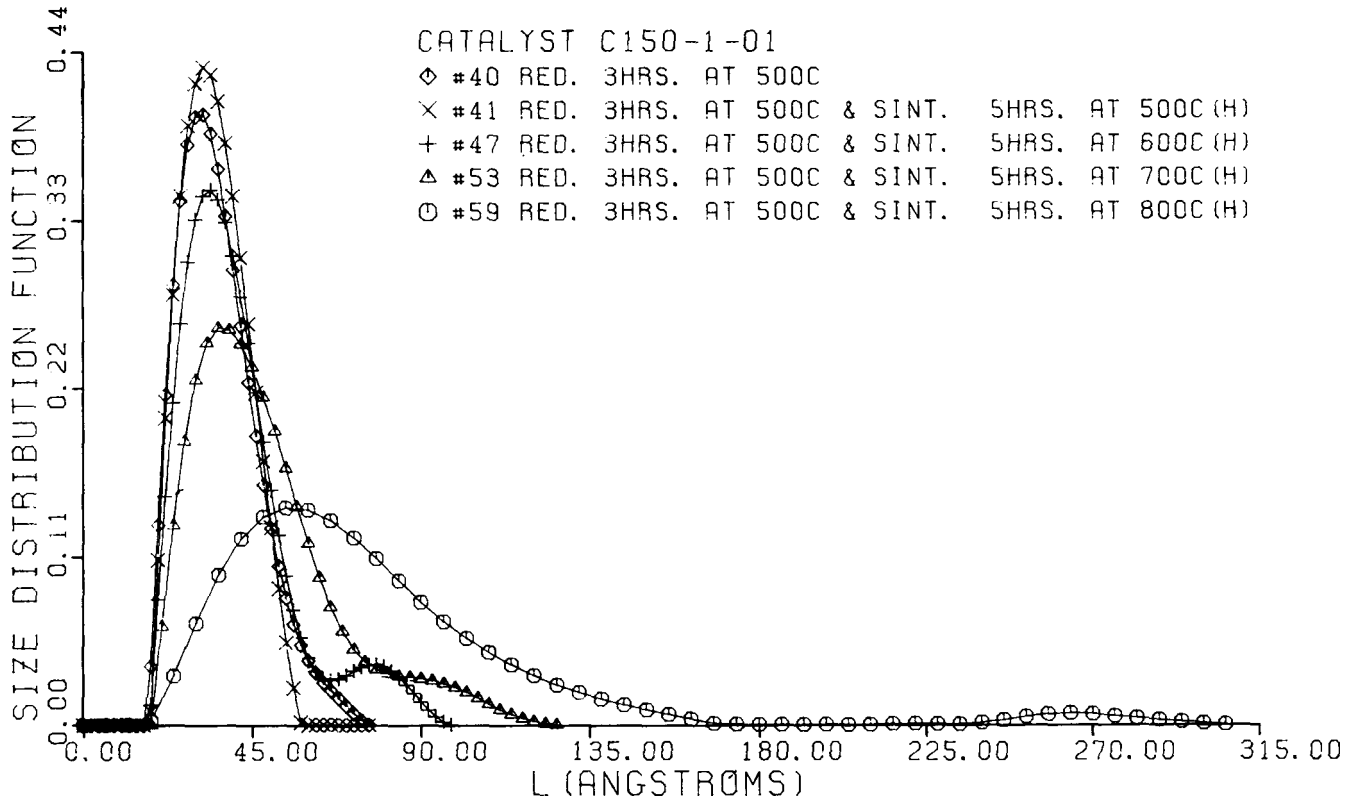


**Figure 1. Particle size distribution functions of catalyst C150-1-01 reduced at 500°C for three hours and sintered at 500, 600, 700 and 800°C for five hours in a hydrogen atmosphere.**

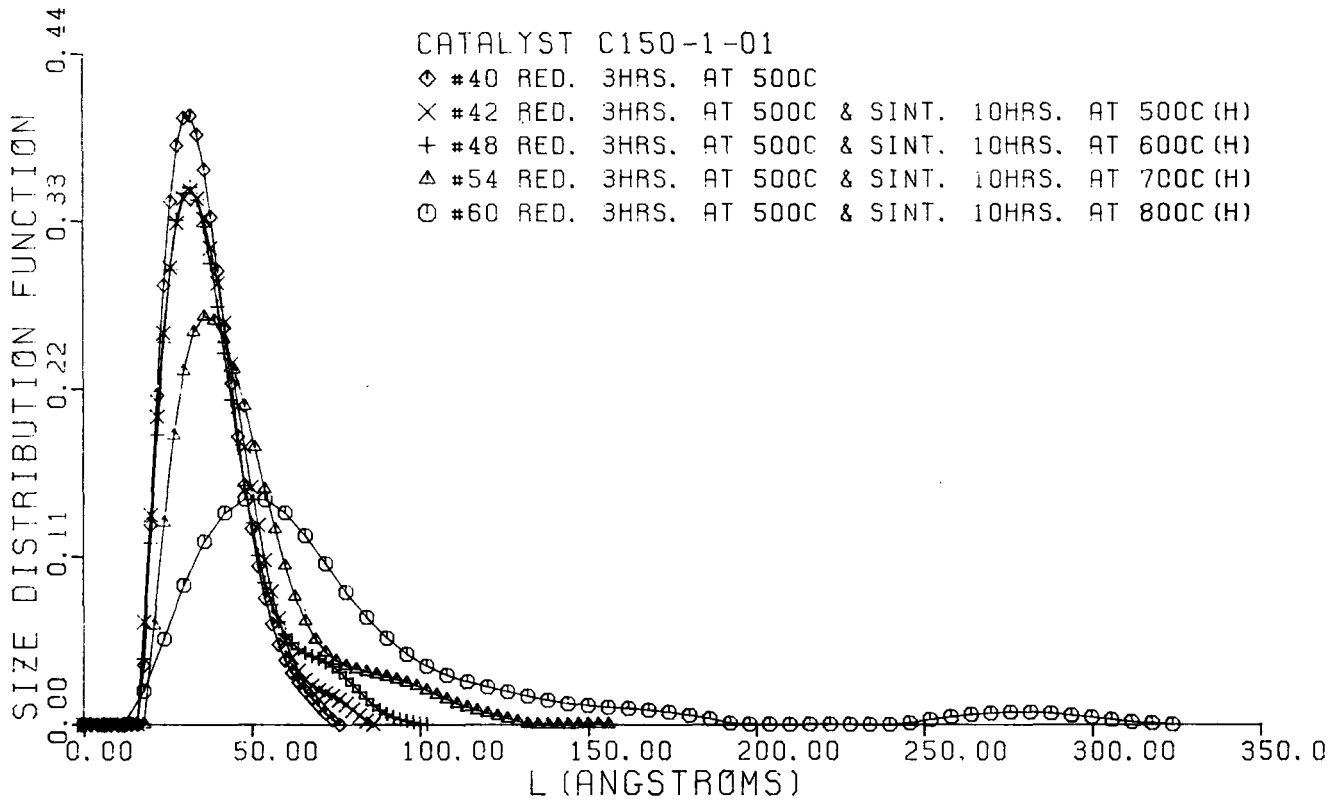


**Figure 2. Particle size distribution functions of catalyst C150-1-01 reduced at 500°C for three hours and sintered at 500, 60( 700 and 800°C for 10 hours in a hydrogen atmosphere.**

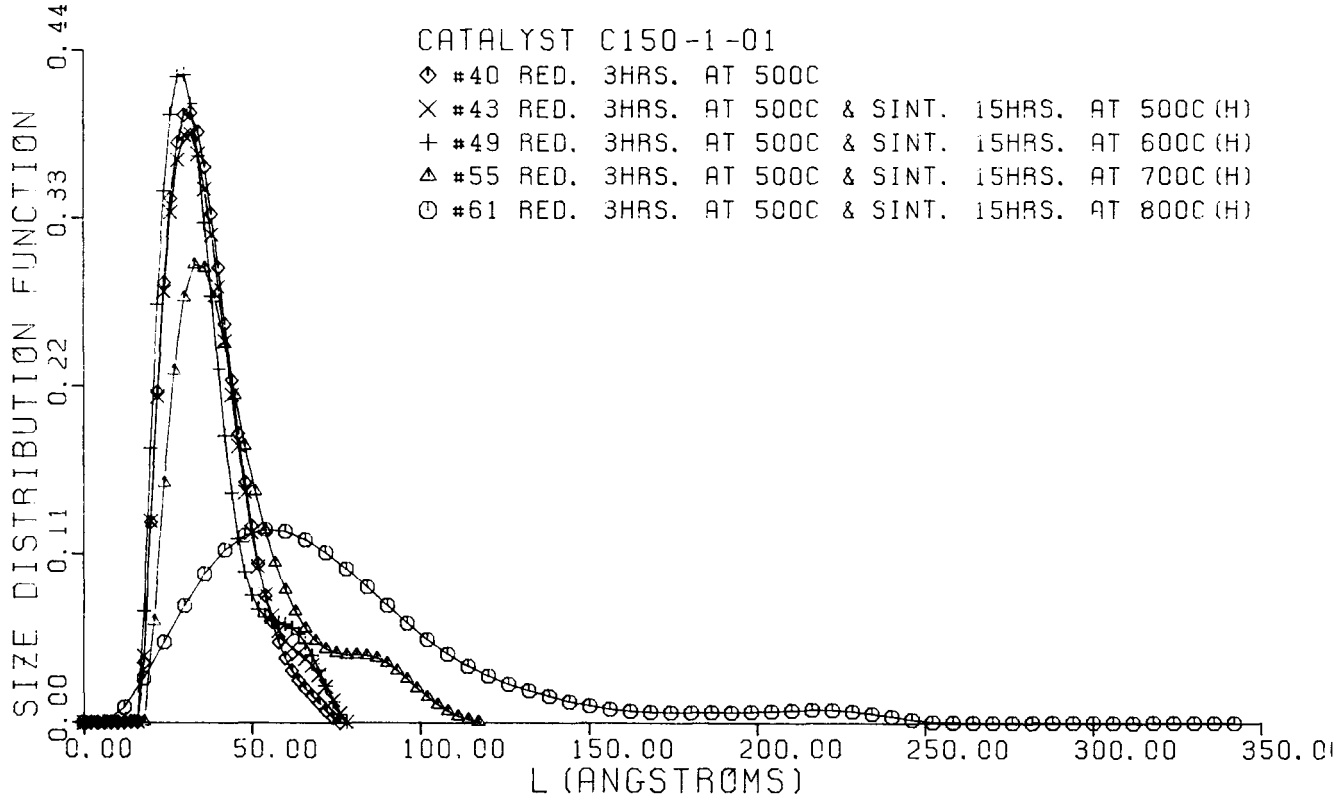


**Figure 3. Particle size distribution functions of catalyst C150-1-01 reduced at 500°C for three hours and sintered at 500, 60( 700 and 800°C for 15 hours in a hydrogen atmosphere.**

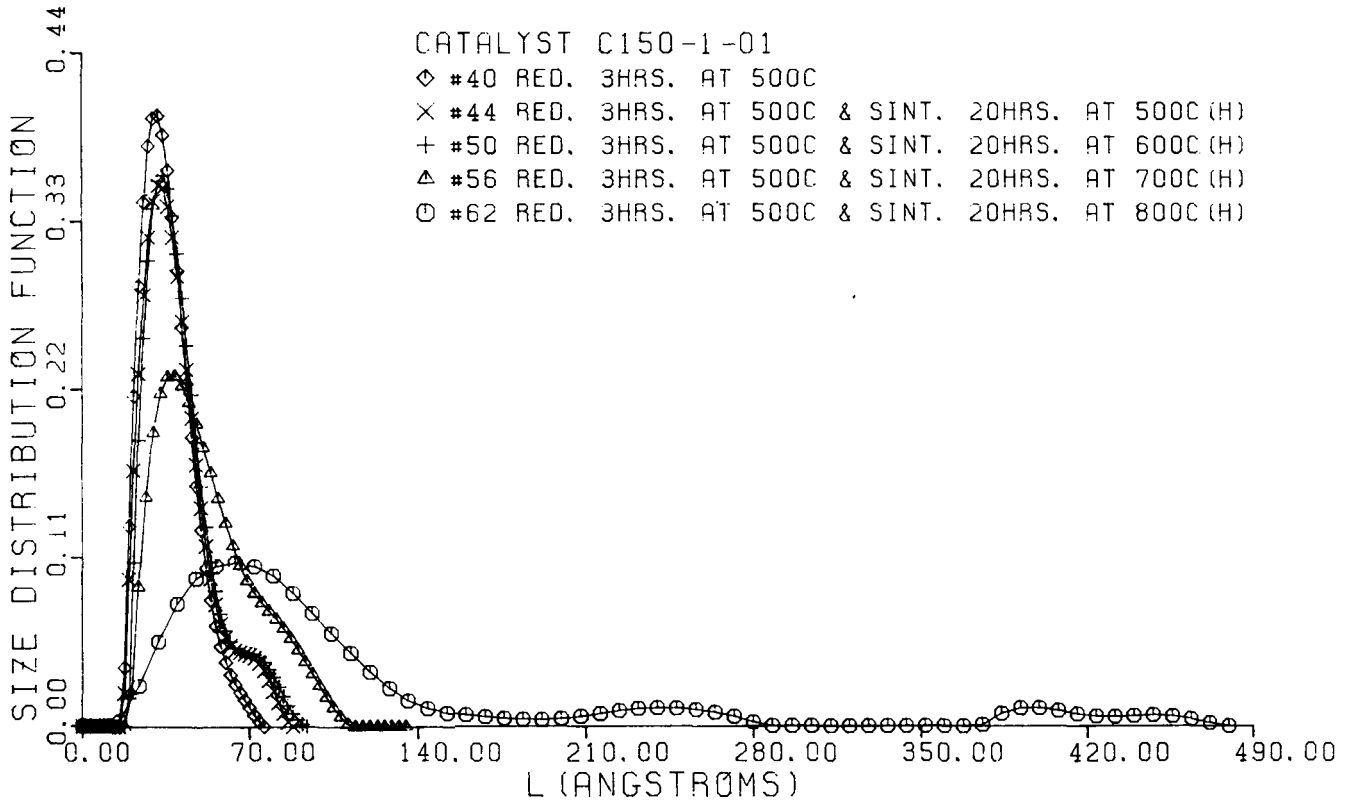


**Figure 4. Particle size distribution functions of catalyst C150-1-01 reduced at 500°C for three hours and sintered at 500, 600, 700 and 800°C for 20 hours in a hydrogen atmosphere.**

hydrogen atmosphere results. Sintering occurs very rapidly at short sintering times and proceeds much more slowly at longer times. The effects of sintering temperature on the particle size distribution are much more pronounced than the effects of sintering time. There appears to be a limiting particle size which increases with increasing sintering temperature. Also, there is a definite formation of tails in the distribution functions to the larger particle size side. This type of tail formation supports a sintering model based on a particle migration mechanism.[14, 15] The lack of formation of particles smaller than the original particles tends to indicate that an atomic migration mechanism was inoperative.[16]

In order to independently check the validity of particle size distribution functions determined by the x-ray diffraction method, transmission electron microscopy studies were conducted on specimens, derived from five selected runs, to obtain the particle size distributions by direct observation. The specimens were prepared by suspending the catalyst powder in methyl alcohol ultrasonically prior to undergoing the TEM analyses. A drop of the suspension solution was placed on a copper grid coated with carbon on formvar, and the alcohol was allowed to evaporate. After drying, the specimens were observed in a Hitachi Hull-B Electron Microscope set for high resolution observations. Photographs of each specimen were enlarged to greater than 500,000 magnification. Tedious and time consuming measurements of images of about 1000 particles were made from photomicrographs of each specimen to determine the PSD.

Figures 5 through 9 are comparisons of the normalized particle size distributions determined by x-ray diffraction and transmission electron microscopy for catalysts that were: reduced three hours at 500°C in hydrogen, reduced three hours at 500°C in hydrogen and sintered 50 hours at 700°C in nitrogen and hydrogen, 100 hours at 700°C in nitrogen, and 20 hours at 800°C in hydrogen.

The agreement between the results obtained from the two techniques is considered to be excellent, especially in the cases of the as-reduced samples sintered at 700°C for 50 hours in nitrogen and hydrogen atmospheres (Figs. 5 to 7). The agreement is not as good in the case of the specimen sintered at 700°C for 100 hours in nitrogen (Fig. 8). However, this specimen was stored in the atmosphere about three weeks after the x-ray work was completed and prior to making the TEM specimens. During this period of time a portion of the nickel metal possibly reoxidized, increasing the apparent size of the particles. The agreement observed, however, was still good, even for this poor specimen. Similar results on domain size distribution

functions in $Cu_3Au$ have been obtained using the Warren double-order, x-ray technique, however, these are the initial data reported which support the single-profile, x-ray technique of determining the particle size distribution function.[17, 13] In addition, although particle size distributions determined by TEM have been compared with small angle x-ray results on a platinum catalyst, this is the first time x-ray line profile analysis and TEM-determined particle size distribution functions have been performed on a supported nickel catalyst.[18]

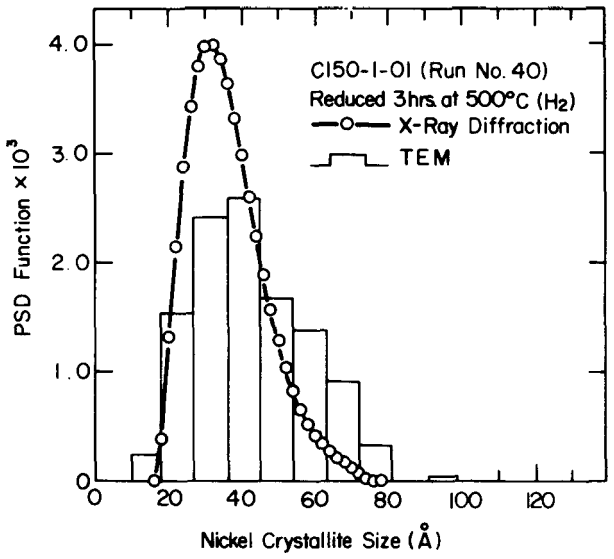


**Figure 5. Particle size distribution functions determined by transmission electron microscopy and x-ray diffraction for catalyst C150-1-01 in the as-reduced condition.**

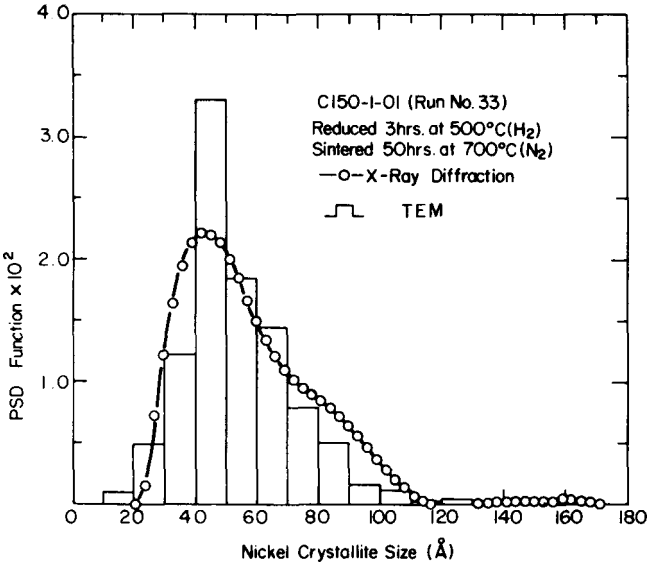


**Figure 6. Particle size distribution functions determined by transmission electron microscopy and x-ray diffraction for catalyst C150-1-01 reduced and sintered at 700°C for 50 hours in a nitrogen atmosphere.**

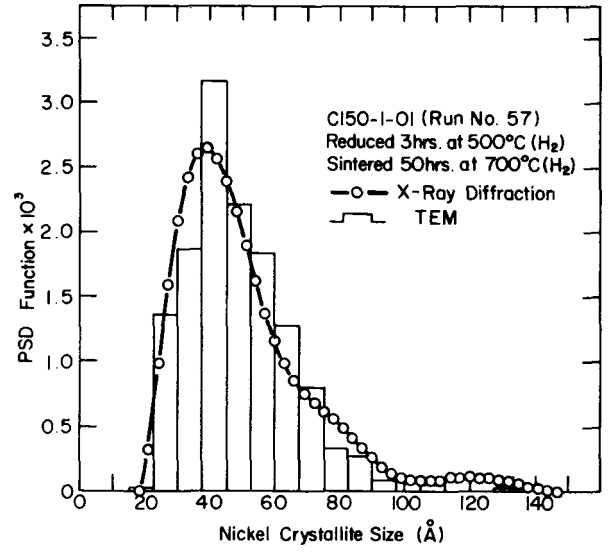


**Figure 7. Particle size distribution functions determined by transmission electron microscopy and x-ray diffraction for catalyst C150-1-01 reduced and sintered at 700°C for 50 hours in a hydrogen atmosphere.**

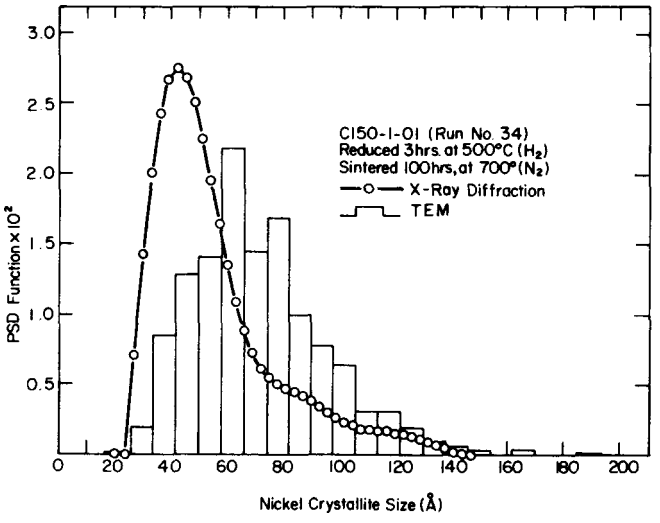


**Figure 8. Particle size distribution functions determined by transmission electron microscopy and x-ray diffraction for catalyst C150-1-01 reduced and sintered at 700°C for 100 hours in a nitrogen atmosphere.**

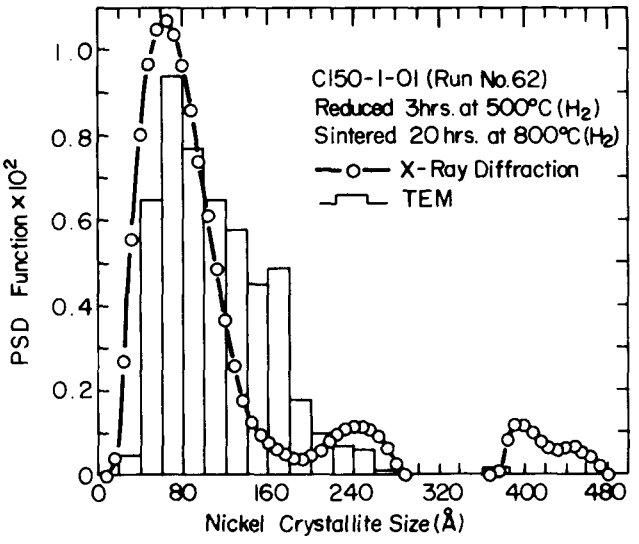


**Figure 9. Particle size distribution functions determined by transmission electron microscopy and x-ray diffraction for catalyst C150-1-01 reduced and sintered at 800°C for 20 hours in a hydrogen atmosphere.**

## Conclusions

(1) An x-ray technique based on the analysis of a single-order profile which allows the reliable determination of the particle size distribution function has been developed. This technique has been successfully applied to monitoring of changes in the particle size distribution of a silica-supported nickel catalyst during sintering.

(2) Sintering of a silica-supported nickel catalyst occurs rapidly at short sintering times and progresses very slowly at longer sintering times.

(3) The extent of sintering observed is strongly dependent on the temperature of sintering and less dependent on the sintering time at a particular temperature.

(4) The operative sintering mechanism is one which contains a particle migration step.

## Acknowledgements

This research was sponsored by the Institute for Mining and Minerals Research, and by the Energy Research and Development Agency through Contract No. E(49-18)2229.

## References

1. S. E. Wanke and P. C. Flynn, **Catalysis Reviews**, Vol. 12, No. 1, pp. 93 (1975).

2. A. D. O. Cinneide and J. K. A. Clarke, **Catalysis Reviews**, Vol. 7, No. 2, pp. 213 (1972).

3. A. Gangulee, **Journal of Applied Crystallography**, Vol. 7, pp. 434 (1974).

4. J. Mignot and D. Rondot, **Acta Metallurgica**, Vol. 23, pp. 1321 (1975).

5. A. R. Stokes, **Proceedings of the American Physical Society**, Vol. 61, p. 382 (1948).

6. R. L. Rothman and J. B. Cohen, **Advanced X-Ray Analysis,** Vol. 12, p. 208 (1969).

7. B. E. Warren and B. L. Averbach, **Journal of Applied Physics,** Vol. 21, p. 595 (1950).

8. B. E. Warren, **Progress in Metal Physics,** Vol. 8, p. 152 (1959).

9. M. McKeehan and B. E. Warren, **Journal of Applied Physics,** Vol. 24, p. 52 (1953).

10. W. P. Evans, R. E. Ricklefs and J. H. Millan, in *"Local Atomic Arrangements Studied by X-Ray Diffraction,"* (J.B. Cohen and J. E. Hilliard, Eds.) Gordon and Breach, New York, p. 271 (1966).

11. R. J. De Angelis in *"Local Atomic Arrangements Studied by X-Ray Diffraction,"* (J. B. Cohen and J. E. Hilliard, Eds.), Gordon and Breach, New York, p. 271 (1966).

12. A. Guinier, *"X-Ray Diffraction in Crystals, Imperfect Crystals and Amorphous Bodies,"* Freeman, San Francisco, (1963).

13. P. Ganesan, H. K. Kuo, A. Saavedra and R. J. De Angelis, **Journal of Catalysis,** Vol. 52, p. 310 (1978).

14. E. Ruckenstein and B. Pulvermacher, **AIChE Journal,** Vol. 19, p. 356 (1973).

15. E. Ruckenstein and B. Pulvermacher, **Journal of Catalysis,** Vol. 29, p. 224 (1973).

16. P. C. Flynn and S. E. Wanke, **Journal of Catalysis,** Vol. 34, pp. 390, 400 (1974).

17. M. Sakai and D. E. Mikkola, **Metallurgical Transactions,** Vol. 2, p. 1635 (1971).

18. A. Renouprez, C. Hoang-Van and P. A. Compagnon, **Journal of Catalysis,** Vol. 34, p. 411 (1974).

# Infrared and Raman Spectra of a Sulfur-Resistant Methanation Catalyst

by

**J. M. Stencel and E. B. Bradley**
Department of Electrical Engineering
University of Kentucky
Lexington, Kentucky 40506

and

**F. R. Brown**
U. S. Department of Energy
Pittsburgh Energy Technology Center
4800 Forbes Avenue
Pittsburgh, Pennsylvania 15213

## Abstract

The infrared and Raman spectra of a sulfur-resistant $NiO/Cr_2O_3/MgSiO_3$ methanation catalyst are presented and compared to the spectra of the catalyst after being reduced, sulfided and tested for methanation activity. The molecular structure of the catalyst is shown to be represented by NiO and MgO dispersed in a quasi-tridimensional Cr-O-Si network. Reduction and sulfiding reorders this network and alters the $SiO_n$ coordination while reducing $Cr^{6+}$ to $Cr^{3+}$ or $Cr^{2+}$. The data indicate that the $SO_4^{-2}$ present after sulfiding and methanation testing may have been formed during the methanation reaction.

## Introduction

The interactions between the components of heterogeneous catalysts have not been studied thoroughly with respect to the contribution of the support material to catalytic activity, stability and specificity.[1] It is known that interactions occur (between the active metal sites and the support) which involve electron donor-acceptor properties of the support.[2] Such interactions play an integral part in the bonding characteristics of adsorbed species and may promote the activity of the catalyst in the presence of poisons such as sulfur. For example, methanation catalysts containing Ni with a $MgSiO_3$ support convert less than 20 percent of the CO to $CH_4$ in a laboratory methanator with five parts per million $H_2S$ in the synthesis gas after being sulfided with approximately 0.6 percent $H_2S$ in $H_2$, whereas incorporating $Cr_2O_3$ in the catalyst increases this conversion activity to 70 percent.[3] These results indicate that it should be possible to prepare methanation catalysts which have suitable long-term activity and stability even in the presence of catalytic poisons. However, such a task relies on the knowledge of the distribution and coordination of the active sites and of the support material which lead to catalytic stability.

The structure of the catalytic surface has been shown to be altered during adsorption of sulfur.[4,5] The support is not an inert substance, and hence, the reconstruction of the active catalytic surface is expected to alter the state of the support.

Thus, it may be possible to describe structural characteristics, such as the coordination of the support, which lead to a stable methanation catalyst by analyzing its infrared and Raman spectra before and after typical use. Monitoring of the reaction *in situ* would be more beneficial, but is extremely difficult.

We have obtained the infrared and Raman spectra of a $NiO/Cr_2O_3/MgSiO_3$ catalyst which has been shown to have suitable methanation activity even in the presence of high sulfur concentrations.[3] The spectra of the as-prepared catalyst were compared to those obtained after reduction and sulfiding, as well as after methanation testing. These spectra show that structural changes do occur to the support material during sulfur treatment and methanation testing. Such reconstruction is related to the catalytic activity and sulfur adsorption.

## Experimental Technique

The $NiO/Cr_2O_3/MgSiO_3$ catalyst samples were supplied by United Catalysts, Inc., Louisville, Kentucky. The methods of preparation are proprietary, but include precipitation methods, along with pellet pressing which include the addition of carbon as a pellet binder. Some chemical and physical properties of the catalyst are shown in Table 1. The representation of the catalyst as $NiO/Cr_2O_3/MgSiO_3$ is expected to give only the most general description of the molecular structure of the catalyst. Catalyst samples were obtained and prepared under the conditions described earlier, except the infrared transmission pellets were pressed under 100,000 psi.[6]

Reference spectra of various substances were obtained to facilitate assignments of the infrared and Raman bands which were observed for the catalyst. These samples included technical grade $Na_2CrO_4$, $MgCrO_4$, $Al_2(CrO_4)_3$, $K_2Cr_2O_7$, $Cr_2(SO_4)_3$, $NiSO_4$ and amorphous $SiO_2$. Spectra were also obtained for NiO, $MgSiO_3$ and $Cr_2O_3$ samples which were used in similar catalyst preparations. Mixtures of these compounds were also made to enable spectral acquisition of $NiO + Cr_2O_3$ and $NiO + Cr_2O_3 + MgSiO_3$.

The Raman spectra were recorded on a Spex Ramalog spectrometer equipped with holographic gratings. The 5145 Å line from a Spectra Physics Model No. $126Ar^+$ laser was used as the exciting source. Spectral slit width was typically 8 $cm^{-1}$ and the laser power at the sample was approximately 50 mW. A description of the rotating Raman sample cell used to hold the catalyst pellets has been published previously.[7]

## Experimental Results

Figure 1a shows the infrared spectrum of the as-prepared $NiO/Cr_2O_3/MgSiO_3$, and Figure 1b shows the spectrum of the reduced, sulfided and methanation-tested catalyst. The intense 3400 $cm^{-1}$ band and the 1610 $cm^{-1}$ absorption are due to adsorbed $H_2O$. These bands are common to all powdered samples which have been exposed to the atmosphere, but are more intense for high-surface area adsorbents. Infrared absorption from 1200 to 400 $cm^{-1}$ results from the fundamental vibrational modes of the catalyst material. The 1135 $cm^{-1}$ shoulder, the intense band at 670 $cm^{-1}$ and the intensity decrease from 930 to

**Table 1. Composition and Surface Area of the $NiO/Cr_2O_3/MgSiO_3$ Methanation Catalyst.**

| Surface Area of Catalyst ($m^2/g$) | | Weight Percents of Constituents | |
|---|---|---|---|
| New | 191 | NiO | 49.7 |
| Sulfided; Methanation Tested | 96 | $Cr_2O_3$ | 25.3 |
| | | $MgSiO_3$ | 25.0 |

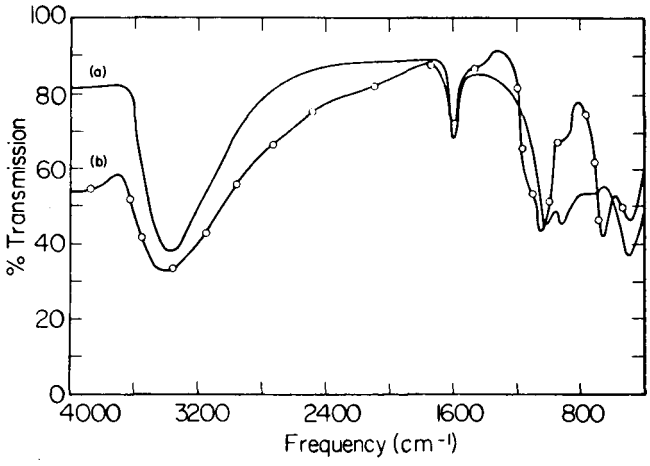


**Figure 1. Infrared spectra of the $NiO/Cr_2O_3/MgSiO_3$ catalyst in the (a) as-prepared form, and (b) after reduction, sulfiding and methanation testing.**

730 $cm^{-1}$ and 600 to 400 $cm^{-1}$ in Figure 1b are discussed later in terms of structural changes of the support material. Also, the band at 1015 in Figure 1a shifts to 1035 $cm^{-1}$ for the tested catalyst, Figure 1b.

Figure 2 shows the Raman spectra of the as-prepared catalyst (Fig. 2a), the as-prepared catalyst after exposure to 1.5 watts of laser irradiation at 5145 Å for 10 minutes (Fig. 2b),and the spectrum of the methanation-tested catalyst (Fig. 2c). The intense band at 815 $cm^{-1}$ in (a) is absent from both (b) and (c). Also, band intensities in the 1370 and 1590 $cm^{-1}$ regions increase for the tested catalyst, while the 595 $cm^{-1}$ band is approximately equal in (a) and (c).

Figure 3 shows the infrared spectra from 1300 to 400 $cm^{-1}$ for (a) the as-prepared catalyst, (b) the reduced and sulfided catalyst, (c) the reduced and sulfided catalyst which had been heated in air at 350°C for 30 minutes, and (d) the reduced, sulfided and methanation-tested catalyst. These spectra show intensity changes near 800 $cm^{-1}$ which are similar to those in Figure 1. The absorption at 920 $cm^{-1}$ decreases for the consecutive spectra, Figure 3(a,b,c,d); frequency shifts toward larger values are observed for the band in the 1020 $cm^{-1}$ region for the same spectral sequence. After oxidation of the sulfided catalyst at 350°C, increased absorption is noted at 1135 $cm^{-1}$ in Figure 3c which is similar to that in Figure 3d. Small differences are observed from 650 to 400 $cm^{-1}$ between (a), (b) and (c), while the methanation tested sample has approximately 25 percent less absorption in this region.

## Discussion

The effects of adsorption of atmospheric gases on the methanation-tested catalyst are expected to be minimal because of the $N_2$ cooling process at the conclusion of the test. Here, the $N_2$ purge acts to passivate the high-area adsorbate.[8] Similarly, a catalyst at ambient room temperature is less reactive, which decreases the possibility of structural changes due to adsorption when the catalyst is removed from the reactor. The stability of the tested catalysts is observed in the sulfided catalyst which had to be heated to 350°C before the 1135 $cm^{-1}$ band in Figure 3c appeared. Heating of the as-prepared and methanation-tested catalysts did not alter their band structure in this region. Similarly, $H_2O$ adsorption is not expected to contribute to this band structure, or that in the 500 $cm^{-1}$ region, since the absorption characteristics in these regions were approximately constant for the as-prepared and methanation-tested samples which had been dehydrated at 250°C. Adsorption of atmospheric gases other than oxygen is expected to produce infrared bands in the 3000 to 1300 $cm^{-1}$ region; however, no samples had infrared absorption other than that due to $H_2O$ in this region. Thus, the 1135 $cm^{-1}$ band, and the

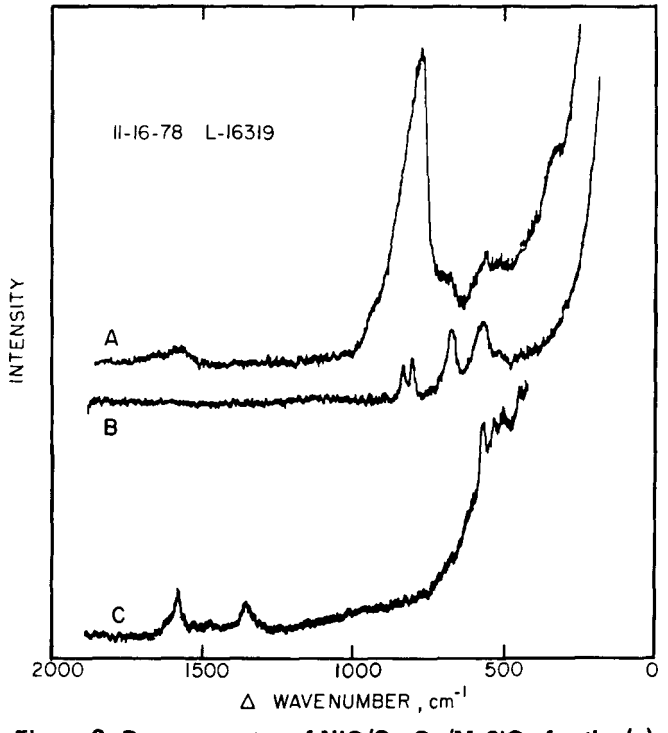


**Figure 2. Raman spectra of $NiO/Cr_2O_3/MgSiO_3$ for the (a) as-prepared catalyst, (b) after 1.5 watt laser irradiation at 5145 Å for 10 minutes, and (c) the methanation tested catalyst.**

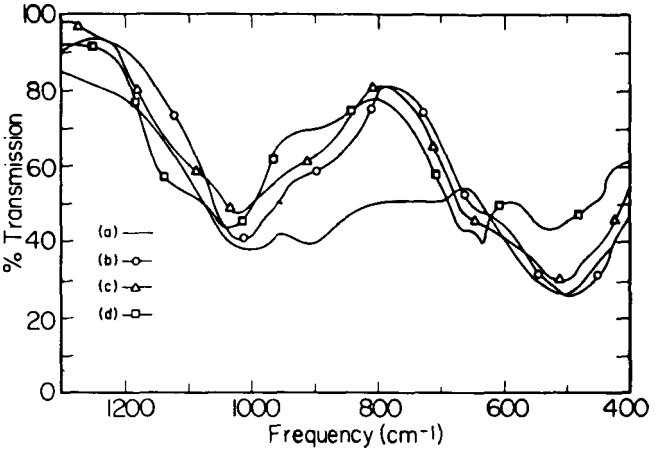


**Figure 3. Infrared spectra of $NiO/Cr_2O_3/MgSiO_3$ from 1300-400 $cm^{-1}$ for (a) the as-prepared catalyst, (b) the reduced and sulfided catalyst, (c) reduced and sulfided catalyst after heating in air at 350°C, and (d) the reduced, sulfided and methanation tested catalyst.**

decreased band intensity in the 500 $cm^{-1}$ region of Figure 3d, are thought to be directly related to structural changes to the catalyst which occur during the methanation reaction.

The broad, ill-defined infrared absorption increases the difficulty of spectral interpretation. Fortunately, the Raman spectra are more definitive, particularly with regard to the coordination of the Cr in the as-prepared catalyst. This in turn defines the origin of the 920 $cm^{-1}$ infrared band.

The most prominent feature of the Raman spectrum of the as-prepared catalyst is the intense, asymmetric band centered at approximately 820 $cm^{-1}$ (see Fig. 2a). Raman spectra of $SiO_2$, $MgSiO_3$ and zeolites obtained in conjunction with the present work show no intense band in this region. This is in agreement with prior work on compounds containing $SiO_n$ groupings.[9] The most intense Raman band for these compounds is the SiO bending mode near 470 $cm^{-1}$, followed in intensity by the weaker SiO stretching modes in the 1050 $cm^{-1}$ region. The corresponding SiO stretching mode in the infrared spectra is located between 120 and 950 $cm^{-1}$, depending on the $SiO_n$ coordination and the degree of cross-linking.

Raman spectra of powdered samples of $Na_2CrO_4$, $MgCrO_4$ and $Al_2(CrO_4)_3$ obtained in this study have intense bands in the 830 to 850 $cm^{-1}$ region. These bands are similar in frequency to those found for the CrO symmetric stretch in $CrO_4^{-2}$ units.[10] The undistorted $CrO_4^{-2}$ group has $T_d$ symmetry and bands at 847 and 884 $cm^{-1}$ are assigned to the A and $F_2$ modes, respectively.[10] In addition, the $F_2$ mode can be split, depending upon the environment of the $CrO_4^{-2}$ units, because of a lowering of the local site symmetry.[11] In dichromates, the CrO symmetric stretch is located near 900 $cm^{-1}$ and this increase in frequency can be related to the decreased coordination of the $CrO_n$ units.[12] In addition, $CrO_2$ and $Cr_2O_3$ have no Raman bands in this region.[13, 14] Accordingly, the intense band in Figure 2a is assigned to the $CrO_4^{-2}$ unit. The high frequency-side asymmetry of the band is attributable to the presence of the two $CrO_4^{-2}$ fundamentals (A and $F_2$), and the possible splitting of the $F_2$ fundamental. Correspondingly, the 920 $cm^{-1}$ band in the infrared spectrum is assigned to the asymmetric stretch of the $CrO_4^{-2}$.

Other Raman bands at 585 and 540 $cm^{-1}$ present in the spectrum of the as-prepared catalyst are also present in another catalyst ($NiO/Cr_2O_3/MgAl_2O_4$) which has been investigated. Upon comparison with $Cr(OH)_3$, which has a band at 535 $cm^{-1}$, it is felt these bands are due to hydrogen bonded $H_2O$ and terminal $OH^-$, respectively.

The spectrum shown in Figure 2b enhances the interpretation that $CrO_4^{-2}$ units are present in the as-prepared catalyst. This spectrum was recorded after exposing the as-prepared catalyst to high-intensity laser irradiation (approximately 1.5 watts for 10 minutes). The large decrease in scattering in the 900 to 800 $cm^{-1}$ region results from thermal decomposition caused by the laser beam. Figure 2b shows some residual Raman scattering in the 850 $cm^{-1}$ region, indicating that the decomposition was incomplete. More significantly, two well-defined bands appear in this region. These are assigned to the A and $F_2$ modes of $CrO_4^{-2}$. The absence of splitting in the higher frequency $F_2$ mode indicates that this residual $CrO_4^{-2}$ is located in a distortion-free environment. Finally, this noted thermal decomposition affirms the necessity for the care that must be taken when recording Raman spectra of absorbing materials.

The $CrO_4$ coordination is not just a geometric surface effect because the 820 $cm^{-1}$ band is observed in Raman spectra of external and internal layers of the catalyst. It is also observed in the infrared spectra where both bulk and surface are analyzed as a result of the infrared pellet pressing technique. The Raman band centered at approximately 1600 $cm^{-1}$ in the as-prepared catalyst correlates with that observed for graphite, and is expected to result from the graphite binder.[15] The absence of this band in Figure 2b (spectrum of the as-prepared catalyst after intense laser irradiation) is interpreted as showing that the graphite binder was oxidized during the laser treatment. It is interesting that two bands associated with carbon are present in the spectrum of the sulfided-methanation tested catalyst (Fig. 2c). The intensity of the second band ($\cong$1365 $cm^{-1}$) has been shown to be inversely proportional to the size of the graphitic crystallites.[16] Thus, the catalyst testing is seen to decrease the size of these crystallites. Carbon deposition during the methanation reaction is expected and the spectra indicate that some ordering exists within this deposit.

The infrared band, which is centered at 1015 $cm^{-1}$ in Figure 3a and b, 1020 $cm^{-1}$ in Figure 3c and 1035 $cm^{-1}$ in Figure 3d, is due to an SiO stretching mode. In general, increasing the value of the coordination number n in $SiO_n$ groups decreases the SiO stretching frequency.[17,18] For example, silicon monoxide absorbs at 125 $cm^{-1}$,[19] the stretching mode of $SiO_2$ appears in the 1210 to 1100 $cm^{-1}$ region, and $SiO_4$ and $Si_2O_7$ groups absorb in the 1050 to 950 $cm^{-1}$ region.[18,20] Thus, the 1010 $cm^{-1}$ SiO absorption indicates that the as-prepared catalyst has $SiO_4$ and/or $Si_2O_7$ coordination. Such coordination would be expected to promote cross-linking, e.g., $SiO_4$ with $CrO_4$, to produce a Si-O-Cr array. This does not imply long-range order, as in a crystal, since x-ray diffraction measurements show very broad bands due to the support which is characteristic of amorphous material. Similarly, the large particle size of the Ni (approximately 30 Å for the as-prepared catalyst) would cause distortion of such an Si-O-Cr complex.

It is known that poorly ordered Si-O-Al units in zeolites, which have coordinated $H_2O$ units, produce broad absorption near 750 $cm^{-1}$, and that this absorption can be used to measure the degree of crystallinity in these materials.[21] Similar effects could cause the broad, undefined absorption in Figure 3a from 830 to 670 $cm^{-1}$. Thus, the infrared absorption from 1200 to 600 $cm^{-1}$ for the as-prepared sample is thought to be the result of a quasi-tridimensional array of Si-O-Cr·$H_2O$ units. The 600 to 400 $cm^{-1}$ region can then be explained by absorption due to MgO and NiO stretching modes.[22, 23] It is possible that the

Mg is also associated with the Si-O-Cr structure which would perturb its vibrational modes and increase the absorption in the 750 $cm^{-1}$ region.

Reducing and sulfiding the catalyst decreases the $CrO_4^{-2}$ concentration, as is observed in the decrease in intensity of the CrO vibrational mode of Figure 2c and 3b. No bands which are explicitly associated with sulfur are found in the 1300 to 400 $cm^{-1}$ infrared region of Figure 3b; adsorbed sulfur is expected to be in sulfide form which does not absorb in this region. ESCA data for this catalyst prove that sulfide species are present after the reduction and sulfide treatment.[24] Subsequent oxidation of this sample allows the infrared absorption due to $SO_4^{-2}$ to be observed near 1135 $cm^{-1}$ (Fig. 3a).[25, 26] Similar band structure is observed for the reduced/sulfided/methanation-tested catalyst, which also has a narrow band at 630 $cm^{-1}$ characteristic of $SO_4^{-2}$. ESCA data show that the $SO_4^{-2}$ concentration is large and evenly distributed throughout the reduced/sulfided/methanation-tested catalyst, while $SO_4^{-2}$ is primarily located on the surface of the reduced/sulfided sample which had been oxidized in air.[24] Other methanation catalysts examined during these analyses, which have low methanation conversion rates after sulfiding, do not have an even distribution of $SO_4^{-2}$. It is thought that formation of bulk $SO_4^{-2}$ during room-temperature air exposure will be minimal, considering the cooling process after the methanation tests and high temperature which was necessary to oxidize the sulfide species. Oxidized forms of sulfur have not been shown to be catalytic poisons.[1] Thus, the high activity of this catalyst, even after sulfur treatment, may be partially explained by the oxidation of the sulfide species during the methanation reaction. The site of the $SO_4^{-2}$ is not completely known, but it may be associated with NiMg or NiCr sites as it is in $NiO/Cr_2O_3/MgAl_2O_4$.[6] It is fair to note that this interpretation relies on the formation of bulk $SO_4^{-2}$ during the methanation reaction and not during the possible, but improbable, oxidation of bulk sulfur during air exposure.

In Figure 3, the increase in the SiO stretching frequency with reduction, sulfiding and methanation testing could be related to a change in the coordination number n of the $SiO_n$ groups. This is especially true in Figure 3d which shows that the infrared absorption at 1035, 650 and 480 $cm^{-1}$ closely resembles that for our reference spectrum of $MgSiO_3$. However, the 650 $cm^{-1}$ band is more pronounced than for $MgSiO_3$, which indicates intensity contributions from the $SO_4^{-2}$ and $Cr_2O_3$ vibrational modes. Thus, decreased band intensity in the 1000 to 700 $cm^{-1}$ region, in conjunction with the increased SiO stretching frequency, indicates that the silicate support can be more nearly described by isolated $SiO_n$ groups after being methanation tested.

## Conclusion

It has been shown that infrared and Raman spectra can determine the structural changes which occur to the support of a methanation catalyst during reducing, sulfiding and methanation testing. During these processes, $Cr^{+6}$ is reduced to $Cr^{+3}$ and/or $Cr^{+2}$ for $NiO/Cr_2O_3/MgSiO_3$ which increases the electron density near the Cr sites. The ability to prepare sulfur-resistant catalysts is shown to be possible by the high-methanation activity of the $NiO/Cr_2O_3/MgSiO_3$ catalyst. However, the description of the physical and chemical properties of this catalyst that introduce high activity rely on an understanding of the role and structure of the support in which the active sites are distributed.

## Acknowledgment

The authors wish to thank P. J. Reucroft and R. B. Shalvoy for the ESCA information on this catalyst, and United Catalysts, Inc., Louisville, Kentucky, for supplying and methanation testing the catalysts used in this research. This work was supported in part by DOE Contract No. EX-76-C-01-2229.

## References

1. R. J. Madon and H. Shaw, **Catalysis Reviews – Science and Engineering**, Vol. 15, p. 69 (1977).

2. L. H. Little, **Infrared Spectra of Adsorbed Species**, Academic Press, p. 205 (1966).

3. A. Hausberger, United Catalysts, Inc., private communication.

4. G. A. Somorjai, **Journal of Catalysis**, Vol. 27, p. 453 (1972).

5. J. L. Oliphant, R. W. Fowler, R. B. Pannell and C. H. Bartholomew, **Journal of Catalysis**, Vol. 51, p. 229 (1978).

6. J. M. Stencel and E. B. Bradley, **Applied Spectroscopy**, Vol. 33, p. 118 (1979).

7. F. R. Brown, L. E. Makovsky and K. H. Rhee, **Applied Spectroscopy**, Vol. 31, p. 563 (1977).

8. J. W. E. Coenen and B. G. Linsen, **Physical and Chemical Aspects of Adsorbents and Catalysis**, Academic Press, p. 471 (1970).

9. C. L. Angell, **Journal of Physical Chemistry**, Vol. 77, p. 222 (1973).

10. W. P. Doyle and P. Eddy, **Spectrochimica Acta**, Vol. 23A, p. 1903 (1967).

11. W. B. Grant and S. Rodhokrishna, **Solid State Communications**, Vol. 13, No. 1, p. 109 (1973); W. Scheuermann, **Proceedings, Symposium on Molecular Spectroscopy**, 4, Morning Session, p. 14 (1973).

12. W. Scheuermann and G. J. Ritter, **Journal of Molecular Structure**, Vol. 6, p. 240 (1970).

13. R. Srivastova and L. L. Chase, **Solid State Communications**, Vol. 11, No. 2, p. 349 (1972).

14. T. R. Hart, R. L. Aggarwal and B. Lax, **Proceedings of the Second International Conference on Light Scattering of Solids**, p. 174 (1971).

15. P. Tarte and G. Nizet, **Spectrochimica Acta**, Vol. 20, p. 503 (1964).

16. E. Tuinstra and J. L. Koenig, **Journal of Chemical Physics**, Vol. 53, p. 1126 (1970).

17. P. Tarte, **Spectrochimica Acta**, Vol. 23A, p. 2127 (1967).

18. P. H. Gaskell, **Physics and Chemistry of Glasses**, Vol. 8, p. 69 (1967).

19. J. S. Anderson and J. S. Ogden, **Journal of Chemical Physics**, Vol. 51, p. 4189 (1969).

20. A. N. Lazarev, **Optics and Spectroscopy**, Vol. 9, p. 103 (1960).

21. C. E. Stroud, Masters Thesis, Electrical Engineering, University of Kentucky (1979).

22. O. Kammori, K. Sato and N. Yamaguchi, **Japan Anal**, Vol. 16, p. 1050 (1967).

23. R. A. Nyquist and R. O. Kagel, **Infrared Spectra of Inorganic Compounds**, Academic Press, p. 207 (1971).

24. P. J. Reucroft and R. B. Shalvoy, Kentucky Center for Energy Research, personal communication.

25. A. Hezel and S. D. Ross, **Spectrochimica Acta**, Vol. 22, p. 1949 (1966).

26. M. Haas and G. B. B. M. Sutherland, **Proceedings of the Royal Society**, Vol. 236A, p. 427 (1956).

# Studies of the Metal-Support Interaction in Coprecipitated Nickel on Alumina Methanation Catalysts Using X-Ray Photoelectron Spectroscopy (XPS)

by

**R. B. Shalvoy and B. H. Davis**
Institute for Mining and Minerals Research
University of Kentucky
Iron Works Pike, Box 13015
Lexington, Kentucky 40583

and

**P. J. Reucroft**
Department of Metallurgical Engineering and Materials Science
and the Institute for Mining and Minerals Research
University of Kentucky
Lexington, Kentucky 40506

## Abstract

Characterization studies on a series of coprecipitated alumina supported nickel methanation catalysts by x-ray photoelectron spectroscopy (XPS) are described. Binding energies and spectral shapes have been determined for several standard compounds (Ni, NiO, $Ni(OH)_2$, $NiAl_2O_4$, $Al_2O_3$) to provide background information for interpreting the catalyst spectra.

The results indicate that the surface regions of the fresh (unreduced) catalysts are composed primarily of amorphous $NiAl_2O_4$ with some NiO particles present either within the pores of the support or covered by a $NiAl_2O_4$ layer. In comparison with similarly prepared silica supported catalysts, reducibility is more difficult, indicating the presence of stronger support interactions.

## Introduction

Recent emphasis on the need for improved methanation catalysts has stimulated new research efforts which have the broad objective of developing a better understanding of the chemical and physical characteristics of typical methanation catalysts.[1-4] The initial catalyst characterization effort in this laboratory was focused on coprecipitated nickel methanation catalysts since such catalysts have provided a good balance of methanation activity, selectivity, thermal stability and reducibility.[5-10] The good balance of properties was attributed to the metal-support interaction. These catalysts are similar to ones developed for use in commercial coal gas methanation reactors.[10]

X-ray photoelectron spectroscopy (XPS) has been found to provide valuable information on the surface chemical state and abundance of supported, finely dispersed metals and has become widely used to study fresh and treated catalysts.[11-21] In a

recent study, XPS was employed to study silica supported nickel methanation catalysts.[9] Some interaction of the metal with the support was observed. A related series of coprecipitated nickel on alumina catalysts has been studied. The dependence of the interaction on the alumina support and the metal loading was the primary emphasis of this study. These samples extended the metal loading range beyond those of the silica supported nickel catalysts that were studied previously. The strength of the metal-support interaction may vary with the different support and metal loading as was observed in impregnated nickel on alumina catalysts.[22] The nature of the metal-support interaction is a key factor in the preparation of catalysts which are both highly active and thermally stable.

## Experimental Details

The data were recorded using a Kratos ES200B electron spectrometer. Data acquisition was computer controlled. Unmonochromatized Mg radiation was employed. Other experimental details were the same as are given elsewhere, except as noted below.[9]

The spectrometer binding energy scale was calibrated so that the spacing of the $2p_{3/2}$ and $3p_{3/2}$ peaks obtained from an argon ion etched Cu metal foil was 857.6 electronvolts. This procedure is in agreement with that suggested elsewhere and appears to be gaining wide acceptance.[24] The spectrometer work function term in the computer program was then set to give the Au $4f_{7/2}'$ peak binding energy of 84.0 (obtained from a clean Au foil).[25]

Most of the standard samples and the catalysts charged from one to four electronvolts. The charging was measured by monitoring the shift of the contaminent C ls line from a neutral value of 285.0 electronvolts. This technique appears to be as effective as any other and is very convenient for use with catalyst samples.[19-26] As a check, the binding energy shift of the Al 2s peak from the value determined for $Al_2O_3$ was monitored for those catalysts with low nickel contents (L141, L142). A good agreement of the two charging monitors was observed. The binding energies given here are felt to contain uncertainties of ±0.3 to 0.5 electronvolts. It should be noted that a core level binding energy for a strong peak in an identical clean metal foil can differ by as much as one electronvolt when measured at different laboratories, all using presumably correct techniques.[19, 26]

The standard samples (Ni, NiO, $Ni(OH)_2$) were obtained as high purity commercial samples. The oxide and hydroxide were examined as powders pressed onto a copper backed adhesive tape. The nickel aluminate sample was prepared in this laboratory and its composition was verified by x-ray diffraction.

The catalyst samples were supplied by United Catalysts, Inc., Louisville, Kentucky. Catalysts were obtained by precipitating a complex carbonate from an aqueous solution which contained nickel nitrate and aluminum nitrate. After aging for one hour at 82°C, the precipitate was filtered, washed, dried and calcined for 8 to 16 hours at 371°C. The material was then ground to a fine powder, mixed with graphite (two to three percent), and pressed into 1/8 or 3/16-inch tablets. The sample was then calcined further to remove any remaining water. Catalysts obtained by these techniques typically display good methanation activity and small catalyst particle size.[10] Physical properties of the catalysts investigated are summarized in Table 1.

**Table 1. Physical Properties of Catalysts.**

| | C150-1-03 | C150-4-03 | L141 | L142 | L143 | L144 |
|---|---|---|---|---|---|---|
| Percent Nickel (by weight) | 47 | 55.6 | 10 | 20 | 30 | 40 |
| Percent Carbon | 5.8 | 2.7 | | | | |
| Total Surface Area ($m^2\ g^{-1}$) | 155 | 176 | 144 | 96 | 97 | 194 |
| Metal Surface Area ($m^2\ g^{-1}$ (Ni)) (Reduced 400°C) | 26.6 | 35.5 | 9.0 | 18.8 | 30.5 | 37.6 |
| Pore Volume ($cm^3\ g^{-1}$) | 0.33 | 0.51 | 0.37 | 0.33 | 0.36 | 0.50 |
| NiO Crystallite Size (Å) | 19 | 26 | – | – | – | 35 |
| Density ($g\ cm^{-3}$) | 1.01 | 0.93 | 1.01 | 1.01 | 0.94 | 0.82 |

## Results and Discussions

The project was divided into two areas. A series of known compounds (standards) was first examined extensively. The catalyst samples were then examined and the results analyzed in relation to the findings derived for the known compounds.

### Standard Samples

The results for the standard samples are shown in Table 2 and Figures 1 and 2. A detailed discussion of these findings is given elsewhere.[9] The significant findings relevant to the characterization of the $Ni/Al_2O_3$ catalysts are repeated here. All binding energy values have been corrected for sample charging.

The spectra of Ni, NiO, and $Ni(OH)_2$ may be readily distinguished by examining the peak shapes (Ni $2p_{3/2}$ , 0 ls) and the associated binding energies in unknown samples. NiO has a characteristic doublet structure to the Ni 2p peak and a low binding energy to the 0 ls peak. These characteristics have been widely observed, and allow the presence of bulk NiO to be easily discerned.[27-33] The binding energies of the Ni and O peaks in $Ni(OH)_2$ are higher than those observed in NiO. $Ni(OH)_2$ also is much more resistant to argon ion etch reduction than is NiO. The data obtained for $Al_2O_3$ are in agreement with results given elsewhere.[19]

$NiAl_2O_4$ was prepared in this laboratory using standard techniques. The final product was sintered at 1300°C for eight hours before the examination procedures were begun, to ensure the completeness of the reaction.[34] The spectrum of $NiAl_2O_4$ is distinct from those of the other standard samples (Figure 3). The splitting of the Ni and O peaks binding energies is larger than that observed in the other standard samples. The Ni 2p binding energy is also higher than that observed in the other standard samples. These values are in agreement with some of those reported in the literature and in disagreement with others.[35, 16] The data reported here will be used to interpret the catalyst spectra because round robin studies conducted by the ASTM have shown that the greatest consistency in data results when all data being compared are taken in the same laboratory.[19] The spectrum of the Al 2s peak in $NiAl_2O_4$ and the catalysts is complicated by the presence of the Ni 3s peak, which overlaps the low binding energy side of the Al peak. The Ni 3s peak does not overwhelm the Al 2s peak nearly as much as the Ni 3p peak does the Al 2p peak. This situation necessitates use of the Al 2s level rather than the somewhat more

**Table 2. Standard Sample Binding Energies (in eV).**

| Sample | Ni $2p_{3/2}$ | O $1s_{1/2}$ | Al 2s |
|---|---|---|---|
| Ni | 852.8 | | |
| NiO | 854.6 | 529.6 | |
| | 856.0 | | |
| $Ni_2O_3$* | 855.8 | 531.4 | |
| $Ni(OH)_2$ | 855.5 | 531.0 | |
| $Al_2O_3$ | | 531.3 | 119.0 |
| $NiAl_2O_4$ | 856.1 | 531.2 | 119.3 |

*Reference 27

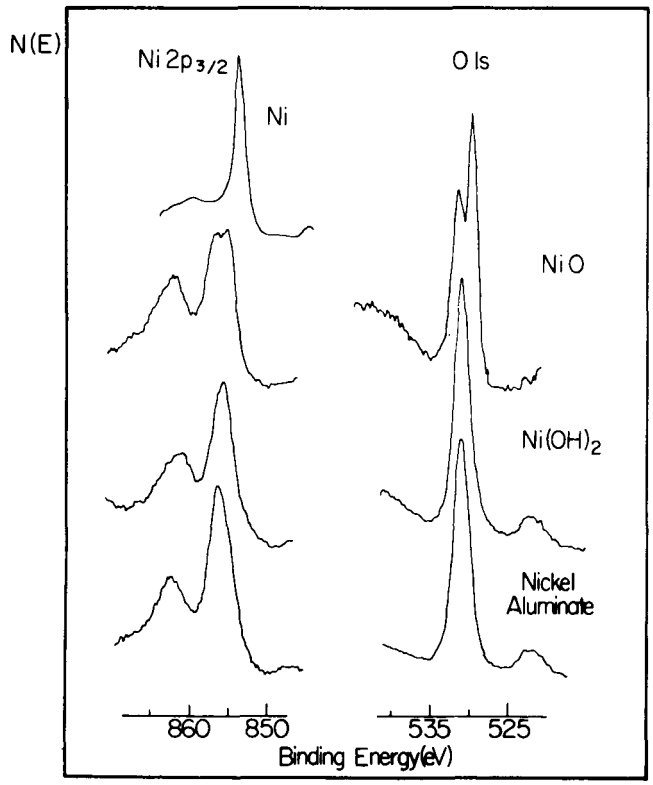


**Figure 1. Spectra of the Ni $2p_{3/2}$ and 0 ls core levels for Ni, NiO, $Ni(OH)_2$ and $NiAl_2O_4$.**

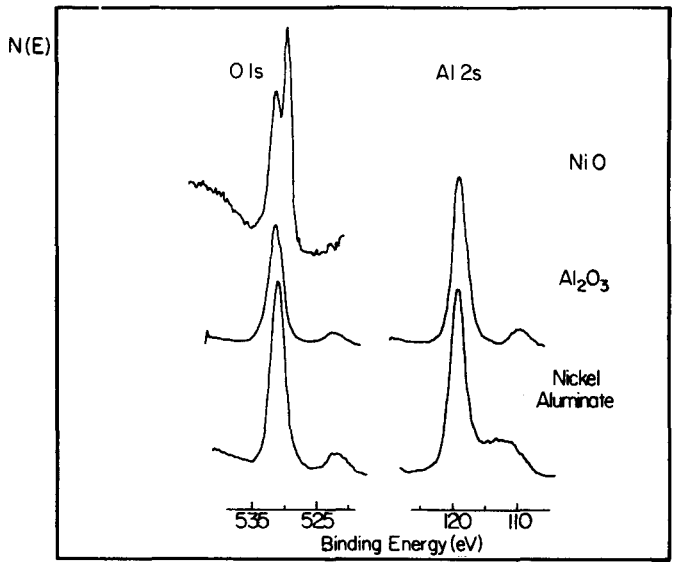


**Figure 2. Spectra of the Al 2s and O 1s core levels in NiO, $Al_2O_3$ and $NiAl_2O_4$.**

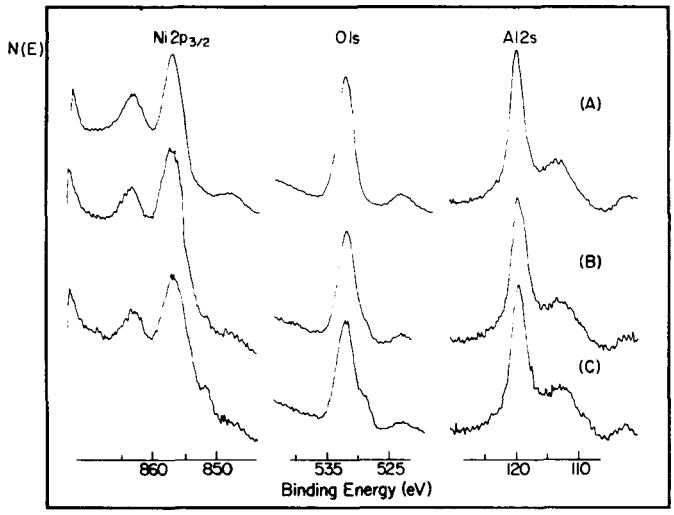


**Figure 3. Spectra for the $NiAl_2O_4$ standard sample: (A) unetched; (B) etched 10 minutes (1 keV); and (C) etched 20 minutes (1 keV).**

intense 2 p level. The effect of the Ni 3s peak on the spectrum of the Al 2s peak can be most easily observed by comparing the Al 2s peaks for $Al_2O_3$ and $NiAl_2O_4$ in Figure 2. This overlap did not pose a significant problem in the analysis of the Al peak energy.

It was observed that in contrast with a similarly prepared $NiSiO_3$ sample, the Ni in the $NiAl_2O_4$ sample was not readily reduced by the conventional argon ion etching treatment (one keV ion energy, 10 to 30-minute etching) that caused the Ni in NiO, and to a lesser extent $NiSiO_3$, to reduce to the metallic state (Figure 3).[9] The results from the argon ion etch reduction studies parallel those obtained from thermal gravimetric analysis (TGA) studies of the reduction of N in flowing $H_2$.[36] The effects of argon etching on Ni compounds, as reported by different laboratories, vary.[28, 37] Since the exact etching procedure differs from laboratory to laboratory (beam energy, geometry, and size and sample mounting procedures), it is best to rely on data taken in one place using a fixed set of etching procedures. The etching results obtained from the standard samples, as reported earlier, will therefore be used to interpret the spectra of the catalysts. Nonetheless, chemical state identification, while aided by information from the etching routine, cannot be solely based on this sort of information. Peak positions and shapes must also agree with the proposed identification of the chemical state.

### Fresh (Unreduced) Catalysts

The photoelectron spectra of the Ni $2p_{3/2}$, O 1s and Al 2s core levels for the catalysts listed in Table 3, in general, closely resembled, in binding energy and spectral shape, the spectra of nickel aluminate. A careful examination of the catalyst and $NiAl_2O_4$ binding energies given in Table 2 reveals a systematic difference between the binding energies of the catalysts and those of $NiAl_2O_4$. The binding energy separation of the Ni $2p_{3/2}$, O 1s and Al 2s peaks are in agreement, however. Since the catalysts charged up by about three to four electronvolts, this difference is attributed to an incomplete correction for the charging of the catalysts. The separation of peaks is independent of charging, and hence, the good agreement of peak separations that was found for the catalysts and $NiAl_2O_4$ helps to confirm the identification of the surface spaces as $NiAl_2O_4$. This is illustrated in Figure 4, where spectra of the C150-1-03 and C150-4-03 catalysts are compared with the spectra of nickel aluminate, and Figure 5, where the principal core level spectra are shown for the catalysts L141 and L144. The spectra are quite different, both in peak binding energy and spectral shape, from the spectra of NiO. It should be noted that the catalysts as-prepared are nominally $NiO/Al_2O_3$, and that x-ray diffraction (XRD) data obtained for the catalysts are consistent, with NiO being the only crystalline phase of nickel present in the catalysts.[6, 7]

The apparent conflict of the XRD and XPS results over the presence of NiO is a matter of some concern. NiO, as indicated by the doublet Ni $2p_{3/2}$ peak, has been observed by XPS for $NiO/Al_2O_3$ and $NiO/MgSiO_3$, particularly at higher metal loadings on catalysts prepared by impregnation.[22, 35, 38] Hence, small (30 Å) particles of supported NiO can have the doublet

**Table 3. Catalyst Binding Energies (in eV).**

| Sample | Ni $2p_{3/2}$ | O 1s | Al 2s |
|---|---|---|---|
| C150-1-03 | 856.8 | 531.8 | 119.4 |
| C150-4-03 | 856.9 | 531.5 | 119.8 |
| L141 | 856.7 | 531.9 | 119.4 |
| L141 | 857.2 | 532.2 | 120.2 |
| L143 | 856.4 | 531.6 | 119.4 |
| L144 | 857.0 | 531.8 | 119.9 |
| $NiAl_2O_4$ | 856.1 | 531.2 | 119.3 |
| $Al_2O_3$ | – | 531.4 | 119.2 |

structure of the Ni $2p_{3/2}$ peak. The NiO fingerprint still applies in this case. The absence of the NiO XPS spectrum from the catalysts spectra may then be attributed to masking of the NiO from the XPS analyzer. This can occur when the NiO particles are under an amorphous $NiAl_2O_4$ overlayer, or are within pores in the alumina support, thus the NiO would be visible to XRD but not XPS due to the differences in their respective sampling depths.[9]

A second explanation has recently been proposed by Vedrine, et al.[39] They contend that the NiO interacts with the support by a modification of the electron properties of the NiO particles undergoing a large unpaired spin delocalization toward the insulator. This interaction would not alter the crystal structure of the NiO particle and hence the XRD spectra. The spin delocalization would serve to alter the doublet structure of the Ni $2p_{3/2}$ peak of NiO removing that XPS fingerprint of NiO from the supported catalyst's spectrum.

Neither argument is completely convincing, but each does have merit and does reconcile the XRD and XPS data in a reasonable fashion. The conclusion remains that the nickel has interacted with the support in a real and substantial way, as evidenced by the change in shape of the Ni $2p_{3/2}$ peak. Nonetheless, as will be presented later, there is good evidence that much of the nickel is present in the form of $NiAl_2O_4$.

The reducibility of the catalysts has been investigated by argon ion etching and thermal gravimetric analysis (TGA). The strength of the metal-support interaction affects the reducibility of the nickel.[39] This property is of concern because, the easier the nickel is to reduce, the more readily an active catalyst can be prepared. A higher nickel loading may also be needed to obtain a satisfactory activity in the presence of a strong metal-support interaction. The silica support nickel has been found to reduce to a moderate extent (approximately 50 percent). The reducibility of $NiSiO_3$ in flowing $H_2$ reflects this.[9] In combination with the XPS spectral information, the nickel in coprecipitated $NiO/SiO_2$ was identified as $NiSiO_3$.

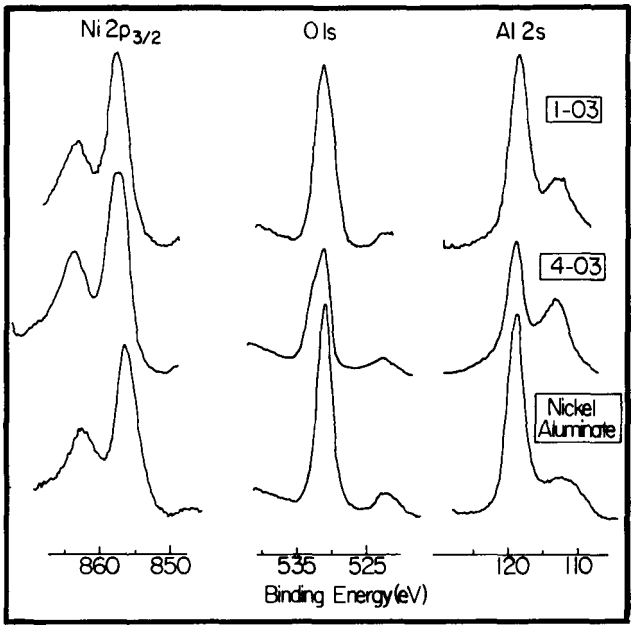


**Figure 4. The principal core level spectra for the C150-1-03 and C150-4-03 catalysts compared with those for $NiAl_2O_4$.**

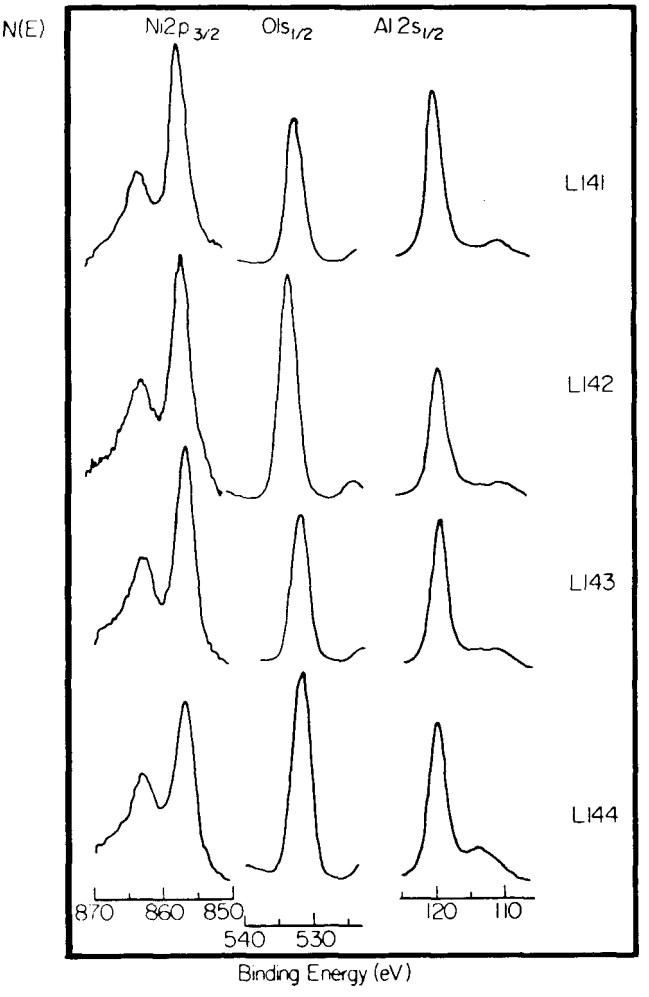


**Figure 5. The principal spectra for the L140 catalyst series. Argon etching did not change the spectra appreciably.**

The argument for the identification of the nickel in these catalysts as $NiAl_2O_4$ is similar. $NiAl_2O_4$ is significantly more difficult to reduce than $NiSiO_3$. The nickel in the catalysts is difficult to reduce either in flowing $H_2$ or by argon ion etching.[14] Figures 6-8 show the effect of argon ion etching in the C150-1-03, 4-03 and L141 catalysts. The results typically indicate very little reduction of nickel to nickel metal (Figure 9). It was estimated that with this treatment and the 1-03 catalyst, no more than nine percent of the nickel in the catalyst becomes reduced to metal. In the case of the C150-4-03 catalyst, a similar etching procedure again yielded a small amount of metal reduction (approximately 12 percent). These results, illustrated in Figure 7, are in agreement with reduction studies carried out on the catalysts in a stream of hydrogen (five $cm^3$/min). From these studies, it was found that only 10 to 20 percent of the nickel could be reduced at 400°C, and that no more than 90 percent could be reduced, even at 500°C.[36] The observed reduction is much less than that found for NiO when similarly treated, and indicates that a large portion of the nickel present in the catalyst occurs in a hard-to-reduce form. For comparison, 25 to 40 percent of the nickel in the $Ni/SiO_2$ catalysts was reduced by etching.[9] The amount of reduction observed in the catalysts is similar to that observed for $NiAl_2O_4$. These data, together with the agreement of the XPS spectra for $NiAl_2O_4$ and the catalysts, support the identification of the nickel in the catalysts as $NiAl_2O_4$. This identification is by no means conclusive because another form of nickel could have similar XPS spectra and reducibilities, but this other form is likely to be similar to $NiAl_2O_4$.

The presence of $Ni(OH)_2$ on the surface of the catalysts is a possibility, since NiO exposed to air can form an overlayer of the hydroxide.[40] The ESCA spectrum of $Ni(OH)_2$ is somewhat similar to that of $NiAl_2O_4$, but its behavior during argon ion etching is noticeably different, and on that basis, its concentration can be seen to be small relative to that of the aluminate. $Ni(OH)_2$ is reducible by the argon ion etching procedure, while $NiAl_2O_4$ (Figure 3) is not readily reduced by a similar etching treatment. The Ni in the catalysts is not reduced by argon ion etching, which is counter to the results expected if the surface Ni was present as a hydroxide. It is possible that a thin layer of $Ni(OH)_2$ could be present on the catalysts, but its abundance would have to be small relative to that for the aluminate, and it would likely be removed by the brief argon ion etching (B) in Figures 6 and 7 that did not cause any significant change in the catalyst's ESCA spectra. All evidence does strongly indicate

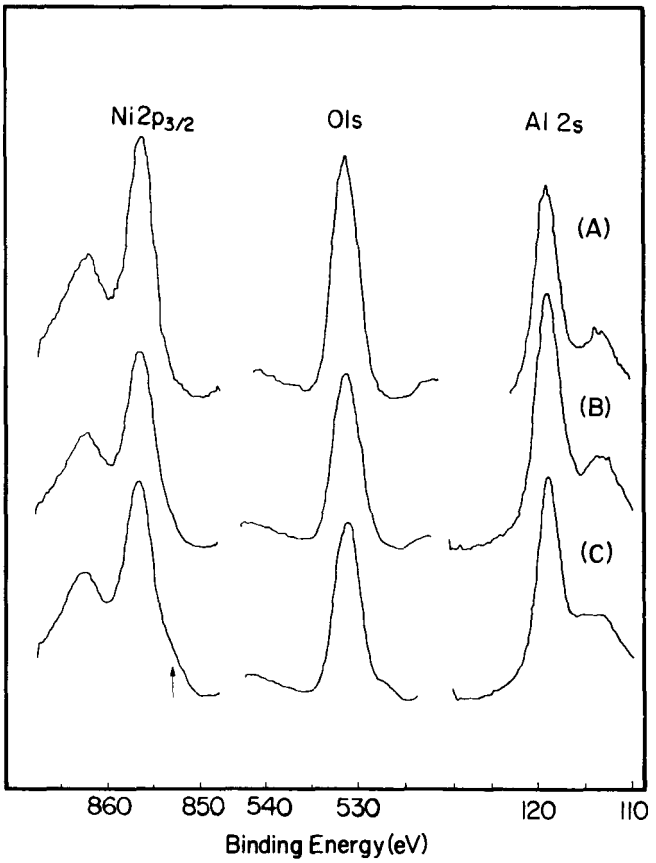


**Figure 6. Etching study spectra for the C150-1-03 catalyst: (A) unetched; (B) etched seven minutes (1 keV); and (C) etched 40 minutes (1 keV).**

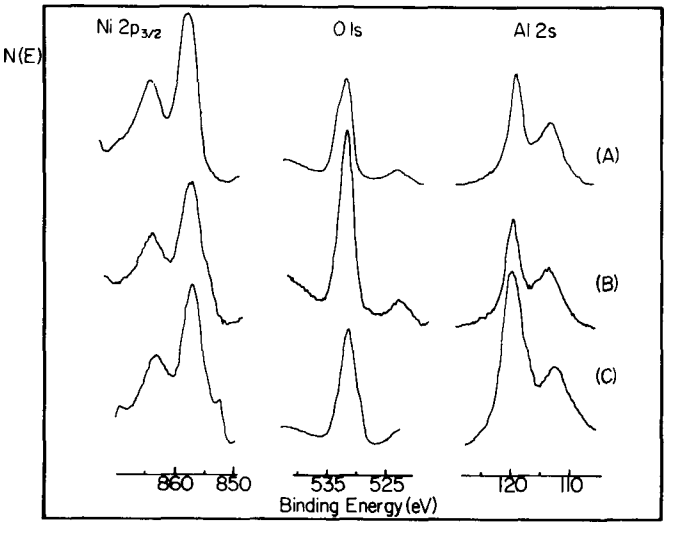


**Figure 7. Etching study spectra for the C150-4-03 catalyst: (A) unetched; (B) etched 12 minutes (1 keV); and (C) etched 40 minutes (1 keV).**

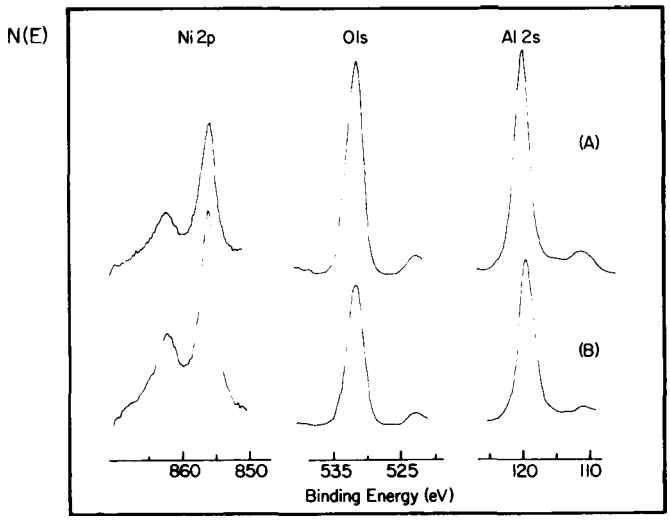


**Figure 8. Etching study spectra for the L141 catalyst: (A) unetched; and (B) etched 20 minutes (1 keV).**

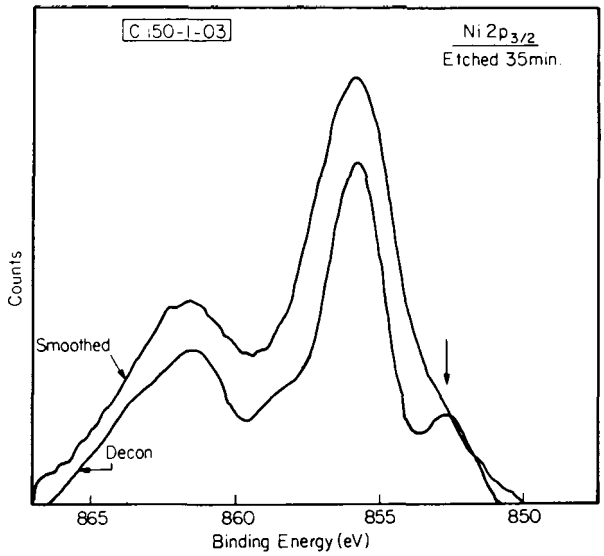


**Figure 9. Deconvolution of the final etched Ni peak for the C150-1-03 catalyst.**

an interaction of the supported nickel and the $Al_2O_3$ support. From the amount of nickel reduced, the strength of the interaction with the alumina support is seen to be stronger than that with the silica support. This is in agreement with other reports.[22, 41, 42] The interaction also appears to be stronger (due to the absence of any ESCA NiO signal) in these coprecipitated catalysts than for impregnated catalysts where NiO has been observed under certain conditions.[22, 35, 42] It seems reasonable that the thermal stability of these catalysts may be attributed to this strong metal-support interaction.[10, 36] A challenge in catalyst preparation is to balance the ease of reducibility and the thermal stability of the dispersed metal by adjusting the metal-support interaction. As has been seen, the type of support and technique of preparation used can play a role in the strength of this interaction.

The L140 series of catalysts was examined with the goal of detecting changes in the chemical state of the nickel as the metal loading decreased. Such an effect has been seen for impregnated $Ni/Al_2O_3$ catalysts.[22] NiO was observed for higher (23.9 percent) loadings, while it was not seen for lower loadings (seven percent).

The changes observed for the L140 series are less pronounced (Figure 8 for example). Indeed, the changes in peak shape and binding energy are quite small. These values are similar to those observed in the higher metal content C150 series catalysts. (The values for L142 appear to be inadequately charging corrected; however, the spacings of the Ni, Al, and O peaks are similar to those observed for the other L140 catalysts). These materials were also quite resistant to argon ion etch reduction, as were the C150 catalysts. The chemical state of the nickel is thus relatively unchanged by the changes in metal loading, in contrast to results for impregnated catalysts. Since the alumina surface areas are similar in each case (100-150 $m^2/gm$), this suggests that the coprecipitation technique disperses the nickel more thoroughly across the available surface area of the support so that more nickel can interact with the support before larger particles of NiO form.

An important consequence of the metal-support interaction in these catalysts can be seen in Table 1. The metal surface area *per gram of Ni* in the reduced catalysts increased significantly as the metal loading of the catalysts increases. This indicates that the interaction is stronger and more complete in the catalysts with the lower metal loadings. To obtain an active coprecipitated catalyst, the metal loading must be higher than that required for an impregnated catalyst.[10] Indeed, it is possible to prepare an inactive coprecipitated $Ni/Al_2O_3$ catalyst with a nickel loading of $30^{w}/o$.[10]

## Conclusions

Photoelectron spectroscopy studies on a series of nickel compounds and coprecipitated nickel on alumina catalysts have shown that the surface regions of the fresh (unreduced) catalysts are dominated by amorphous nickel aluminate with nickel oxide present, either within the pores of the support, or covered by a layer of nickel aluminate. The results, taken in conjunction with chemical and argon ion reducing studies, indicate that up to 80 percent of the nickel is combined with the support in a hard-to-reduce form in the higher metal loading samples, and even higher fractions have interacted with the support in the case of lower metal loading. The degree and strength of the interaction is stronger than for silica supported catalysts or alumina supported catalysts prepared by an impregnation technique.

## Acknowledgements

This research was supported by U.S. Department of Energy Contract No. EX-76-C-01-2229, and by the Institute for Mining and Minerals Research, University of Kentucky. Catalyst samples and useful technical information were provided by A. L. Hausberger, W. A. Kustes and M. Miller, United Catalysts, Inc., Louisville, Kentucky.

## References

1. W. L. Lom and A. F. Williams, **Substitute Natural Gas**, John Wiley and Sons, New York (1976).
2. G. A. Mills and F. W. Steffgen, **Catalysis Reviews**, Vol. 8, p. 159 (1973).
3. G. A. Mills, **Catalysis Reviews**, Vol. 14, p. 69 (1976).
4. M. A. Vannice, **Catalysis Reviews**, Vol. 14, p. 153 (1976).
5. R. B. Shalvoy and P. J. Reucroft, **Journal of Electron Spectroscopy**, Vol. 12, p. 351 (1977).
6. A. Kidron, R. J. De Angelis and P. J. Reucroft, **Journal of Applied Physics**, Vol. 48, p. 5296 (1977).
7. P. Ganesan, H. K. Kuo, A. Saavedra and R. J. De Angelis, **Journal of Catalysis**, Vol. 52, p. 310 (1978).
8. E. B. Bradley and J. M. Stencel, **Journal of Applied Spectroscopy**, in press.
9. R. B. Shalvoy, P. J. Reucroft and B. H. Davis, **Journal of Catalysis**, Vol. 56, p. 336 (1979).
10. A. L. Hausberger, K. Atwood and C. B. Knight, **Advances in Chemistry**, Series 146, p. 47 (1975).
11. T. A. Carlson, **Photoelectron and Auger Spectroscopy**, Plenum Press, New York (1975).
12. C. R. Brundle, **Journal of Electron Spectroscopy**, Vol. 5, p. 291 (1976).
13. C. R. Brundle, **Journal of Vacuum Science Technology**, Vol. 11, p. 212 (1976).
14. W. N. Delgass, T. R. Hughes and C. S. Fadley, **Catalysis Reviews**, Vol. 4, p. 179 (1970).
15. J. S. Brinen, **Accounts of Chemical Research**, Vol. 9, p. 86 (1976).
16. K. T. Ng and D. M. Hercules, **Journal of Physical Chemistry**, Vol. 80, p. 2096 (1976).
17. H. Vinek, H. Nolles, M. Ebel and K. Schwartz, **Journal of the Chemical Society**, Faraday Transactions I, Vol. 73, p. 734 (1977).
18. D. Briggs, **Journal of Electron Spectroscopy**, Vol. 9, p. 687 (1976).
19. T. E. Madey, C. D. Wagner and A. Joshi, **Journal of Electron Spectroscopy**, Vol. 10, p. 359 (1977).
20. M. Batista-Leal, J. E. Lester and C. A. Lucchesi, **Journal of Electron Spectroscopy**, Vol. 11, p. 333 (1977).
21. C. R. Helms and J. H. Sinfelt, **Surface Science**, Vol. 72, p. 229 (1978).
22. Milton Wu, Roland Chin and David M. Hercules, **Spectroscopy Letters**, Vol. 11, p. 615 (1978).
23. Milton Wu and David M. Hercules, **Journal of Physical Chemistry**, Vol. 83, p. 2003 (1979).
24. C. D. Wagner, W. M. Riggs, L. E. Davis, J. F. Moulder and G. E. Muilenberg, *"Handbook of X-Ray Photoelectron Spectroscopy,"* Perkin Elmer Corp., Eden Prairie, Minnesota (1979).

25. W. P. Dianis and J. E. Lester, **Analytical Chemistry**, Vol. 45, p. 1416 (1973).

26. C. J. Powell, N. E. Erickson and T. E. Madey, unpublished results.

27. K. S. Kim and N. Winograd, **Surface Science**, Vol. 43, p. 625 (1974).

28. K. S. Kim, W. E. Battinger, J. W. Amy and N. Winograd, **Journal of Electron Spectroscopy**, Vol. 5, p. 351 (1974).

29. R. Holm and S. Storp, **Journal of Electron Spectroscopy**, Vol. 8, p. 139 (1976).

30. N. S. McIntyre and M. G. Cook, **Analytical Chemistry**, Vol. 47, p. 2208 (1973).

31. S. Evans, J. Pielaszek and J. M. Thomas, **Surface Science**, Vol. 56, p. 644 (1976).

32. J. Haber, J. Stoch and L. Ungier, **Journal of Electron Spectroscopy**, Vol. 9, p. 459 (1976).

33. M. Oku and K. Kirokawa, **Journal of Electron Spectroscopy**, Vol. 10, p. 103 (1977).

34. M. Shelef, M. A. Z. Wheeler and H. C. Yao, **Surface Science**, Vol. 47, p. 697 (1975).

35. Petra Lorenz, J. Finster, G. Wendt, J. V. Salyn, E. K. Zumadilov and V. I. Nefedov, **Journal of Electron Spectroscopy**, Vol. 16, p. 267 (1979).

36. P. J. Reucroft, E. B. Bradley, R. J. De Angelis and G. A. Sargent, Reports Nos. 5-7, *"Surface Structure and Mechanisms of Gasification Catalysts Deactivation,"* U.S. Department of Energy Contract No. EX-76-C-01-2229, February 1 to October 31, 1977.

37. N. S. McIntyre and F. W. Stanchell, **Journal of Vacuum Science Technology**, Vol. 16, p. 798 (1979).

38. R. B. Shalvoy, unpublished results.

39. Jacques C. Vedrine, Guy Hollinger and Tran Minh Duc, **Journal of Physical Chemistry**, Vol. 82, p. 1515 (1978).

40. Tery L. Barr, **Journal of Physical Chemistry**, Vol. 82, p. 1801 (1978).

41. Dirk Reinen and P. W. Selwood, **Journal of Catalysis**, Vol. 2, p. 109 (1963).

42. Vernon C. F. Holm and Alfred Clark, **Journal of Catalysis**, Vol. 11, p. 305 (1968).

ABSTRACT OF DISSERTATION

# A Surface Analysis Study of Carbon Monoxide and Hydrogen Adsorption and Desorption on Ni(111) Crystals

A dissertation submitted in partial fulfillment of the
requirements for the degree of Doctor of Philosophy
at The University of Kentucky

by

James Lih-Ren Chao
Taipei, Taiwan. R.O.C.

Director

Dr. Gordon A. Sargent
Professor of Metallurgical Engineering
and Materials Science
University of Kentucky
Lexington, Kentucky
1979

Most industrial chemical processes are promoted by catalysts. The transition metals have strong catalytic ability for many chemical reactions. Among these transition metals, nickel has been found to be a very efficient and specific catalyst for the methanation process. This process is becoming more important because of the need for synthetic fuels.

In order to understand the nickel catalytic reactivity, a surface analysis study was made on nickel single crystal surfaces of Ni(111) by using such new research techniques as low energy electron diffraction (LEED) and auger electron spectroscopy (AES). The adsorption and desorption of CO and $H_2$ on the nickel surface was investigated. An additional Ni(111) sample with small angle boundaries (SAB) was employed in the present research in order to examine the effect on the reactivity of the discontinuity caused by the boundary lines. Sulfur poisoned samples were also examined to investigate the sulfur poisoning problem in the nickel catalytic reaction.

A $(\sqrt{7} \times \sqrt{7})R19.1^\circ$ LEED pattern was observed for CO adsorbed on Ni(111) with a CO gas adsorption pressure of $1.6 \times 10^{-6}$ torr. The same pattern was also observed at the region of the surface between the boundaries for the Ni(111)-SAB sample.

Sulfur impurity appears to inhibit the nickel catalytic reactivity by simply blocking the active sites on the nickel surface. The number of gas molecules adsorbed per unit area is thus severely reduced. The sulfur impurity was diffused from the bulk of the nickel crystal to the surface and the boundary lines on the nickel surface did not provide an enhanced path for sulfur diffusion.

Nickel enhances the dissociation of the adsorbed CO molecules, especially, at high temperatures ($\geq 100^\circ C$). The boundary lines on Ni(111)-SAB provide a good place for this dissociation even at room temperature.

Two desorption states were observed for CO adsorption on Ni(111) at room temperature. The overall activation energy for desorption was measured to be 32 Kcal/mole. When CO adsorption was taken at $100^\circ C$, there was only one desorption state observed with an activation energy of 7.7 Kcal/mole.

In determining the maximum coverage of CO on Ni(111) at room temperature, a value of 0.28 was obtained in this study. The present results agree quite well with the work done by Erley, et al. They suggested the maximum coverage of CO on Ni(111) was 0.28 and criticized that the value of 0.57, observed by other workers, could be explained by multiple scattering of the adsorbed species.

For the adsorption of $H_2$ on Ni(111), no additional spots due to adsorbed $H_2$ molecules were observed on LEED pattern. When the $H_2$ adsorption pressure is relatively high ($\geqslant 10^{-5}$ torr), the nickel (10) and (01) diffracted beams decrease in intensity to the point that they can not be seen. There was one desorption state observed for $H_2$ desorption. The temperature corresponding to this desorption state changed from 127°C to 262°C as the adsorption temperature changed from 20°C to 100°C for the $H_2$ adsorption pressure of $\approx 5.0 \times 10^{-5}$ torr. As a conclusion, the present work suggests that there could be a surface reconstruction occurring when $H_2$ gas adsorption pressure is high ($\geqslant 10^{-5}$ torr).

# Appendix II.

# Abstracts of Papers Presented at Technical Meetings

# Appendix II.

# Abstracts of Papers Presented at Technical Meetings

**Title:** *"Investigation of the Metal-Support Interaction in Coprecipitated Nickel on Alumina Methanation Catalysts Using X-Ray Photoelectron Spectroscopy."*

**Principal Investigators:** R. B. Shalvoy, P. J. Reucroft and B. H. Davis, Institute for Mining and Minerals Research and Department of Metallurgical Engineering and Materials Science, University of Kentucky, Lexington, Kentucky 40583.

**Presented by:** R. B. Shalvoy at the 26th National Meeting of the American Vacuum Society, New York, New York, October 1-5, 1979.

**Abstract:** X-ray photoelectron spectroscopy (XPS) characterization studies on a series of commercial coprecipitated nickel on alumina catalysts are described. These catalysts have demonstrated both a high degree of activity and selectivity for the methanation of low-Btu coal gas and a resistance to deactivation by thermal sintering. The results of this study show a high degree of interaction between the supported nickel and the alumina support. An excellent agreement of both core level spectra and reducibility is observed between the catalyst samples and a $NiAlO_2$ standard sample. Surface NiO was not found. The resistance to thermal sintering is attributable to the metal-support interaction. In comparison with similarly prepared silica supported catalysts, reducibility is more difficult, indicating the presence of stronger support interactions. The high metal content of the commercial catalysts provides sufficient available nickel for good activity.

**Title:** *"Surface Characterization of Methanation Catalysts"*

**Principal Investigators:** P. J. Reucroft, E. B. Bradley, G. A. Sargent and R. J. De Angelis, Department of Metallurgical Engineering and Materials Science, University of Kentucky, Lexington, Kentucky 40506

**Presented by:** P. J. Reucroft at the Fifth Annual DOE/Fossil Energy Conference on University Coal Research, Lexington, Kentucky, August 23-24, 1978.

**Period of Performance:** February 1, 1976 to January 31, 1979

**Objective:** To study catalyst deactivation and the mechanism of catalyzed methanation by surface characterization techniques.

**Abstract:** Significant conclusions that have emerged from the project to date can be summarized as follows:

1. In coprecipitated alumina and silica supported nickel catalysts, a high fraction, ranging from 20 to 70 percent depending on the catalyst, of the active metal (nickel), is complexed with the support material in a difficult-to-reduce, spinel-like form. In the case of magnesium silicate supported nickel catalysts, the support interactions appear to be much less.

2. The higher methanation activity observed in heavily sulfided magnesium silicate and magnesium aluminate

supported nickel-chromium catalysts may be associated with the formation of sulfate in competition with sulfide in these systems.

3. CO + $H_2$ adsorption on Ni(111) at 300°C creates an intense Raman band at 80 $cm^{-1}$ when observed using 4880A exciting radiation. The surface species which is adsorbed appears to be similar to a cyclic hydrocarbon and is very stable with respect to thermal decomposition (150 to 400°C).

4. Auger studies showed that the adsorption of CO on a sulfur contaminated catalyst sample surface was slow. The sticking coefficient was $<3 \times 10^{-3}$, the adsorption of CO probably proceeding through the substitution of S and O on the active site of nickel.

5. Studies of the temperature and pressure dependence of the interaction of CO with a sulfur poisoned Ni(111) surface have indicated the presence of two CO adsorption states: a dissociated state and a nondissociated state. At high temperatures (100°C) pyrolysis of CO takes place which results in the formation of a carbide-like species on the surface.

6. The thermal sintering behavior of supported nickel catalysts has been followed by determination of the changes which occur in the particle size distribution function from x-ray diffraction data.

7. Particles of NiO and nickel in coprecipitated catalysts have been found to contain appreciable microstrains. The source of these strains is not completely understood and their role in catalytic activity is unclear at this time.

8. In coprecipitated $NiO\text{-}Al_2O_3$ and $NiO\text{-}SiO_2$ catalysts, it is necessary to use hydrogen chemisorption data combined with TGA data to determine the average metallic particle size. Excellent agreement with x-ray measured particle sizes is then obtained.

9. ESCA can be used to determine the average catalysts particle size and should be useful in studying sintering effects. Such studies can be conveniently carried out on *in situ* reduced catalysts avoiding complications that can occur due to sample partial reoxidation.

**Significance to the Fossil Energy Program:** Improvements in catalyst design that will result from obtaining a better understanding of catalyzed surface phenomena should ultimately lead to the realization of more economical processes for gasifying coal.

**Plans for the Coming Year:** During the next period, the surface characterization studies will be closely correlated with catalyst activity studies that are being initiated at the Kentucky Center for Energy Research. It is also planned to initiate preliminary studies on Fischer-Tropsch and methanol synthesis catalysts.

## Title: *"Surface Structure and Mechanisms of Gasification Catalyst Deactivation"*

**Principal Investigators:** P. J. Reucroft, E. B. Bradley, R. J. De Angelis and G. A. Sargent, University of Kentucky, Lexington, Kentucky 40506

**Presented by:** P. J. Reucroft at the ERDA/NSF/EPRI University Principal Investigators Conference – Coal Research, Colorado School of Mines, Golden, Colorado, September 3-4, 1976.

**Period of Performance:** February 1, 1976 – January 31, 1979

**Abstract:** The objective of the program is to characterize the surface structure of methanation catalysts in order to relate structural features to catalytic activity and catalyst deactivation. Surfaces to be examined include:

(a) Single-crystal nickel with well-defined crystal planes; and
(b) Dispersed samples of nickel and nickel alloys on alumina and silica supports.

The chemical composition and surface concentration will be measured by ESCA and Auger spectroscopy. Chemical bonding information will be determined by Raman and infrared spectroscopy. Structural changes in the surface lattice will be investigated by LEED characterization. The catalyst surface will be investigated in the presence of CO, $H_2$, $CH_4$ and $H_2S$ in the initial stages of the program. Other potential poisons and deactivating agents, such as chlorides, cyanides, and nitrogen oxides, and carbon depositors, such as ethylene and benzene, will be investigated as the program develops. The validity of currently accepted models of catalyst thermal deactivation, i.e., sintering, will be evaluated and assessed for accuracy and applicability. Parameters to be monitored include:

(a) Particle size and particle size distribution,
(b) The effect of temperature on particle size distribution, and
(c) The effect of particle size distribution on the rate of thermal sintering.

## Title: *"Surface Analysis of Nickel Methanation Catalysts by ESCA"*

**Principal Investigators:** P. J. Reucroft and R. B. Shalvoy, Department of Metallurgical Engineering and Materials Science, University of Kentucky, Lexington, Kentucky 40506

**Presented by:** P. J. Reucroft at the Ninth Central Regional Meeting, American Chemical Society, Charleston, West Virginia, October 12-14, 1977.

**Research Sponsor:** U. S. Energy Research and Development Administration (ERDA Contract No. EX-76-C-01-2229) and the Institute for Mining and Minerals Research, University of Kentucky, Lexington, Kentucky 40506

**Abstract:** The relationship between ESCA signal intensity and chemical bulk composition has been determined for a range of alumina supported coprecipitated methanation catalysts containing 10 to 47 percent nickel, by weight. If the nickel particle size is similar to the mean free path of photoelectrons, the ratio of intensities of the Ni $2p_{3/2}$ and Al $2s_{1/2}$ core levels should be determined by the relative abundance of Ni and Al atoms in the catalyst. In the case of particle sizes greater than the photoelectron mean free path, the measured intensity ratio is expected to be less than that predicted by the relative atomic abundance. In catalyst samples where the nickel content varied from 10 to 40 percent, the measured intensity ratio R(Ni/Al), was found to agree closely with intensity ratios predicted from atomic abundances, indicating nickel particle size of approximately 15 to 20Å. In the case of a catalyst containing 47 percent nickel, which had been previously reduced, the measured intensity ratio was significantly less than the predicted value. The latter result was attributed to particle size increase during the reduction process (sintering). The relationship between the observed intensity ratio and the nickel content was similar to results obtained for ion exchanged catalysts, but different from the relationship observed for impregnated catalysts.

## Title: *"Particle Size Distribution Function of Supported Metal Catalysts by X-Ray Diffraction"*

**Principal Investigators:** R. J. De Angelis, Department of Metallurgical Engineering and Materials Science, P. Ganesan, Institute for Mining and Minerals Research, University of Kentucky, Lexington, Kentucky 40506, and A. Saavedra, Instituto Militar de Engenharia, Urca ZC 82, Rio de Janeiro, Brazil.

**Presented by:** R. J. De Angelis at the Symposium on Catalysis of Coal Conversion Processes, Joint CIC/ACS Conference, Montreal, Canada, May 29-June 2, 1977.

**Abstract:** The sintering of nickel methanation catalysts proposed to be used in coal gasification reduces catalytic activity and leads to catalyst deactivation. Before the sintering problem can be controlled, knowledge of the mechanism of sintering is required. Two mechanistic models have been proposed to describe the sintering process in supported metal catalyst.[1,2] Each model predicts different behavior of the particle size distribution during sintering. Therefore, changes in the particle size distribution during sintering will provide information concerning the active sintering mechanism. An x-ray diffraction method based on the analysis of a single diffraction profile has been developed which provides the required particle size distribution function. This method will be presented with results obtained from silica and alumina supported nickel catalysts. These initial results indicate that the atomic transport mechanism of sintering is operative. These results will be discussed along with possible methods to reduce the rate of sintering. This work was partially supported by the Energy Research and Development Administration, contract number E(49-18)2229.

**References:**

1. E. Ruckenstein and B. Pulvermacher, **AIChE Journal**, Vol. 19, 224, 356 (1973).

2. P. C. Flynn and S. E. Wanke, **Journal of Catalysis**, Vol. 34, 390, 400 (1974).

## Title: *"ESCA Characterization of Methanation Catalysts"*

**Principal Investigators:** P. J. Reucroft, B. H. Davis and R. B. Shalvoy, Department of Metallurgical Engineering and Materials Science, University of Kentucky, Lexington, Kentucky 40506.

**Presented by:** P. J. Reucroft at the Symposium on Catalysis of Coal Conversion Processes, Joint CIC/ACS Conference, Montreal, Canada, May 29-June 2, 1977.

**Research Sponsor:** U. S. Energy Research and Development Administration (ERDA Contract No. E(49-18)-2229) and the Institute for Mining and Minerals Research, University of Kentucky, Lexington, Kentucky 40506

**Abstract:** Studies on the surface chemical composition of nickel methanation catalysts will be described. The catalysts were obtained by coprecipitation methods and contain approximately 50 percent nickel, by weight. The support material is alumina ($Al_2O_3$) or silica ($SiO_2$). Surface areas are in the range of 200 to 300 $m^2g^{-1}$. Ni $2p_{3/2}$ and O $1s_{1/2}$ ESCA spectra have been obtained for the catalysts in the reduced and prereduced state and compared with similar spectra obtained for standard samples, such as nickel silicate, nickel aluminate, NiO, $Ni_2O_3$, NiO-$Ni_2O_3$ and nickel metal. Binding energy shifts due to surface charge occur to different extents in these materials, greatly complicating the interpretation of data. Initial ESCA spectra obtained for the catalysts indicate that the surface regions of the catalysts are dominated by nickel silicate in the case of the

silica supported catalysts, or by nickel aluminate in the case of the alumina supported catalysts. Removing surface regions by argon ion bombardment yields ESCA peaks that are characteristic of nickel oxide and, in the case of the reduced catalysts, metallic nickel. Studies on the nickel oxide powder samples show that the surface region of each oxide always contains nickel in two valence states, independent of the bulk composition.

## Title: *"On Measuring the Average Particle Size of Nickel in Coprecipitated $NiO$-$Al_2O_3$ and $NiO$-$SiO_2$ Catalytic Materials"*

**Principal Investigators:** K. B. Patel, C. H. Lin, P. Ganesan, P. J. Reucroft and R. J. De Angelis, Department of Metallurgical Engineering and Materials Science, and Institute for Mining and Minerals Research, University of Kentucky, Lexington, Kentucky 40506.

**Presented by:** P. Ganesan at the Conference on Catalyst Deactivation and Poisoning, Lawrence Berkeley Laboratory, Berkeley, California, May 24-26, 1978.

## INTRODUCTION

Several methods can be used to determine the average crystallite size in supported metal catalysts.[1] X-ray diffraction and electron microscopy can also provide information on the crystallite size distribution. Hydrogen chemisorption, which depends upon determining the hydrogen uptake corresponding to monolayer coverage on the reduced active metal surface, requires information on the amount of reduced metal in the sample. In many cases, such as platinum catalysts, the reduced metal content will be the same as the total metal content of the catalyst under most reducing conditions that are employed. In catalysts where incomplete reduction is obtained, it is necessary to apply a correction for the fraction of metal that remains unreduced. In this paper, average crystallite size data obtained from hydrogen chemisorption are found to be in good agreement with similar data, obtained from x-ray diffraction studies, when corrections are applied for incomplete reduction.

**Table 1. Physical and Chemical Properties of Methanation Catalysts.**

| | C150-1-01 | C150-4-03 |
|---|---|---|
| Carrier Material | $SiO_2$ | $Al_2O_3$ |
| %Ni (Initial form NiO) | 51.7 | 55.6 |
| %C (binder) | 2.94 | 2.7 |
| %Cl | – | 0.013 |
| %S | 0.06 | 0.09 |
| $N_2$ Surface area ($m^2/g$) | 211 | 177 |
| Pore Volume ($cm^3/g$) | 0.34 | 0.514 |
| Density lbs/cu ft | 65.6 | 58.0 |

## MATERIALS

The methanation catalysts used for this investigation were supplied by United Catalysts, Inc., Louisville, Kentucky. The general properties of these catalysts are summarized in Table 1. These were made by coprecipitation of the carrier with the metal oxides in the form of metal salt solutions with $Na_2CO_3$ or $NH_4OH$.

## EXPERIMENTAL RESULTS

### Thermogravimetric Analysis

Hydrogen reduction experiments on approximately 10 milligram samples of as-received pellets were performed using a DuPont thermogravimetric analyzer. During the initial heating, under nitrogen, to the reduction temperature, there is weight loss due to removal of moisture and possibly adsorbed oxygen. Once a steady state is reached, hydrogen is passed at a predetermined flow rate as measured by a flow meter. The fraction of oxygen reduction was calculated based on the sample weight after the moisture was removed and by assuming all nickel to be in the form of NiO.

Reduction experiments were carried out on both catalysts at 400, 450 and 500°C using hydrogen flow rates between 4.8 and 8.0 cc/min. The reduction time required to attain 50 to 70 percent reduction, along with sample weight loss due to moisture for different flow rates and temperatures, are recorded in Table 2.

In the case of silica supported C150-1-01 catalysts, almost 50 percent of NiO was reduced in five minutes, the reaction rate reduced considerably thereafter, and complete reduction was not usually obtained. These results support the assumption that part of the nickel oxide is readily accessible to hydrogen and is reduced easily, and the other portions of NiO are nearly completely encapsulated or complexed by the support which make reductions difficult.

The values of activation energy for 50 and 70 percent reduction obtained for various hydrogen flow rates on the catalyst C150-1-01 are given in Table 2. The reported activation energies of 13.8 and 18.7 kcal/mole for the permeability and diffusion of hydrogen in nickel agree with the activation energies obtained on the silica supported catalysts.[2] Thus, it can be reasonably concluded that the permeability of hydrogen in the initial period and diffusion of hydrogen in the latter part of the reduction process control the reaction kinetics.[3]

For the case of the alumina supported C150-4-03 catalyst at a reduction temperature of 400°C, the fractional

**Table 2. Experimental Data for Reduction of Different Catalytic Materials.**

| Catalyst | Sample Wt. (mg) | Moisture Cont. (mg) | Red. Temp. (°C) | $H_2$ Flow Rate (cc/min) | $t_{0.5}$* (min) | Q (kcal/mole) | $t_{0.7}$* (min) | Q (kcal/mole) |
|---|---|---|---|---|---|---|---|---|
| C150-1-01 | 9.10 | 1.54 | 400 | 4.8 | 18 | – | 76.8 | – |
| C150-1-01 | 9.30 | 1.15 | 450 | 4.8 | 5.6 | – | 14.9 | – |
| C150-1-01 | 8.42 | 1.54 | 500 | 4.8 | 5.0 | 13.5 | 12.6 | 19.0 |
| C150-1-01 | 8.25 | 0.90 | 400 | 8.0 | 8.2 | – | 82.0 | – |
| C150-1-01 | 9.05 | 1.01 | 450 | 8.0 | 2.6 | – | 15.0 | – |
| C150-1-01 | 8.10 | 1.48 | 500 | 8.0 | 2.5 | 12.5 | 5.26 | 28.5 |
| C150-4-03 | 9.40 | 0.66 | 400 | 4.8 | – | | – | |
| C150-4-03 | 9.00 | 0.67 | 450 | 4.8 | 28.8 | | 77.6 | |
| C150-4-03 | 10.92 | 0.88 | 500 | 4.8 | 60.9 | | 60.9 | |

*$t_{0.50}$ and $t_{0.7}$ refers to time taken for 50 and 70 percent reduction, respectively.

Research support through DOE Contract No. EX-76-C-01-2229 is acknowledged.

reduction is only 25 percent and increases to 80 percent as the reduction temperature is increased to 500°C. The data also indicate that the kinetics of reduction at 500°C is lower than at 450°C.[4]

### Batch Process

Batch type reductions (250-gram samples) were made using C150-1-01 material at 400 and 500°C employing hydrogen flow rates of 1.2 and 2.9 ℓ/min. The results obtained were very similar to the TGA results.

### Chemisorption

Hydrogen chemisorption isotherms were determined by the conventional volumetric adsorption technique employing a vacuum system similar in design to a system described previously.[5] The surface area per gram of metal was determined from the mass of catalyst sample employed, the metal content of the catalyst and assuming an area of 6.5Å$^2$ per atom of hydrogen.

## DISCUSSION

Average particle sizes calculated from the hydrogen chemisorption data obtained on C150-1-01 and C150-4-03 (samples reduced at 400°C) were 67Å and 200Å, respectively. These values were obtained assuming a spherical shape factor and complete reduction of the NiO to metallic nickel. However, the TGA indicated that the fractional reduction of NiO was between 0.2 and 0.8 for the alumina supported catalysts, and 0.7 and 0.8 for the silica supported catalysts. Introducing the fractional reduction (F) into the calculation of the average particle size from the surface area(s) leads directly to:

$$\begin{aligned} d\ \text{sphere} &= 0.6734\ F/S\ (Å), \\ d\ \text{cube} &= 0.5612\ F/S\ (Å). \end{aligned} \qquad (1)$$

Using Coenen's proposed model in which hemispherical crystallite gives the formula:[6]

$$d_{\text{hemisphere}} = 0.4310\ F/S\ (Å). \qquad (2)$$

Table 3 contains the values of the average crystallite size calculated from the data obtained on catalysts using the above three particle models. The x-ray determined particle sizes obtained from these catalysts after a reduction of two hours at 500°C were 35 to 40Å.[7] A comparison of the x-ray results with the values in Table 3 indicates that there is a good agreement with the crystallite sizes determined from the surface area measurements. The hemispherical particle shape model had the closest agreement.

## REFERENCES

1. T. E. Whyte, Jr., **Catalysis Reviews**, Vol. 8, pp. 117 (1973).

2. W. Jost, **Diffusion in Solids, Liquids and Gases**, Academic Press, N.Y., 1960.

**Table 3. Hydrogen Chemisorption, Thermogravimetric and Average Particle Size Data.**

| Reduc. Temp. | Surface Area ($m^2/g$) | Fract. Reduc. | Aver. Particle Size (Å) Sphere | Cube | Hemi. |
|---|---|---|---|---|---|
| C150-1-01 | | | | | |
| 400 | 85 | 0.74 | 56 | 46 | 36 |
| 450 | 76 | 0.90 | 76 | 64 | 49 |
| C150-4-03 | | | | | |
| 400 | 28.0 | 0.24 | 59 | 49 | 39 |
| 450 | 61.5 | 0.80 | 87 | 73 | 55 |

3. K. B. Patel, Ph.D. Research in Progress, University of Kentucky.

4. P. J. Reucroft, E. B. Bradley, R. J. De Angelis and G. A. Sargent, *"Surface Structure and Mechanisms of Gasification Catalyst Deactivation,"* First Annual Report, Feb. 1, 1976 to Jan. 31, 1977, ERDA Contract No. E(49-18)2229.

5. K. A. Krieger, **Industrial and Engineering Chemistry,** Vol. 16, pp. 398 (1944).

6. J. W. Coenen and B. G. Linsen, **Physical and Chemical Aspects of Adsorbents and Catalysts,** B. G. Linsen, Ed., Academic Press, London, p. 471 (1970).

7. P. Ganesan, H. K. Kuo, A. Saavedra and R. J. De Angelis, **Journal of Catalysis,** in press.

## Title: *"Surface Structure and Mechanisms of Gasification Catalyst Deactivation"*

**Principal Investigators:** P. J. Reucroft, E. B. Bradley, R. J. De Angelis and G. A. Sargent, College of Engineering, University of Kentucky, Lexington, Kentucky 40506

**Presented by:** P. J. Reucroft at the ERDA/EPRI/NSF-RANN University Principal Investigators Conference on Fossil Energy Research Related to Coal, Carnegie-Mellon Institute for Research, Pittsburgh, Pennsylvania, April 25-26, 1977

**Research Sponsor:** ERDA (Contract No. EX-76-C-01-2229)

**Abstract:** Improvements are generally needed in the following areas if catalyzed methanation processes are to develop further and become more economical:

(1) Catalysts are needed that are much less susceptible to sulfur poisoning. Current catalysts require $H_2S$ levels below 0.1 ppm in the gas stream to avoid deactivation.

(2) Catalysts with improved metal structure stability at high temperatures are needed. At the high temperatures employed in a typical methanation process, sintering can occur resulting in increased metal particle size and loss of catalytic activity.

(3) It would generally be desirable to have a better understanding of the factors governing catalysts specificity. Such knowledge would be useful, for example, in designing special catalysts which would favor the production of $C_2$ or $C_3$ hydrocarbons.

The general research approach to these problems is to characterize the surface structure of methanation catalysts in order to relate structural features to catalytic activity and catalyst deactivation. Surfaces under examination include dispersed samples of nickel and nickel alloys on alumina and silica supports, and single-crystal nickel with well-defined crystal planes. The coprecipitated methanation catalysts being studied were supplied by Catalysts and Chemicals, Inc., Louisville, Kentucky, who are investigating the effect of catalyst composition and support on methanation activity in the presence of sulfur. The experimental techniques employed included ESCA, auger spectroscopy, LEED, x-ray diffraction, thermogravimetric analysis (TGA), laser Raman and infrared spectroscopy, and gas adsorption.

In the first phase of the program emphasis was placed on coprecipitated dispersed metal catalysts. Catalysts which have been examined include fresh catalysts, both reduced and unreduced, used catalysts which gave good methanation activity in a sulfur-free gas stream, and sulfur deactivated catalysts.

The following are examples of significant accomplishments that have resulted from the investigation to date:

ESCA, hydrogen adsorption on reduced catalysts, infrared spectroscopy and thermogravimetric analysis indicated that reduction to metal is incomplete at 400 to 450°C. Reduction at 500°C is 100 percent complete, but increases in catalyst particle size result at these temperatures and increases in metal surface area are not commensurate. ESCA and laser Raman studies on these catalysts indicated that the incomplete reduction at 400°C occurs because a significant fraction of the nickel is complexed with the alumina or silica support. ESCA and laser Raman studies on sulfided catalysts showed that presulfiding treatment effectively saturates the catalyst with sulfur. Sulfur in the sulfide, sulfate and sulfite forms has been detected.

Particle size distribution functions have been obtained on as-received and sintered catalysts in the unreduced form (NiO). Studies to determine the particle size distribution function of reduced and passivated catalyst samples have been initiated.

Future plans include further characterization studies on supported catalysts and fundamental studies on gas-solid interactions at single crystal metal surfaces.

## Title: *"Characterization of a Sulfur Resistant Methanation Catalyst by XPS"*

**Principal Investigators:** R. B. Shalvoy and P. J. Reucroft, Department of Metallurgical Engineering and Materials Science, University of Kentucky, and Institute for Mining and Minerals Research, Kentucky Center

for Energy Research Laboratory, Lexington, Kentucky.

**Presented by:** R. B. Shalvoy at the 25th National Vacuum Symposium, American Vacuum Society, San Francisco, California, November 27-December 1, 1978.

**Research Sponsor:** Department of Energy (Contract No. EX-76-C-01-2229)

**Abstract:** A Ni-Cr on $MgSiO_3$ catalyst has been developed by United Catalysts, Inc., which converts 60 percent of the input CO to $CH_4$ after a heavy presulfiding treatment that reduces the CO conversion of conventional catalysts to less than 10 percent. The unsulfided conversion rate is better than 95 percent. X-ray photoemission spectra obtained from a series of untreated and sulfided and methanation tested Ni and Ni-Cr on $MgSiO_3$ catalysts show the presence of nickel sulfide in catalysts which are deactivated by the sulfiding, and of both nickel sulfide and nickel sulfate in the catalysts which retain appreciable methanation activity. The relationship between the resistance to sulfur poisoning and the presence of Cr and $MgSiO_3$ is discussed.

## Title: *"ESCA Characterization of Nickel Methanation Catalysts"*

**Principal Investigators:** R. B. Shalvoy and P. J. Reucroft, Department of Metallurgical Engineering and Materials Science, University of Kentucky, Lexington, Kentucky 40506.

**Presented by:** R. B. Shalvoy at the 175th ACS National Meeting, Anaheim, California, March 13-17, 1978.

**Research Sponsors:** U.S. Energy Research and Development Administration (Contract No. EX-76-C-01-2229) and the Institute for Mining and Minerals Research, University of Kentucky, Lexington, Kentucky

**Abstract:** The average particle size of dispersed metal is an important characteristic of heterogeneous catalysts. This parameter is conventionally determined from the angular width of x-ray diffraction lines or electron microscopy. These techniques are time consuming. Since the escape depth of photoelectrons is on the order of the average particle size for a typical coprecipitated nickel methanation catalyst (50 percent nickel on alumina), it is expected that a comparison of the peak areas for the nickel and aluminum core lines will contain information on the particle size. An empirical test of this approach resulted in a good correlation between the calculated and experimental Ni to Al peak area ratios for unreduced catalyst samples (R. B. Shalvoy and P. J. Reucroft, **Journal of Electron Spectroscopy**, in press). This approach has been extended to samples with a wide range of metal loadings and average particle sizes with promising results. The information provided by this quick, surface sensitive technique is a useful complement to the chemical state data conventionally obtained by ESCA.

## Title: *"Infrared and Raman Spectra of a Heterogeneous Nickel-Alumina Catalyst"*

**Principal Investigators:** J. M. Stencel and E. B. Bradley, Department of Electrical Engineering, University of Kentucky, Lexington, Kentucky 40506

**Presented by:** J. M. Stencel at the 32nd Symposium on Molecular Spectroscopy, Ohio State University, Columbus, Ohio, June 13-17, 1977.

**Research Sponsor:** ERDA Contract No. E(49-18)-2229 and Institute for Mining and Minerals Research, University of Kentucky.

**Abstract:** The infrared and Raman spectra of a heterogeneous nickel-alumina catalyst, that could be used in a coal methanation reactor is presented. They will be compared to the spectra of these catalysts which have been exposed to synthesis gas ($CO + H_2$) with temperatures near 350°C and pressures up to $35 \times 10^5$ $N/m^2$. The spectral effects of sulfur poisoning will be described. Spectral interpretation of adsorbed acetylenic and olefinic compounds is accomplished through this comparison and through the use of group theoretical analysis, desorption experiments and characteristic vibrational frequencies. A possible methanation reaction mechanism is presented and compared to previously proposed mechanisms.

## Title: *"A Cell for* in situ *Infrared and Raman Adsorption Studies"*

**Principal Investigators:** J. M. Stencel, D. M. Noland and E. B. Bradley, College of Engineering, University of Kentucky, Lexington, Kentucky 40506.

**Presented by:** J. M. Stencel at the 1977 Fall Meeting of the American Physical Society, Miami, Florida, November 21-24, 1977.

**Research Sponsor:** ERDA Contract EX-76-C-01-2229

**Abstract:** Details of an oil-free, stainless steel, ultrahigh vacuum system, which is being used to obtain infrared reflection and Raman spectra of gases adsorbed on oriented Ni surfaces, are presented. This design allows temperature-dependent adsorption-desorption studies to be performed from approximately 80 to 600°K on oriented metal surfaces which are cleaned by $H_2$ reduction and/or $Ar^+$

bombardment. Adsorbed species are distinguished from free gaseous species by multiple reflection attachments. Raman spectral results for adsorbed CO and $H_2$ on clean Ni(111) surfaces will be presented and the sensitivity of the Raman cassegrain optics will be discussed for these gases.

## Title: *"Comparison of the Infrared Spectra of Coal Methanation Catalysts"*

**Principal Investigators:** E. B. Bradley, E. Heinz and J. M. Stencel, College of Engineering, University of Kentucky, Lexington, Kentucky 40506.

**Presented by:** J. M. Stencel at the 1977 Fall Meeting of the American Physical Society, Miami, Florida, November 21-24, 1977.

**Research Sponsor:** ERDA Contract EX-76-C-01-2229

**Abstract:** Greater than 90 percent conversion of CO to $CH_4$ can be accomplished with the catalytically induced CO + $3H_2 \rightarrow CH_4$ reaction. This conversion rate decreases rapidly as catalyst sintering and sulfur poisoning occurs during this high-temperature, high-pressure reaction, e.g., a $NiO/Al_2O_3$ catalyst gives approximately a 20 percent conversion rate after exposure to sulfur. However, some heterogeneous catalysts can maintain a 70 percent conversion rate after identical sulfur treatment. These differences in methanation activity are investigated through the comparison of the infrared spectra of commercial silica- and alumina-support catalysts. Structural changes in the catalysts which result from the methanation tests will be described and related to their observed methanation activity.

## Title: *"Raman Spectra Associated with Gas Adsorption on Ni(111)"*

**Principal Investigators:** J. M. Stencel and E. B. Bradley, Department of Electrical Engineering, University of Kentucky, Lexington, Kentucky 40506.

**Presented by:** J. M. Stencel at the Molecular Spectroscopy Symposium, The Ohio State University, Columbus, Ohio, June 12-16, 1978

**Abstract:** An experimental system for studying the Raman spectra of adsorbed gases on clean, oriented crystalline surfaces and high-surface-area catalysts will be described. This ultrahigh vacuum system, which enables sample temperature variation between -120°C and 700°C, can also be used for obtaining infrared reflection spectra of adsorbed gases on smooth crystalline surfaces. The Raman spectral results from temperature dependent adsorption of $O_2$, $H_2$, $D_2$, CO and $CO_2$ on Ni(111) will be presented and discussed in relation to catalytic activity associated with the methanation reaction (CO + $3H_2 \rightarrow CH_4 + H_2O$). The effects of surface cleaning procedures which involve high-temperature oxidation/reduction cycles and $Ar^+$ bombardment will also be discussed.

## Title: *"UHV Chamber for Reflection-Absorption Spectroscopy"*

**Principal Investigators:** E. Heinz, J. M. Stencel and E. B. Bradley, Department of Electrical Engineering, University of Kentucky, Lexington, Kentucky 40506

**Presented by:** E. Heinz at the APS Southeastern Section Meeting, Blacksburg, Virginia, October 26, 1978.

**Research Sponsor:** DOE Contract No. EX-76-C-01-2229

**Abstract:** An infrared system and ultrahigh vacuum cell have been designed to measure the infrared absorption spectra of gases adsorbed on oriented single crystals of metal. The optical design features a single reflection from the metal surface at grazing incidence. The vacuum cell, equipped with an argon ion sputter gun for cleaning the crystal surface, can be operated at $10^{-11}$ torr to maintain an oxide-free surface for several hours. Heaters, coolers, and thermometers are mounted to vary the sample temperature from -190 to +650°C. The cell mounts with a standard flange on an existing ultrahigh vacuum system equipped with gas cylinders, a mixing chamber, and a leak valve to supply gases for adsorption on the metal surface at pressures as low as $10^{-10}$ torr. The system is compatible with most single- and double-beam infrared spectrophotometers. For reference spectra, the sample beam can be adjusted to by-pass the sample and still follow the same optical path it follows during absorption measurements.

## Title: *"Raman Spectra Associated with Gas Adsorption on Ni(110)"*

**Principal Investigators:** E. B. Bradley and J. M. Stencel, Department of Electrical Engineering, University of Kentucky, Lexington, Kentucky 40506

**Presented by:** E. B. Bradley at the Annual Meeting of the Optical Society of America, San Francisco, California, October 31-November 4, 1978

**Research Sponsor:** ERDA Contract No. EX-76-C-01-2229

**Abstract:** An ultrahigh vacuum cell for studying the Raman spectra of adsorbed gases on clean, oriented crystalline surfaces will be described. This cell which enables temperature variation between -170°C and 700°C can also be used for

obtaining infrared reflection spectra of adsorbed gases on smooth crystalline surfaces. The Raman spectral results from temperature-dependent adsorption of CO, $O_2$, $H_2$ and $D_2$ on Ni(110) will be presented and compared with the results of similar studies on Ni(111). It is shown that dispersion occurs for the observed bands as a function of the exciting frequency. The symmetry of the excitation centers which produce these bands, as obtained from polarization-dependent studies, will be discussed.

## Title: *"Raman Spectra of CO Adsorbed on Oriented Nickel Surfaces"*

**Principal Investigators:** E. B. Bradley and J. M. Stencel, Department of Electrical Engineering, University of Kentucky, Lexington, Kentucky 40506

**Presented by:** E. B. Bradley at the Annual Meeting of the Optical Society of America, Rochester, New York, October 8-12, 1979

**Research Sponsor:** ERDA Contract No. EX-76-C-01-2229

**Abstract:** Laser Raman spectroscopy has been used to investigate the adsorption of CO on Ni(111), Ni(110) and Ni(100). The spectra were obtained with the oriented Ni crystals at temperatures from 100 to 210°K for near grazing incidence of the laser excitation. Adsorbed CO is observed to have similar Raman frequencies on the various Ni surfaces at 5 x $10^4$ Pa CO pressure and 210°K. A Raman band at 2141 $cm^{-1}$ is also observed for the Ni(100) surface at 5 x $10^4$ Pa CO pressure at 205°K. This band is related to physically adsorbed CO.

## Title: *"Apparatus for the Measurement of the Infrared and Raman Spectra of Gases Adsorbed on Clean Metal Surfaces"*

**Principal Investigators:** J. M. Stencel and E. B. Bradley, Department of Electrical Engineering, University of Kentucky, Lexington, Kentucky 40506

**Presented by:** E. Heinz at the Molecular Spectroscopy Symposium, Columbus, Ohio, June 11-15, 1979.

**Research Sponsor:** ERDA Contract No. EX-76-C-01-2229

**Abstract:** The vibrational spectra of molecules adsorbed on metal surfaces usually are measured with electron energy loss spectroscopy.[1] In recent years there has been a renewal of interest in measuring these spectra with infrared absorption[2] and Raman scattering.[3]

Apparatus for making these measurements will be discussed, and a report on the infrared and Raman spectra of acetone and of CO adsorbed on low Miller index planes of nickel crystals will be presented. The samples are cleaned by thermal desorption and ion bombardment in an ultra-high vacuum monitored by a residual gas analyzer. Spectra are compared from samples at room temperature and at liquid nitrogen temperature. The polarization dependence of the spectra will be discussed.

**References**

1. G. A. Somorjai, **Science**, Vol. 201, pp. 489 (1978).

2. H. J. Krebs and H. Luth, **Applied Physics**, Vol. 14, pp. 337-342 (1977).

3. T. H. Wood and M. V. Klein, **Journal of Vacuum Science and Technology**, in press.

## Title: *"Auger Electron Spectroscopy and Desorption Studies of CO on Sulfur-Poisoned Nickel (111) Single-Crystal Surfaces"*

**Principal Investigators:** G. A. Sargent, Department of Metallurgical Engineering and Materials Science, University of Kentucky, Lexington, Kentucky 40506, and J. Chao and G. Freeman, Institute for Mining and Minerals Research, Kentucky Center for Energy Research Laboratory, P. O. Box 13015, Lexington, Kentucky 40583

**Presented by:** G. Freeman at the 176th National Meeting of the American Chemical Society, Miami Beach, Florida, September 10-15, 1978

**Abstract:** Adsorption isotherms of CO have been measured at temperatures between -50 and 600°C on Ni(111) single-crystal surfaces poisoned by a sulfur surface impurity estimated at about 0.13 monolayer. Adsorption levels were determined by measuring normalized Ni, S, C and O AES transition peak to peak heights. Pressure ranges from $10^{-9}$ to $10^{-5}$ torr were examined and desorption data were compiled by flashing the crystal to 770°C and monitoring mass peaks of interest to identify adsorbed species and energies of desorption, as well as coverage. The ambient hydrogen pressure was monitored by the residual gas analyser used in the desorption studies. Carbon monoxide dissociation on the Ni(111) surface was examined as a function of the $H_2$ partial pressure, as well as the temperature of the Ni crystal surface and the CO pressure. LEED studies of the CO adsorption states were also carried out.

## Title: *"Auger Electron Spectroscopy (AES), Low-Energy Electron Diffraction (LEED) and Thermal Desorption Studies of CO on Clean and Sulfur Poisoned Ni(111) Single Crystals"*

**Principal Investigators:** G. A. Sargent, Department of Metallurgical Engineering and Materials Science, University of Kentucky, Lexington, Kentucky 40506, J. Chao and G. Freeman, Institute for Mining and Minerals Research, Kentucky Center for Energy Research Laboratory, Lexington, Kentucky 40583

**Presented by:** G. A. Sargent at the 1979 International Metallographic Society Meeting, Tamiment, Pennsylvania, July 8-11, 1979.

**Abstract:** The techniques of auger electron spectroscopy (AES), low energy electron diffraction (LEED), and thermal desorption have been used to study CO on clean and sulfur poisoned Ni(111) single-crystal surfaces at room temperature. The activation energy for desorption of CO was measured using a mass spectrometer. The CO coverage was determined by LEED for both the clean and sulfur poisoned conditions. It was determined that sulfur reduces catalytic activity of the surface simply by blocking adsorption sites.

## Title: *"The Sintering Behavior of a Silica Supported Nickel Catalyst"*

**Principal Investigators:** H. K. Kuo, P. Ganesan and R. J. De Angelis, Department of Metallurgical Engineering and Materials Science, University of Kentucky, Lexington, Kentucky 40506, and Institute for Mining and Minerals Research, Kentucky Center for Energy Research Laboratory, Iron Works Pike, Lexington, Kentucky 40583.

**Presented by:** R. J. De Angelis at the Twelth Annual International Metallographic Convention, Tamiment, Pennsylvania, July 8-11, 1979.

**Research Sponsors:** U.S. Department of Energy (Contract No. E(49-18)2229) and Institute for Mining and Minerals Research, University of Kentucky, Lexington, Kentucky.

**Abstract:** Changes in the nickel particle size distribution function was monitored during sintering of a silica supported nickel catalyst. Sintering was carried out in hydrogen and nitrogen atmospheres at 100°C temperature intervals between 500 and 800°C. Particle size distributions determined both by x-ray line profile analysis and electron transmission microscopy compared well. Clear indications are that the sintering process occurs very rapidly initially, and then proceeds much more slowly at longer times. The changes in the particle size distribution function tend to indicate that the probable sintering mechanism is one associated with particle migration and coalescense.

The maximum average nickel particle size, after 100 hours of sintering, increases with sintering temperature from 50 to 75 Å as the temperature increases from 500 to 700°C. After sintering 100 hours at 800°C, the particle size increased to over 100 Å.

The particle size distribution function changes during sintering were presented and discussed in terms of existing models of sintering in supported metal catalysts.

This work was sponsored by the Institute for Mining and Minerals Research and the Department of Energy through Contract No. E(49-18)2229.

# Appendix III.

# Concise Statements of Research Accomplishments

(Prepared for the U.S. Department of Energy
Conference on University Coal Research,
August 23-16, 1978)

# Appendix III.

# Concise Statements of Research Accomplishments

(Prepared for the U.S. Department of Energy
Conference on University Coal Research,
August 23-16, 1978)

## Title: *"Support Interactions and the Reducibility of Nickel Methanation Catalysts"*

**Principal Investigator:** P. J. Reucroft, Department of Metallurgical Engineering and Materials Science, University of Kentucky, Lexington, Kentucky 40506

**Abstract:** Characterization studies on commercial alumina- and silica-supported nickel methanation catalysts have shown that a significant fraction of the metal catalyst is complexed with the support material in a difficult-to-reduce form. Techniques that have been employed to characterize the catalysts include ESCA, infrared and Raman spectroscopy, thermogravimetric analysis, hydrogen chemisorption and x-ray diffraction. At a reduction temperature of 400°C, which is typically employed in methanation reactions, the fraction of nickel that becomes reduced was as low as 0.24 to 0.3 in coprecipitated alumina supported catalysts. The fractional reduction for a similarly prepared silica-supported catalyst at 400°C was 0.4. In the case of a catalyst prepared by precipitation of nickel on to a slurry of $SiO_2$, the fractional reduction at 400°C was 0.74.

These studies indicate that the optimum reduction temperature to maximize catalyst surface area in commercial methanation catalysts will depend upon the support employed. If the temperature is too low, a small fraction of the active metal becomes reduced. At too high a temperature, although a greater fraction of metal is reduced, thermal sintering effects leading to increased catalyst particle size causes reduced catalyst surface area and activity.

## Title: *"Sulfide and Sulfate Retention in Ni/Cr Methanation Catalysts"*

**Principal Investigators:** P. J. Reucroft and E. B. Bradley, Departments of Metallurgical and Electrical Engineering, University of Kentucky, Lexington, Kentucky 40506

**Abstract:** Characterization studies on sulfided, methanation tested $Ni/Al_2O_3$, $Ni/MgSiO_3$ and $Ni/Cr/MgSiO_3$ catalysts by ESCA and infrared spectroscopy show that a significant fraction of the retained sulfur is in the sulfate form in the $Ni/Cr/MgSiO_3$ catalyst in comparison with the single metal systems. In addition, the total sulfur retention in the Ni/Cr system is approximately one half that observed in the Ni systems.

Activity tests carried out at United Catalysts, Inc., Louisville, Kentucky, have shown that $Ni/Cr/MgSiO_3$ catalysts retain greater methanation activity (60 to 80 percent CO conversion at 593°C) after severe sulfiding treatment, in contrast to other Ni based catalysts. The latter systems are rapidly deactivated after sulfiding treatments (7 to 12 percent CO conversion). The characterization studies on sulfided catalysts indicate that the improved performance of the $Ni/Cr/MgSiO_3$ system may be associated with a lower affinity for sulfur in this system and a greater tendency to retain sulfur as sulfate rather than sulfide.

## Title: *"Sintering Behavior of Nickel Methanation Catalysts"*

**Principal Investigators:** P. Ganesan and R. J. De Angelis, Department of Metallurgical Engineering and Materials Science, University of Kentucky, Lexington, Kentucky 40506

**Abstract:** An x-ray diffraction line broadening technique has been developed to obtain the particle size distribution function of metal in a supported metal catalyst using a single x-ray diffraction profile. This analysis technique has been employed to obtain particle size distribution functions in reduced and sintered samples of a commercial methanation catalyst obtained by coprecipitation of NiO on silica support. The results obtained from samples reduced at 500°C and sintered at 500 and 600°C for various times indicate that the rate of sintering is very slow. Also, the

development of the tails on the large diameter side of the distribution function indicate that the sintering takes place by a particle migration and coalescence mechanism.

The slow rate of sintering indicates that the commercial catalyst investigated is thermally stable. This stability is due either to strong interaction of the metal with the support or the particle growth is inhibited by the pore structure of the support.

## Title: *"Surface Characterization of Nickel Catalysts by Laser Light Scattering"*

**Principal Investigator:** E. B. Bradley, Department of Electrical Engineering, University of Kentucky, Lexington, Kentucky 40506

**Abstract:** Studies of the frequency shifts of $Ar^+$ laser light (Raman effect) reflected from CO, $O_2$, $H_2$ and $D_2$ adsorbed on an oriented single crystal of nickel have furnished new information on: molecular bonding of these gases on the surface of the nickel; the surface sensitivity of nickel to the adsorption of these gases; and, surface modes in nickel which affect the adsorption of these gases as a function of pressure and temperature. The sensitivity of these moles to energy exchange with the adsorbed gases may have implications in the methanation reaction.

Knowledge of the bonding and reaction mechanisms of synthesis gases on methanation catalysts will aid in improving efficiency and poison resistance of nickel catalysts.

## Title: *"A Study of Catalysts Using Auger Electron Spectroscopy and Low Energy Electron Diffraction"*

**Principal Investigator:** G. A. Sargent, Department of Metallurgical Engineering and Materials Science (and associated with the Institute for Mining and Minerals Research), University of Kentucky, Lexington, Kentucky 40506

**Abstract:** Studies of the temperature and pressure dependence of the interaction of CO with a sulfur poisoned Ni (111) surface by the techniques of low energy electron diffraction (LEED) and auger spectroscopy (AES) have indicated the presence of two CO adsorption states: a dissociated state and a nondissociated state. At high temperatures ($100^\circ C$) pyrolysis of CO was found to occur, resulting in the formation of a carbide-like species on the surface. It was also found that S appears to be inert to the adsorption of CO on the Ni surface. However, its presence limits the interaction of CO with the surface, which consequently reduces the efficiency of the Ni catalysis effect.



☆ U.S. GOVERNMENT PRINTING OFFICE: 1980-640-258/149